VINESEG

MEJS

MIDDLE EAST JOURNAL OF SCIENCE

CONTENTS

Research Articles

Review

ON DECAY AND BLOW UP OF SOLUTIONS FOR A SYSTEM OF KIRCHHOFF TYPE EQUATIONS WITH DAMPING TERMS

Erhan Pişkin*

Dicle University, Department of Mathematics, Diyarbakır, Turkey; Orcid: 0000-0001-6587-4479

* Corresponding author: episkin@dicle.edu.tr

Abstract: In this paper, we investigate system of Kirchhoff type equations with bounded domain. We obtain decay of solutions by using multiplier method. Later, we will prove blow up results for negative inital energy.

Keywords: Decay, Blow up, Kirchhoff type equation.

Mathematics Subject Classification (2010): 35B40, 35B44.

1. Introduction

In this paper, we consider the following initial boundary value system

$$
\begin{cases}
u_{tt} - M\left(\|\nabla u\|^2\right)\triangle u + \gamma_2 u_t + |u_t|^p u_t = F_u(u,v), & (x,t)\in\Omega\times(0,T), \\
v_{tt} - M\left(\|\nabla v\|^2\right)\triangle v + \gamma_2 v_t + |v_t|^q v_t = F_v(u,v), & (x,t)\in\Omega\times(0,T), \\
u(x,t) = v(x,t) = 0, & (x,t)\in\partial\Omega\times(0,T), \\
u(x,0) = u_0(x),\ u_t(x,0) = u_1(x), & x\in\Omega, \\
v(x,0) = v_0(x),\ v_t(x,0) = v_1(x), & x\in\Omega,
\end{cases}
\tag{1.1}
$$

where Ω is a bounded domain with smooth boundary $\partial\Omega$ in R^n $(n=1,2,3)$, $p,q>0$, $\gamma_2>0$. Let $\triangle = \sum_{j=1}^{n}\frac{\partial^2}{\partial x_j^2}$ be the Laplace operator, and $M(s)$ be a nonnegative locally Lipschitz function, and $F:R^2\longrightarrow R$ is a C^1 function given by

$$
F(u,v) = a|u+v|^{r+2} + 2b|uv|^{\frac{r+2}{2}},
\tag{1.2}
$$

where $r\geq 2$, $a>1$ and $b>0$, which implies

$$
F_u(u,v) = (r+2)\left[a|u+v|^r(u+v) + b|u|^{\frac{r-2}{2}}|v|^{\frac{r+2}{2}}u\right],
$$

$$
F_v(u,v) = (r+2)\left[a|u+v|^r(u+v) + b|v|^{\frac{r-2}{2}}|u|^{\frac{r+2}{2}}v\right].
$$

Also, we have

$$
uF_u(u,v) + vF_v(u,v) = (r+2)F(u,v) \quad \forall(u,v)\in R^2.
\tag{1.3}
$$

Lemma 1.1 [10]. Let c_0 and c_1 be positive constants, such that

$$c_0 \left(|u|^{r+2} + |v|^{r+2} \right) \le F(u, v) \le c_1 \left(|u|^{r+2} + |v|^{r+2} \right).\tag{1.4}$$

Throughout this paper, we define $M(s)$ by

$$M(s) = \alpha + \beta s^\gamma, \; s \ge 0, \; \alpha, \; \beta > 0, \; \gamma \ge 0.\tag{1.5}$$

Obviously, $M(s)$ is a nonnegative locally Lipschitz function.

The problem (1.1) is a generalization of a model introduced by Kirchhoff [5]. More precisely, Kirchhoff proposed a model given by the equation for $f = g = 0$,

$$\rho h \frac{\partial^2 u}{\partial t^2} + \delta \frac{\partial u}{\partial t} + g \left(\frac{\partial u}{\partial t} \right) = \left\{ \rho_0 + \frac{Eh}{2L} \int_0^L \left(\frac{\partial u}{\partial x} \right)^2 dx \right\} \frac{\partial^2 u}{\partial x^2} + f(u),\tag{1.6}$$

for $0 < x < L, \; t \ge 0$.

The qualitative analysis of solutions for a single Kirchhoff type equation

$$u_{tt} - M \left(\|\nabla u\|^2 \right) \triangle u + g(u_t) = f(u), \; x \in \Omega, \; t > 0,\tag{1.7}$$

has been discussed by many authors, see [3, 7, 12, 18, 20].

When $M(s) = 1$, (1.1) become the following system

$$\begin{cases} u_{tt} - \triangle u + \gamma_2 u_t + |u_t|^p u_t = F_u(u, v), \\ v_{tt} - \triangle v + \gamma_2 v_t + |v_t|^q v_t = F_v(u, v). \end{cases}\tag{1.8}$$

Many authors studied the existence, blow up and decay of solutions of (1.8) (see [6, 11, 13, 14, 19, 21]). Also, many authors studied the existence and nonexistence of solutions (1.8) with $\gamma_2 = 0$ ([2, 16, 17]).

Motivated by previous works, we study the decay of solutions and the blow up of solutions with negative initial energy for the system of Kirchhoff type equations with damping terms.

The outline of this paper is as follows. In section 2, we give some lemmas and notations. In section 3, the decay of the solution is given. Section 4, we show the blow up properties of solution.

2. Preliminaries

In this paper, $\|.\|$ and $\|.\|_p$ denote the usual $L^2(\Omega)$ norm and $L^p(\Omega)$ norm, respectively. Firstly, we give the following lemmas:

Lemma 2.1 [8]. Suppose that, $0 < p \; (n = 1, 2)$ or $0 < p \le 2\frac{n-1}{n-2} \; (n \ge 3)$ holds. Then there exists a positive constant $C > 1$ depending only on Ω, such that

$$\|u\|_p^s \le C \left(\|\nabla u\|^2 + \|u\|_p^p \right),$$

for any $u \in H_0^1(\Omega), \; 2 \le s \le p$.

Lemma 2.2 (Sobolev-Poincare inequality) [1]. Let p be a number with $2 \leq p < \infty$ $(n = 1, 2)$ or $2 \leq p \leq 2n/(n-2)$ $(n \geq 3)$, such that

$$\|u\|_q \leq C_* \|\nabla u\| \text{ for } u \in H_0^1(\Omega) \tag{2.1}$$

where $C_* = C_*(\Omega, q)$ is a constant.

We introduce the following functionals

$$
\begin{aligned}
J(t) &= J(u(t), v(t)) = \frac{\alpha}{2}\left(\|\nabla u\|^2 + \|\nabla v\|^2\right) \\
&+ \frac{\beta}{2(\gamma+1)}\left(\|\nabla u\|^{2(\gamma+1)} + \|\nabla v\|^{2(\gamma+1)}\right) - \int_\Omega F(u,v)\,dx,
\end{aligned}
\tag{2.2}
$$

and

$$
\begin{aligned}
I(t) &= I(u(t), v(t)) = \alpha\left(\|\nabla u\|^2 + \|\nabla v\|^2\right) \\
&+ \beta\left(\|\nabla u\|^{2(\gamma+1)} + \|\nabla v\|^{2(\gamma+1)}\right) - (r+2)\int_\Omega F(u,v)\,dx.
\end{aligned}
\tag{2.3}
$$

Next, we introduce the energy functional

$$
\begin{aligned}
E(t) &= \frac{1}{2}\left(\|u_t\|^2 + \|v_t\|^2\right) + \frac{\alpha}{2}\left(\|\nabla u\|^2 + \|\nabla v\|^2\right) \\
&+ \frac{\beta}{2(\gamma+1)}\left(\|\nabla u\|^{2(\gamma+1)} + \|\nabla v\|^{2(\gamma+1)}\right) - \int_\Omega F(u,v)\,dx.
\end{aligned}
\tag{2.4}
$$

We also define

$$W = \left\{(u,v) : (u,v) \in \left(H_0^1(\Omega) \cap H^2(\Omega)\right) \times \left(H_0^1(\Omega) \cap H^2(\Omega)\right), \ I(u,v) > 0\right\} \cup \{(0,0)\}. \tag{2.5}$$

Lemma 2.3. Let $u(x, t)$ be the solution of (1.1). Then

$$E'(t) = -\gamma_2\left(\|u_t\|^2 + \|v_t\|^2\right) - \left(\|u_t\|_{p+2}^{p+2} + \|v_t\|_{q+2}^{q+2}\right) \leq 0. \tag{2.6}$$

Proof. By multiplying the first equation of (1.1) by u_t and the second equation by v_t, integrating over Ω, we obtain

$$E(t) - E(0) = -\int_0^t \left[\gamma_2\left(\|u_\tau\|^2 + \|v_\tau\|^2\right) + \left(\|u_\tau\|_{p+2}^{p+2} + \|v_\tau\|_{q+2}^{q+2}\right)\right]d\tau \text{ for } t \geq 0. \tag{2.7}$$

We state a local existence result without a proof here (see [4, 15, 18])

Theorem 2.1 . Suppose that $\min\{p, q\} > r$ such that

$$
\begin{cases}
0 < p, q, \ 0 < r, & n = 1, 2 \\
0 < p, q \leq \frac{2}{n-2}, \ 0 < r, & n \geq 3,
\end{cases}
$$

and let $(u_0, v_0) \in \left(H_0^1(\Omega) \cap H^2(\Omega)\right) \times \left(H_0^1(\Omega) \cap H^2(\Omega)\right)$, $(u_1, v_1) \in H_0^1(\Omega) \times H_0^1(\Omega)$ be given. Then the problem (1.1) has a unique local solution

$$u, v \in C\left([0, T]; H_0^1(\Omega) \cap H^2(\Omega)\right) \text{ and } u_t, v_t \in C\left([0, T]; H_0^1(\Omega)\right),$$

for any fixed time $T > 0$.

3. The decay result

In this section, we consider the energy decay of the solution to (1.1). For this purpose, we use the functional

$$\Phi(t) = E(t) + \epsilon \int_\Omega (uu_t + vv_t) \, dx + \frac{\epsilon \gamma_2}{2} \left(\|u\|^2 + \|v\|^2 \right), \tag{3.1}$$

where ϵ is a positive constant. Inspiring by idea in [9], we will show in the next lemma that $\Phi(t)$ and $E(t)$ are equivalent.

Lemma 3.1. For $\epsilon > 0$ small enough, the relation

$$\alpha_1 E(t) \leq \Phi(t) \leq \alpha_2 (E(t))^{\frac{1}{\gamma+1}} \tag{3.2}$$

holds for two positive constants α_1 and α_2.

Proof. Applying Young inequality and Sobolev embedding theorem, we obtain

$$\begin{aligned}
\Phi(t) &\leq E(t) + \frac{\epsilon}{2} \left(\int_\Omega u^2 dx + \int_\Omega u_t^2 dx + \int_\Omega v^2 dx + \int_\Omega v_t^2 dx \right) + \frac{\epsilon \gamma_2}{2} \left(\|u\|^2 + \|v\|^2 \right) \\
&\leq \left(1 + \frac{\epsilon}{2} \right) E(t) + C_* \frac{\epsilon \gamma_2}{2} C^{\frac{1}{\gamma+1}} \left(\|\nabla u\|^{2(\gamma+1)} + \|\nabla v\|^{2(\gamma+1)} \right)^{\frac{1}{(\gamma+1)}},
\end{aligned}$$

where $(a+b)^\lambda \leq C \left(a^\lambda + b^\lambda \right)$, $a,b > 0$ was used. After that we obtain

$$\begin{aligned}
\Phi(t) &\leq \left(1 + \frac{\epsilon}{2} \right) E(t) + C_* \frac{\epsilon \gamma_2}{2} C^{\frac{1}{\gamma+1}} (E(t))^{\frac{1}{(\gamma+1)}} \\
&\leq \left(\left(1 + \frac{\epsilon}{2} \right) (E(t))^{\frac{\gamma}{\gamma+1}} + C_* \frac{\epsilon \gamma_2}{2} C^{\frac{1}{\gamma+1}} \right) (E(t))^{\frac{1}{(\gamma+1)}} \\
&\leq \left(\left(1 + \frac{\epsilon}{2} \right) (E(0))^{\frac{\gamma}{\gamma+1}} + C_* \frac{\epsilon \gamma_2}{2} C^{\frac{1}{\gamma+1}} \right) (E(t))^{\frac{1}{(\gamma+1)}} \\
&= \alpha_2 (E(t))^{\frac{1}{(\gamma+1)}}, \tag{3.3}
\end{aligned}$$

and

$$\begin{aligned}
\Phi(t) &\geq E(t) - \epsilon \left[\frac{1}{4\tau} \left(\|u_t\|^2 + \|v_t\|^2 \right) + \tau \left(\|u\|^2 + \|v\|^2 \right) \right] + \frac{\epsilon \gamma_2}{2} \left(\|u\|^2 + \|v\|^2 \right) \\
&\geq E(t) - \frac{\epsilon}{4\tau} \left(\|u_t\|^2 + \|v_t\|^2 \right) + \epsilon \left(\frac{\gamma_2}{2} - \tau \right) \left(\|u\|^2 + \|v\|^2 \right) \\
&\geq E(t) - \frac{\epsilon}{4\tau} \left(\|u_t\|^2 + \|v_t\|^2 \right) \\
&= J(t) + \left(\frac{1}{2} - \frac{\epsilon}{4\tau} \right) \left(\|u_t\|^2 + \|v_t\|^2 \right) \\
&\geq J(t) + \frac{\alpha_1}{2} \left(\|u_t\|^2 + \|v_t\|^2 \right) \\
&\geq \alpha_1 E(t). \tag{3.4}
\end{aligned}$$

for small enough τ. This completes the proof.

Theorem 3.1. Suppose that $\min \{p, q, r\} > 2\gamma$ and

$$\frac{\beta(2\gamma+1)}{2(\gamma+1)} > 2 c_*^{r+2} c_1 (r+1) \left(\frac{2(r+2)(\gamma+1)}{\beta(r-2\gamma)} E(0) \right)^{\frac{r-2\gamma}{2(\gamma+1)}}$$

4

such that (2.5) is satisfied and let $(u_0, v_0) \in W$ be given. Then the solution satisfies

$$
E(t) \leq \begin{cases} Ke^{-kt}, & \gamma = 0, \\ (kt + K)^{-\frac{1}{\gamma}}, & \gamma > 0, \end{cases} \tag{3.5}
$$

where K and k are positive constants which will be defined later.

Proof. Now differentiate (3.1) and use Eq. (1.1) and Young inequality, we have

$$
\begin{aligned}
\Phi'(t) &= -\gamma_2 \left(\|u_t\|^2 + \|v_t\|^2 \right) - \left(\|u_t\|_{p+2}^{p+2} + \|v_t\|_{q+2}^{q+2} \right) + \epsilon \left(\|u_t\|^2 + \|v_t\|^2 \right) \\
&\quad - \epsilon\alpha \left(\|\nabla u\|^2 + \|\nabla v\|^2 \right) - \epsilon\beta \left(\|\nabla u\|^{2(\gamma+1)} + \|\nabla v\|^{2(\gamma+1)} \right) \\
&\quad - \epsilon \left(\int_\Omega u u_t |u_t|^p \, dx + \int_\Omega v v_t |v_t|^q \, dx \right) + \epsilon(r+2) \int_\Omega F(u,v) \, dx \\
&\leq -(\gamma_2 - \epsilon) \left(\|u_t\|^2 + \|v_t\|^2 \right) - \left(\|u_t\|_{p+2}^{p+2} + \|v_t\|_{q+2}^{q+2} \right) \\
&\quad - \epsilon\alpha \left(\|\nabla u\|^2 + \|\nabla v\|^2 \right) - \epsilon\beta \left(\|\nabla u\|^{2(\gamma+1)} + \|\nabla v\|^{2(\gamma+1)} \right) \\
&\quad + \epsilon \left(\delta \|u\|_{p+2}^{p+2} + c(\delta) \|u_t\|_{p+2}^{p+2} + \delta \|v\|_{q+2}^{q+2} + c(\delta) \|v_t\|_{q+2}^{q+2} \right) \\
&\quad + \epsilon(r+2) \int_\Omega F(u,v) \, dx. \tag{3.6}
\end{aligned}
$$

By using the definition of the $E(t)$, we get

$$
\begin{aligned}
\Phi'(t) &\leq -\epsilon E(t) - \left(\gamma_2 - \frac{3\epsilon}{2} \right) \left(\|u_t\|^2 + \|v_t\|^2 \right) - \frac{\epsilon\alpha}{2} \left(\|\nabla u\|^2 + \|\nabla v\|^2 \right) \\
&\quad - (1 - c(\delta)) \left(\|u_t\|_{p+2}^{p+2} + \|v_t\|_{q+2}^{q+2} \right) + \epsilon \left(\delta \|u\|_{p+2}^{p+2} + \delta \|v\|_{q+2}^{q+2} \right) \\
&\quad + \epsilon(r+1) \int_\Omega F(u,v) \, dx - \frac{\epsilon\beta(2\gamma+1)}{2(\gamma+1)} \left(\|\nabla u\|^{2(\gamma+1)} + \|\nabla v\|^{2(\gamma+1)} \right).
\end{aligned}
$$

By use of $F(u,v) \leq c_1 \left(|u|^{r+2} + |v|^{r+2} \right)$, we have

$$
\begin{aligned}
\Phi'(t) &\leq -\epsilon E(t) + \epsilon\delta \left(\|u\|_{p+2}^{p+2} + \|v\|_{q+2}^{q+2} \right) + \epsilon c_1(r+1) \left(\|u\|_{r+2}^{r+2} + \|v\|_{r+2}^{r+2} \right) \\
&\quad - \frac{\epsilon\beta(2\gamma+1)}{2(\gamma+1)} \left(\|\nabla u\|^{2(\gamma+1)} + \|\nabla v\|^{2(\gamma+1)} \right). \tag{3.7}
\end{aligned}
$$

Since $I(t) > 0$,

$$
\begin{aligned}
J(t) &= \frac{r}{2(r+2)} \left[\alpha \left(\|\nabla u\|^2 + \|\nabla v\|^2 \right) + \frac{\beta(r-2\gamma)}{(\gamma+1)r} \left(\|\nabla u\|^{2(\gamma+1)} + \|\nabla v\|^{2(\gamma+1)} \right) \right] + \frac{1}{r+2} I(t) \\
&\geq \frac{r}{2(r+2)} \left[\alpha \left(\|\nabla u\|^2 + \|\nabla v\|^2 \right) + \frac{\beta(r-2\gamma)}{(\gamma+1)r} \left(\|\nabla u\|^{2(\gamma+1)} + \|\nabla v\|^{2(\gamma+1)} \right) \right]. \tag{3.8}
\end{aligned}
$$

Thus,

$$
\begin{aligned}
\|\nabla u\|^{2(\gamma+1)} + \|\nabla v\|^{2(\gamma+1)} &\leq \frac{2(r+2)(\gamma+1)}{\beta(r-2\gamma)} J(t) \\
&\leq \frac{2(r+2)(\gamma+1)}{\beta(r-2\gamma)} E(t) \\
&\leq \frac{2(r+2)(\gamma+1)}{\beta(r-2\gamma)} E(0). \tag{3.9}
\end{aligned}
$$

From Poincare inequality, we have

$$
\begin{aligned}
\|u\|_{p+2}^{p+2} &\leq c_*^{p+2} \|\nabla u\|^{p+2} \\
&= c_*^{p+2} \|\nabla u\|^{p-2\gamma} \|\nabla u\|^{2(\gamma+1)} \\
&= c_*^{p+2} \left(\|\nabla u\|^{2(\gamma+1)} \right)^{\frac{p-2\gamma}{2(\gamma+1)}} \|\nabla u\|^{2(\gamma+1)} \\
&\leq c_*^{p+2} \left(\frac{2(r+2)(\gamma+1)}{\beta(r-2\gamma)} E(0) \right)^{\frac{p-2\gamma}{2(\gamma+1)}} \|\nabla u\|^{2(\gamma+1)},
\end{aligned}
\tag{3.10}
$$

and similarly

$$
\|v\|_{q+2}^{q+2} \leq c_*^{q+2} \left(\frac{2(r+2)(\gamma+1)}{\beta(r-2\gamma)} E(0) \right)^{\frac{q-2\gamma}{2(\gamma+1)}} \|\nabla v\|^{2(\gamma+1)}.
\tag{3.11}
$$

Furthermore,

$$
\|u\|_{r+2}^{r+2} \leq c_*^{r+2} \left(\frac{2(r+2)(\gamma+1)}{\beta(r-2\gamma)} E(0) \right)^{\frac{r-2\gamma}{2(\gamma+1)}} \|\nabla u\|^{2(\gamma+1)},
$$

and similarly

$$
\|v\|_{r+2}^{r+2} \leq c_*^{r+2} \left(\frac{2(r+2)(\gamma+1)}{\beta(r-2\gamma)} E(0) \right)^{\frac{r-2\gamma}{2(\gamma+1)}} \|\nabla v\|^{2(\gamma+1)}.
\tag{3.13}
$$

Substituting (3.9)-(3.13) into (3.7), we have

$$
\begin{aligned}
\Phi'(t) \leq & -\epsilon E(t) - \epsilon \left[\frac{\beta(2\gamma+1)}{2(\gamma+1)} - 2c_*^{r+2} c_1 (r+1) \left(\frac{2(r+2)(\gamma+1)}{\beta(r-2\gamma)} E(0) \right)^{\frac{r-2\gamma}{2(\gamma+1)}} \right. \\
& \left. -\delta m \right] \left(\|\nabla u\|^{2(\gamma+1)} + \|\nabla v\|^{2(\gamma+1)} \right)
\end{aligned}
\tag{3.14}
$$

where $m = \max \left\{ c_*^{p+2} \left(\frac{2(r+2)(\gamma+1)}{\beta(r-2\gamma)} E(0) \right)^{\frac{p-2\gamma}{2(\gamma+1)}}, c_*^{q+2} \left(\frac{2(r+2)(\gamma+1)}{\beta(r-2\gamma)} E(0) \right)^{\frac{q-2\gamma}{2(\gamma+1)}} \right\}$. Thus from the assumptions of the theorem and by choosing a sufficiently small $\delta > 0$, we obtain that

$$
\Phi'(t) \leq -\epsilon E(t) \leq -\frac{\epsilon}{(\alpha_2)^{\gamma+1}} (\Phi(t))^{\gamma+1}.
\tag{3.15}
$$

We separate (3.15) into two cases.

Case 1: $\gamma = 0$, then a simply integration of (3.15) over $(0, t)$ yields

$$
E(t) \leq \Phi(t) \leq \Phi(0) e^{-kt},
$$

where $k = \frac{\epsilon}{(\alpha_2)^{\gamma+1}}$.

Case 2: $\gamma > 0$, a simply integration of (3.15) over $(0, t)$ yields

$$
E(t) \leq \Phi(t) \leq \left(kt + \Phi^{-\gamma}(0) \right)^{-\frac{1}{\gamma}},
$$

where $k = \frac{\epsilon \gamma}{(\alpha_2)^{\gamma+1}}$. This completes the proof.

4. Blow up

In this section, we state and prove blow up result.

Theorem 4.1. Suppose that $r > \max\{2\gamma, p, q\}$, $E(0) < 0$, and there exists a constant τ such that $\tau \leq \frac{2\alpha\gamma}{\gamma_2 C_*}$, where C_* is the constant of the Sobolev embedding theorem. Then the solution of this system blows up in finite time T^*, and

$$T^* \leq \frac{1-\sigma}{\xi\sigma\Psi^{\frac{\sigma}{1-\sigma}}(0)},$$

where $\Psi(t)$ and σ are given in (4.1) and (4.2) respectively.

Proof. Define $H(t) = -E(t)$, then $E(0) < 0$ and (2.6) gives $H(t) \geq H(0) > 0$. Define

$$\Psi(t) = H^{1-\sigma}(t) + \varepsilon\left(\int_\Omega uu_t dx + \int_\Omega vv_t dx\right), \tag{4.1}$$

where ε is a small constant to be chosen later and

$$0 < \sigma \leq \min\left\{\frac{r-p}{(r+2)(p+1)}, \frac{r-q}{(r+2)(q+1)}\right\}. \tag{4.2}$$

A direct differentiation of $\Psi(t)$ gives

$$
\begin{aligned}
\Psi'(t) &= (1-\sigma)H^{-\sigma}(t)H'(t) + \varepsilon\left(\|u_t\|^2 + \|v_t\|^2\right) - \varepsilon\alpha\left(\|\nabla u\|^2 + \|\nabla v\|^2\right) \\
&\quad -\varepsilon\beta\left(\|\nabla u\|^{2(\gamma+1)} + \|\nabla v\|^{2(\gamma+1)}\right) + \varepsilon(r+2)\int_\Omega F(u,v)\,dx \\
&\quad -\varepsilon\gamma_2\left(\int_\Omega uu_t dx + \int_\Omega vv_t dx\right) - \varepsilon\left(\int_\Omega uu_t |u_t|^p\,dx + \int_\Omega vv_t |v_t|^q\,dx\right). \tag{4.3}
\end{aligned}
$$

From definition of $H(t)$, it follows that

$$
\begin{aligned}
-\beta\left(\|\nabla u\|^{2(\gamma+1)} + \|\nabla v\|^{2(\gamma+1)}\right) &= 2(\gamma+1)H(t) + (\gamma+1)\left(\|u_t\|^2 + \|v_t\|^2\right) \\
&\quad +\alpha(\gamma+1)\left(\|\nabla u\|^2 + \|\nabla v\|^2\right) \\
&\quad -2(\gamma+1)\int_\Omega F(u,v)\,dx. \tag{4.4}
\end{aligned}
$$

Substitute (4.4) into (4.3) to obtain

$$
\begin{aligned}
\Psi'(t) &= (1-\sigma)H^{-\sigma}(t)H'(t) + \varepsilon\left(\|u_t\|^2 + \|v_t\|^2\right) \\
&\quad -\varepsilon\alpha\left(\|\nabla u\|^2 + \|\nabla v\|^2\right) + 2\varepsilon(\gamma+1)H(t) \\
&\quad +\varepsilon(\gamma+1)\left(\|u_t\|^2 + \|v_t\|^2\right) + \varepsilon\alpha(\gamma+1)\left(\|\nabla u\|^2 + \|\nabla v\|^2\right) \\
&\quad -2\varepsilon(\gamma+1)\int_\Omega F(u,v)\,dx + \varepsilon(r+2)\int_\Omega F(u,v)\,dx \\
&\quad -\varepsilon\gamma_2\left(\int_\Omega uu_t dx + \int_\Omega vv_t dx\right) - \varepsilon\left(\int_\Omega uu_t |u_t|^p\,dx + \int_\Omega vv_t |v_t|^q\,dx\right). \tag{4.5}
\end{aligned}
$$

Now, we make use of the following Young's inequality

$$XY \leq \frac{\delta^k X^k}{k} + \frac{\delta^l Y^l}{l},$$

$X, Y \geq 0$, $\delta > 0$, $k, l \in R^+$ such that $\frac{1}{k} + \frac{1}{l} = 1$. We have

$$\int_\Omega uu_t dx \leq \frac{\tau}{2}\|u\|^2 + \frac{1}{2\tau}\|u_t\|^2, \qquad \int_\Omega vv_t dx \leq \frac{\tau}{2}\|v\|^2 + \frac{1}{2\tau}\|v_t\|^2,$$

$$\int_{\Omega} uu_t \, |u_t|^p \, dx \;\; \leq \;\; \frac{\delta_1^{p+2}}{p+2} \, \|u\|_{p+2}^{p+2} + \frac{(p+1)\,\delta_1^{-\frac{p+2}{p+1}}}{p+2} \, \|u_t\|_{p+2}^{p+2}$$

$$\leq \;\; \frac{\delta_1^{p+2}}{p+2} \, \|u\|_{p+2}^{p+2} + \frac{(p+1)\,\delta_1^{-\frac{p+2}{p+1}}}{p+2} \, H'(t)$$

and similarly

$$\int_{\Omega} vv_t \, |v_t|^q \, dx \leq \frac{\delta_2^{q+2}}{q+2} \, \|v\|_{q+2}^{q+2} + \frac{(q+1)\,\delta_2^{-\frac{q+2}{q+1}}}{q+2} \, H'(t),$$

where δ_1, δ_2 are constants depending on the time t that will be specified later. Thus, (4.5) becomes

$$\begin{aligned}
\Psi'(t) \;\; \geq \;\; & (1-\sigma)\,H^{-\sigma}(t)\,H'(t) + \varepsilon \left(\|u_t\|^2 + \|v_t\|^2 \right) \\
& + \varepsilon\alpha\gamma \left(\|\nabla u\|^2 + \|\nabla v\|^2 \right) + 2\varepsilon\,(\gamma+1)\,H(t) + \varepsilon\,(\gamma+1)\left(\|u_t\|^2 + \|v_t\|^2 \right) \\
& + \varepsilon\,(r-2\gamma)\int_{\Omega} F(u,v)\,dx - \frac{\varepsilon\gamma_2\tau}{2}\left(\|u\|^2 + \|v\|^2 \right) - \frac{\varepsilon\gamma_2}{2\tau}\left(\|u_t\|^2 + \|v_t\|^2 \right) \\
& - \varepsilon \left(\frac{(p+1)\,\delta_1^{-\frac{p+2}{p+1}}}{p+2} + \frac{(q+1)\,\delta_2^{-\frac{q+2}{q+1}}}{q+2} \right) H'(t) - \varepsilon \left(\frac{\delta_1^{p+2}}{p+2}\,\|u\|_{p+2}^{p+2} + \frac{\delta_2^{q+2}}{q+2}\,\|v\|_{q+2}^{q+2} \right) \quad (4.6)
\end{aligned}$$

By using Sobolev-Poincare's inequality, we have

$$\begin{aligned}
\Psi'(t) \;\; \geq \;\; & (1-\sigma)\,H^{-\sigma}(t)\,H'(t) + \varepsilon \left(\alpha\gamma - \frac{\gamma_2\tau C_*}{2} \right) \left(\|\nabla u\|^2 + \|\nabla v\|^2 \right) + 2\varepsilon\,(\gamma+1)\,H(t) \\
& + \varepsilon \left(\gamma + 2 - \frac{\gamma_2}{2\tau} \right) \left(\|u_t\|^2 + \|v_t\|^2 \right) + \varepsilon\,(r-2\gamma)\int_{\Omega} F(u,v)\,dx \\
& - \varepsilon \left(\frac{(p+1)\,\delta_1^{-\frac{p+2}{p+1}}}{p+2} + \frac{(q+1)\,\delta_2^{-\frac{q+2}{q+1}}}{q+2} \right) H'(t) - \varepsilon \left(\frac{\delta_1^{p+2}}{p+2}\,\|u\|_{p+2}^{p+2} + \frac{\delta_2^{q+2}}{q+2}\,\|v\|_{q+2}^{q+2} \right) \quad (4.7)
\end{aligned}$$

Therefore by taking δ_1 and δ_2 so that $\delta_1^{-\frac{p+2}{p+1}} = k_1 H^{-\sigma}(t)$, $\delta_2^{-\frac{q+2}{q+1}} = k_2 H^{-\sigma}(t)$, where k_1, $k_2 > 0$ are specified later, we get

$$\delta_1^{p+2} = k_1^{-(p+1)} H^{\sigma(p+1)}(t) \leq k_1^{-(p+1)} c_1^{\sigma(p+1)} \left(\|u\|_{r+2}^{r+2} + \|v\|_{r+2}^{r+2} \right)^{\sigma(p+1)}, \qquad (4.8)$$

and

$$\delta_2^{q+2} = k_2^{-(q+1)} H^{\sigma(q+1)}(t) \leq k_2^{-(q+1)} c_1^{\sigma(q+1)} \left(\|u\|_{r+2}^{r+2} + \|v\|_{r+2}^{r+2} \right)^{\sigma(q+1)}, \qquad (4.9)$$

since $H(t) = -E(t) \leq \int_{\Omega} F(u,v)\,dx \leq c_1 \left(|u|^{r+2} + |u|^{r+2} \right).$

Substituting (4.8) and (4.9) into (4.7), we have

$$
\begin{aligned}
\Psi'(t) \geq{} & \left(1 - \sigma - \frac{\varepsilon(p+1)k_1}{p+2} - \frac{\varepsilon(q+1)k_2}{q+2}\right) H^{-\sigma}(t) H'(t) + 2\varepsilon(\gamma+1) H(t) \\
& + \varepsilon\left(\alpha\gamma - \frac{\gamma_2 \tau C_*}{2}\right)\left(\|\nabla u\|^2 + \|\nabla v\|^2\right) \\
& + \varepsilon\left(2 + \gamma - \frac{\gamma_2}{2\tau}\right)\left(\|u_t\|^2 + \|v_t\|^2\right) + \varepsilon(r - 2\gamma)\int_\Omega F(u,v)\,dx \\
& - \frac{\varepsilon k_1^{-(p+1)} c_1^{\sigma(p+1)}}{p+2}\left(\|u\|_{r+2}^{r+2} + \|v\|_{r+2}^{r+2}\right)^{\sigma(p+1)}\|u\|_{p+2}^{p+2} \\
& - \frac{\varepsilon k_2^{-(q+1)} c_1^{\sigma(q+1)}}{q+2}\left(\|u\|_{r+2}^{r+2} + \|v\|_{r+2}^{r+2}\right)^{\sigma(q+1)}\|v\|_{q+2}^{q+2}.
\end{aligned}
\tag{4.10}
$$

Since $r > \max\{p, q\}$, we obtain

$$
\|u\|_{p+2}^{p+2} \leq C\|u\|_{r+2}^{p+2} \leq C\left(\|u\|_{r+2} + \|v\|_{r+2}\right)^{p+2},
$$

$$
\|v\|_{q+2}^{q+2} \leq C\|v\|_{r+2}^{q+2} \leq C\left(\|u\|_{r+2} + \|v\|_{r+2}\right)^{q+2}.
$$

Thus

$$
\begin{aligned}
\Psi'(t) \geq{} & \left(1 - \sigma - \frac{\varepsilon(p+1)k_1}{p+2} - \frac{\varepsilon(q+1)k_2}{q+2}\right) H^{-\sigma}(t) H'(t) + 2\varepsilon(\gamma+1) H(t) \\
& + \varepsilon\left(\alpha\gamma - \frac{\gamma_2 \tau C_*}{2}\right)\left(\|\nabla u\|^2 + \|\nabla v\|^2\right) \\
& + \varepsilon\left(2 + \gamma - \frac{\gamma_2}{2\tau}\right)\left(\|u_t\|^2 + \|v_t\|^2\right) + \varepsilon(r - 2\gamma)\int_\Omega F(u,v)\,dx \\
& - \frac{\varepsilon k_1^{-(p+1)} c_1^{\sigma(p+1)} C}{p+2}\left(\|u\|_{r+2} + \|v\|_{r+2}\right)^{\sigma(r+2)(p+1)+p+2} \\
& - \frac{\varepsilon k_2^{-(q+1)} c_1^{\sigma(q+1)} C}{q+2}\left(\|u\|_{r+2} + \|v\|_{r+2}\right)^{\sigma(r+2)(q+1)+q+2},
\end{aligned}
\tag{4.11}
$$

where $(a+b)^\lambda \leq C\left(a^\lambda + b^\lambda\right)$, $a, b > 0$ is used. From (4.2), we have $2 \leq \sigma(p+1)(r+2)+p+2 \leq r+2$, $2 \leq \sigma(q+1)(r+2) + q + 2 \leq r + 2$. By using Lemma 2.1, we have

$$
\|u\|_{r+2}^{\sigma(p+1)(r+2)+p+2} \leq C\left(\|\nabla u\|^2 + \|u\|_{r+2}^{r+2}\right),
$$

$$
\|v\|_{r+2}^{\sigma(q+1)(r+2)+q+2} \leq C\left(\|\nabla v\|^2 + \|v\|_{r+2}^{r+2}\right).
$$

Thus

$$
\begin{aligned}
\Psi'(t) \geq{} & \left(1 - \sigma - \frac{\varepsilon(p+1)k_1}{p+2} - \frac{\varepsilon(q+1)k_2}{q+2}\right) H^{-\sigma}(t) H'(t) + 2\varepsilon(\gamma+1) H(t) \\
& + \varepsilon\left(\alpha\gamma - \frac{\gamma_2 \tau C_*}{2}\right)\left(\|\nabla u\|^2 + \|\nabla v\|^2\right) \\
& + \varepsilon\left(2 + \gamma - \frac{\gamma_2}{2\tau}\right)\left(\|u_t\|^2 + \|v_t\|^2\right) + \varepsilon(r - 2\gamma)\int_\Omega F(u,v)\,dx \\
& + \varepsilon\left(-\frac{k_1^{-(p+1)} c_1^{\sigma(p+1)} C}{p+2} - \frac{k_2^{-(q+1)} c_1^{\sigma(q+1)} C}{q+2}\right)\left(\|u\|_{r+2}^{r+2} + \|v\|_{r+2}^{r+2}\right) \\
& + \varepsilon\left(-\frac{k_1^{-(p+1)} c_1^{\sigma(p+1)} C}{p+2} - \frac{k_2^{-(q+1)} c_1^{\sigma(q+1)} C}{q+2}\right)\left(\|\nabla u\|^2 + \|\nabla v\|^2\right).
\end{aligned}
\tag{4.12}
$$

By using the $c_0 \left(|u|^{r+2} + |v|^{r+2} \right) \leq F(u, v)$ in (4.12) we obtain

$$
\begin{aligned}
\Psi'(t) \geq & \left(1 - \sigma - \frac{\varepsilon(p+1)k_1}{p+2} - \frac{\varepsilon(q+1)k_2}{q+2} \right) H^{-\sigma}(t) H'(t) \\
& + 2\varepsilon(\gamma+1) H(t) + \varepsilon \left(2 + \gamma - \frac{\gamma_2}{2\tau} \right) \left(\|u_t\|^2 + \|v_t\|^2 \right) \\
& + \varepsilon \left(c_0(r - 2\gamma) - \frac{k_1^{-(p+1)} c_1^{\sigma(p+1)} C}{p+2} - \frac{k_2^{-(q+1)} c_1^{\sigma(q+1)} C}{q+2} \right) \left(\|u\|_{r+2}^{r+2} + \|v\|_{r+2}^{r+2} \right) \\
& + \varepsilon \left(\alpha\gamma - \frac{\gamma_2 \tau C_*}{2} - \frac{k_1^{-(p+1)} c_1^{\sigma(p+1)} C}{p+2} - \frac{k_2^{-(q+1)} c_1^{\sigma(q+1)} C}{q+2} \right) \left(\|\nabla u\|^2 + \|\nabla v\|^2 \right) (4.13)
\end{aligned}
$$

where $r > 2\gamma$ is used. We choose $k_1, \ k_2$ large enough so that

$$
c_0(r - 2\gamma) - \frac{k_1^{-(p+1)} c_1^{\sigma(p+1)} C}{p+2} - \frac{k_2^{-(q+1)} c_1^{\sigma(q+1)} C}{q+2} > \frac{c_0(r - 2\gamma)}{2}
$$

and

$$
\alpha\gamma - \frac{\gamma_2 \tau C_*}{2} - \frac{k_1^{-(p+1)} c_1^{\sigma(p+1)} C}{p+2} - \frac{k_2^{-(q+1)} c_1^{\sigma(q+1)} C}{q+2} > \frac{\alpha\gamma}{2} - \frac{\gamma_2 \tau C_*}{4}.
$$

Then, we choose ε small enough so that $1 - \sigma - \frac{\varepsilon(p+1)k_1}{p+2} - \frac{\varepsilon(q+1)k_2}{q+2} \geq 0$. Thus, we have

$$
\begin{aligned}
\Psi'(t) \geq & \ \varepsilon \left(2 + \gamma - \frac{\gamma_2}{2\tau} \right) \left(\|u_t\|^2 + \|v_t\|^2 \right) + 2\varepsilon(\gamma+1) H(t) \\
& + \varepsilon \left(\frac{\alpha\gamma}{2} - \frac{\gamma_2 \tau C_*}{4} \right) \left(\|\nabla u\|^2 + \|\nabla v\|^2 \right) + \varepsilon \frac{c_0(r - 2\gamma)}{2} \left(\|u\|_{r+2}^{r+2} + \|v\|_{r+2}^{r+2} \right) \\
\geq & \ \eta \left(\|u_t\|^2 + \|v_t\|^2 + H(t) + \|\nabla u\|^2 + \|\nabla v\|^2 + \|u\|_{r+2}^{r+2} + \|v\|_{r+2}^{r+2} \right), \qquad (4.14)
\end{aligned}
$$

where $\eta = \min \left\{ \varepsilon \left(2 + \gamma - \frac{\gamma_2}{2\tau} \right), \ 2\varepsilon(\gamma+1), \ \varepsilon \left(\frac{\alpha\gamma}{2} - \frac{\gamma_2 \tau C_*}{4} \right), \ \varepsilon \frac{c_0(r-2\gamma)}{2} \right\}$. Consequently we have

$$
\Psi(t) \geq \Psi(0) = H^{1-\sigma}(0) + \varepsilon \left(\int_\Omega u_0 u_1 dx + \int_\Omega v_0 v_1 dx \right) > 0, \ \forall t \geq 0. \qquad (4.15)
$$

On the other hand, by the Hölder's inequality, we get

$$
\begin{aligned}
\left| \int_\Omega u u_t dx + \int_\Omega v v_t dx \right|^{\frac{1}{1-\sigma}} \leq & \ \|u\|^{\frac{1}{1-\sigma}} \|u_t\|^{\frac{1}{1-\sigma}} + \|v\|^{\frac{1}{1-\sigma}} \|v_t\|^{\frac{1}{1-\sigma}} \\
\leq & \ C \left(\|u\|_{r+2}^{\frac{1}{1-\sigma}} \|u_t\|^{\frac{1}{1-\sigma}} + \|v\|_{r+2}^{\frac{1}{1-\sigma}} \|v_t\|^{\frac{1}{1-\sigma}} \right). \qquad (4.16)
\end{aligned}
$$

Young inequality gives

$$
\left| \int_\Omega u u_t dx + \int_\Omega v v_t dx \right|^{\frac{1}{1-\sigma}} \leq C \left(\|u\|_{r+2}^{\frac{\mu}{1-\sigma}} + \|u_t\|^{\frac{\theta}{1-\sigma}} + \|v\|_{r+2}^{\frac{\mu}{1-\sigma}} + \|v_t\|^{\frac{\theta}{1-\sigma}} \right), \qquad (4.17)
$$

for $\frac{1}{\mu} + \frac{1}{\theta} = 1$. We take $\theta = 2(1-\sigma)$, to get $\mu = \frac{2(1-\sigma)}{1-2\sigma} \leq r + 2$ by (4.2). Therefore (4.17) becomes

$$
\left| \int_\Omega u u_t dx + \int_\Omega v v_t dx \right|^{\frac{1}{1-\sigma}} \leq C \left(\|u_t\|^2 + \|v_t\|^2 + \|u\|_{r+2}^{\frac{2}{1-2\sigma}} + \|v\|_{r+2}^{\frac{2}{1-2\sigma}} \right). \qquad (4.18)
$$

By using Lemma 2.1, we obtain

$$\left| \int_\Omega u u_t dx + \int_\Omega v v_t dx \right|^{\frac{1}{1-\sigma}} \leq C \left(\|u_t\|^2 + \|v_t\|^2 + \|u\|_{r+2}^{r+2} + \|v\|_{r+2}^{r+2} + \|\nabla u\|^2 + \|\nabla v\|^2 \right). \quad (4.19)$$

Thus

$$
\begin{aligned}
\Psi^{\frac{1}{1-\sigma}}(t) &= \left[H^{1-\sigma}(t) + \varepsilon \left(\int_\Omega u u_t dx + \int_\Omega v v_t dx \right) \right]^{\frac{1}{1-\sigma}} \\
&\leq 2^{\frac{\sigma}{1-\sigma}} \left(H(t) + \varepsilon^{\frac{1}{1-\sigma}} \left| \int_\Omega u u_t dx + \int_\Omega v v_t dx \right|^{\frac{1}{1-\sigma}} \right) \\
&\leq C \left(\|u_t\|^2 + \|v_t\|^2 + H(t) + \|u\|_{r+2}^{r+2} + \|v\|_{r+2}^{r+2} + \|\nabla u\|^2 + \|\nabla v\|^2 \right). \quad (4.20)
\end{aligned}
$$

By combining of (4.14) and (4.20) we arrive

$$\Psi'(t) \geq \xi \Psi^{\frac{1}{1-\sigma}}(t), \quad (4.21)$$

where ξ is a positive constant. A simple integration yields

$$\Psi^{\frac{\sigma}{1-\sigma}}(t) \geq \frac{1}{\Psi^{-\frac{\sigma}{1-\sigma}}(0) - \frac{\xi \sigma t}{1-\sigma}},$$

which implies that the solution blows up in a finite time T^*, with

$$T^* \leq \frac{1-\sigma}{\xi \sigma \Psi^{\frac{\sigma}{1-\sigma}}(0)}.$$

References

[1] Adams, R.A., Fournier, J.J.F., *Sobolev Spaces,* Academic Press, New York, 2003.

[2] Agre, K., Rammaha, M.A., "Systems of nonlinear wave equations with damping and source terms", *Diff. Integral Eqns.,* 19, 1235–1270, 2006.

[3] Benaissa, A., Messaoudi, S.A., "Blow-up of solutions for the Kirchhoff equation of q-Laplacian type with nonlinear dissipation", *Colloquium Mathematicum,* 94, 103-109, 2002.

[4] Georgiev, V., Todorova, G., "Existence of a solution of the wave equation with nonlinear damping and source term", J. Differ. Equations, 109 (1994) 295–308.

[5] Kirchhoff, G., *Mechanik,* Teubner, Leipzig, 1883.

[6] Korpusov, M.O., "Blow up the solution of a nonlinear system of equations with positive energy", *Theoretical and Mathematical Physics,* 171, 725-738, 2012.

[7] Matsuyama, T., Ikehata, R., "On global solutions and energy decay for the wave equations of the Kirchhoff type with nonlinear damping terms", *J. Math. Anal. Appl.,* 204, 729-753, 1996.

[8]   Messaoudi, S.A., "Blow up in a nonlinearly damped wave equation", *Math. Nachr.,* 231, 105-111, 2001.

[9]   Messaoudi, S.A., "On the decay of solutions for a class of quasilinear hyperbolic equations with non-linear damping and source terms", *Mat. Meth. Appl. Sci.,* 28, 1819-1828, 2005.

[10] Messaoudi, S.A., Said-Houari, B., "Global nonexistence of positive initial-energy solutions of a system of nonlinear viscoelastic wave equations with damping and source terms", *J. Math. Anal. Appl.,* 365, 277–287, 2010.

[11] Miranda, M.M., Medeiros, L.A., "On the existence of global solutions of a coupled nonlinear Klein-Gordon equations", *Funkcial Ekvac.,* 30, 147-161, 1987.

[12] Ono, K., "Global existence, decay, and blow-up of solutions for some mildly degenerate nonlinear Kirchhoff strings", *J. Differential Equations,* 137, 273-301, 1997.

[13] Pişkin, E., "Uniform decay and blow-up of solutions for coupled nonlinear Klein-Gordon equations with nonlinear damping terms", *Math. Meth. Appl. Sci.,* 37, 3036-3047, 2014.

[14] Pişkin, E., "Blow-up of solutions for coupled nonlinear Klein-Gordon equations with weak damping terms", *Math. Sci. Letters,* 3, 189-191, 2014.

[15] Pişkin, E., "Existence, decay and blow up of solutions for the extensible beam equation with nonlinear damping and source terms", *Open Math.,* 13, 408-420, 2015.

[16] Said-Houari, B., "Global nonexistence of positive initial-energy solutions of a system of nonlinear wave equations with damping and source terms", *Diff. Integral Eqns.,* 23, 79–92, 2010.

[17] Said-Houari, B., "Global existence and decay of solutions of a nonlinear system of wave equations", *Appl. Anal.,* 91, 475-489, 2012.

[18] Taniguchi, T., "Existence and asymptotic behaviour of solutions to weakly damped wave equations of Kirchhoff type with nonlinear damping and source terms", *J. Math. Anal. Appl.,* 361, 566–578, 2010.

[19] Wu, S.T., "Blow-up results for system of nonlinear Klein-Gordon equations with arbitrary positive initial energ", *Electron. J. Diff. Equations,* 2012, 1-13, 2012.

[20] Wu, S.T., Tsai, L.Y., "Blow-up solutions for some nonlinear wave equations of Kirchhoff type with some dissipation", *Nonlinear Anal.,* 65, 243-264, 2006.

[21] Ye, Y., "Global existence and asymptotic stability for coupled nonlinear Klein-Gordon equations with nonlinear damping terms", *Dynamical Syst.,* 28, 287-298, 2013.

INESEG INTERNATIONAL
ENGINEERING, SCIENCE
AND EDUCATION GROUP

EFFECT OF COMPLETE BLOCK OF IRRADIATED LUNG VOLUME IN BREAST CANCER WITH TOMOTHERAPY

[1]Mehmet Hakan Doğan*, [1]Mehmet Ali Kaya
ORCID: 0000000205527587   ORCID: 0000000272660193
[1]Dicle University Faculty of Medicine, Radiation Oncology Department, Diyarbakır/Turkey

*Corresponding author; drmhdogan@outlook.com

Abstract: *The purpose of this study was to evaluate the dosimetric value of the Tomo Helical (TH) plans with the complete block where located posterior of the sided lung compared to TH plans with no block in patients with intact breast cancer. TH plans with intact breast cancer were retrospectively created for 17 patients with blocked or no TH techniques in our clinic. The beam angles were arranged to cover PTV intact breast and to minimize doses to Organ at Risks (OARs), sided lung and contralateral breast in TH plans. There was no difference between the values of Conformity Index (CI) and Homogeneity Index (HI) of both plans (p>0.05). The values of Dmean, V5, and V20 of the sided lung in Tomo Helical with the block (HTb) were significantly lower than that Tomo Helical with no block (TH) for all 17 patients (p=0.01, p=0, p=0.002). The values of Dmean and V5 of heart in HTb were significantly lower than that in TH (p=0.004, p=0). Both of HTb and TH plans produce acceptable target dose coverage in intact breast Radio Therapy (RT). Especially we produce lower dose V5 values in sided lung volume when using complete block posteriorly. Aimed to decrease scattering low dose regions in irradiated volume and around the breast, so we may prevent the probability of secondary malignancy in the breast region.*
Key Word: Breast Cancer, Tomotherapy, Complete Block, Irradiation.

1. Introduction

The number of patients diagnosed with breast cancer increases with more widely used screening mammography programs around the world [1]. Breast-conserving therapy (BCT) has become the method of choice for the treatment of early-stage breast cancer. Conservative surgery plus axillary radiotherapy is superior to axillary node dissection in stage I breast cancer patients [2]. Whole breast radiotherapy has been shown to cause low rates of axillary recurrence after breast-conserving surgery (BCS) [3]. In patients with breast cancer, compliance with adjuvant radiotherapy is good, the rate of toxicity is often acceptable, and the patients often have significantly better survival [4].

Conventional radiotherapy (RT) after conservative breast surgery is performed with 2D and 3D conformal RT with tangential beams and mixed photons/electron beams [5]. Additionally, in

recent decades, various techniques such as intensity-modulated radiotherapy (IMRT) and hybrid IMRT have been developed to improve dose distribution in the breast and to reduce the dose delivered to organs at risk (OAR) [6]. Also, 3D Conformal RT (3DCRT) and rotational IMRT with fixed gantry angles have also been shown to reduce the dose delivered to critical structures and healthy tissues in patients with breast cancer [7].

Radiotherapy to the breast is a complex task which includes numerous different techniques that can be employed to ensure adequate dose target coverage while minimizing doses to OAR [8]. In this study, we aimed to compare the role of two helical techniques, TH with blocking (THb) and TH without blocking (TH), in the reduction of doses delivered to critical organs, by creating an optimal planning target volume (PTV) in breast cancer patients. Block was created by using binary multi-leaf collimator (MLC) in the lower region of the sided lung with the optimization system.

2. Materials and Methods

2.1. Patients

The study included 17 patients with an intact primary breast tumor that underwent helical tomotherapy (TH) for BCT between January 2016 and January 2017 at Dicle University Medical School Department of Radiation Oncology. TH plans were created for each patient after informed consent was obtained from each patient. The eligibility criterion was histopathologically proven early stage I-II breast cancer according to the American Joint Committee on Cancer (AJCC) cancer staging system, We compared two modes of tomotherapy for BCT: (I) TH with blocking (THb) and (II) TH without blocking (TH).

2.2.Simulation, Contouring, Planning, Plan Assessment, and Complete Block

Patients were simulated using computed tomography (CT) simulator and were positioned on a breast board (CIVCO) with their head turned to the contralateral side and their contralateral arm raised above their head. CT images with 3.0 mm thickness were obtained for TH planning. The CT images and the contours of the planning target volume (PTV) and OAR were transferred to the tomotherapy planning system (Accuray Inc., Sunny vale) to create treatment plans.

Helical tomotherapy (TH) plans were generated using IMRT with rotational dose delivery systems to create an optimal PTV and to minimize the doses delivered to OAR, contralateral lung, and contralateral breast. The intact breast was also included in the target volume. The TH plans were created with a pitch, field width, and modulator factor of 0.287, 5.048, 3.0 (range, 0.5-4.0) cm, respectively.

A total of 50 Gy was prescribed in 25 fractions (2 Gy per fraction). In the dose limits for PTV, (I) the minimum dose delivered to 95% of the PTV was defined as D95 and D95%≥95% was achieved and (II) the percentage of the PTV receiving a minimum of 95% of the dose was defined as V95% (V47.5 Gy) and V95%≥95% was achieved. For PTV, the percentage of the PTV receiving a minimum of 107% of the prescribed dose was defined as V107 (V53.5 Gy) and was used for comparing the HT plans.

The conformity Index (CI) was used for the evaluation of the target dose conformity. The CI was calculated according to the following formula defined by ICRU (International Commission on Radiation Units and Measurements) [9]:

CI=the Volume of PTV surrounded by the reference dose /PTV Volume.

CI=1.00 is the optimal case.

The uniformity of dose distribution in the target volume was analyzed based on the Homogeneity Index (HI). HI was calculated using the HI = (D2 - D98) / D50 formula, where D2 and D98 represent the doses delivered to 2% and 98% of the PTV, respectively, and D50 represents the mean target dose (50%) [10]. A lower HI value indicates greater homogeneity, whereas a higher CI value indicates better conformity. The effects of HT on the target and OAR doses and the duration of treatment were assessed for each plan by one radiation oncologist.

The complete block is created with MLC. MLC is made of tungsten and MLC thickness is 6.25 mm. Block has placed the lower part of the lung with the optimization system (Volo planning program). Block is used for decreasing the low dose region in the sided lung.

2.3.Statistical Analysis

All data were analyzed using SPSS 16.0 (SPSS, Chicago, IL, USA). All the variables were expressed as median and mean. Wilcoxon signed-rank test for related samples was used for comparing the dosimetric end-points between the HT plans. A p value of <0.05 was considered significant.

3. Results

The study included 17 patients with breast cancer, of whom 8 (47.1%) patients had right and 9 (52.9%) patients had left breast cancer. The median age was 48 (range, 24-80) years. Median PTV volume in intact breasts was 607.9 cc (range, 338.0-1850.68). The CI values were 0.93 and 0.96 in THb and TH, respectively (p>0.05). The CI values were 0.21 and 0.23 in THb and TH, respectively, and no significant difference was found (p>0.05). Both techniques demonstrated clinically acceptable target dose coverage for the intact breasts. However, a significant difference was found in the Dmax values between the two techniques. Besides, a significant difference was found between the mean values of V107 (the volume receiving 53.5 Gy) between THb and TH (2.5% *vs.* 0.68%) (p=0.01). Table 1 summarizes the PTV dose parameters in the TH plans. A total of 50 Gy doses were given patient, while the dose distribution of PTV and critic organs were shown in Figure 1.

Table 1. Comparison of dosimetric parameters for the PTV between THb and TH plans.

Parameter	TomoBlock		TomoHelical		P value
	Median	**Range**	**Median**	**Range**	
Dmean	50,68	49,12-51,20	50,72	49,93-50,94	0,453
Dmin	25,45	17,5-37,19	35,65	24,32-41,58	0,001
Dmax	57,27	54,61-61,24	55,47	53,66-58,14	0,002
V95	95,63	91,91-99,06	95,09	91,46-98,64	0,148
V107	2,55	0.01-14,65	0,68	0-1,78	0,001
D2	53,72	50,75-55,98	53,06	51,04-53,43	0,025

D50	50,88	49,32-51,4	50,76	50,01-51,08	0,326
D95	47,97	46,13-49,3	48,57	45,8-49,26	0,234
D98	45,4	44,8-48,41	46,37	43,45-47,5	0,255
CI	0,93	0,88-0,97	0,96	0,90-0,99	0,2
HI	0,21	0,09-0,35	0,23	0,08-0,29	0,16
Dmax , maximum dose; Dmean, mean dose; Dmin, minimal dose received by 99% of target target volume; Dx, the dose received x% of the target volume; Vx, the volume of (%)receiving x dose (Gy) or higher; CI, Conformity index; HI, Homogeneity index.					
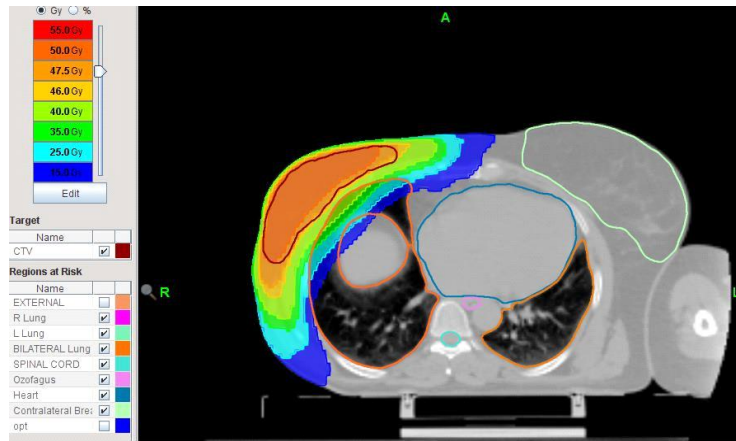
(a)
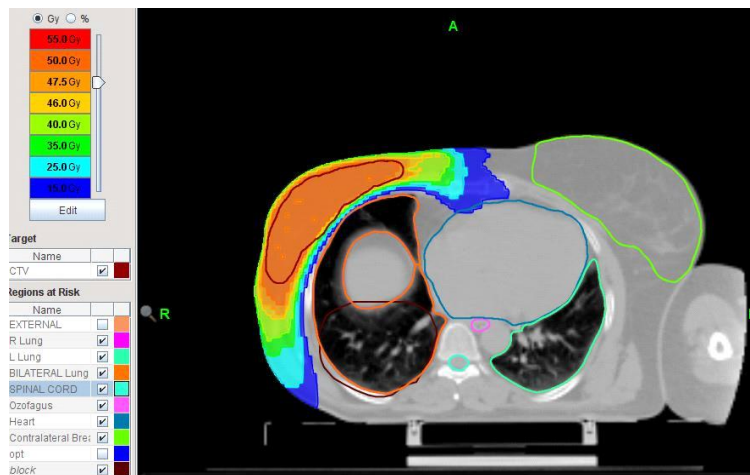
(b)

Figure 1(a). The dose distributions of Tomohelical plan without block. (b) The dose distributions of Tomohelical plan with block.

In the THb technique, the D2 and Dmin values for PTV, the V5 and V20 values for the ipsilateral lung, the Dmean and V5 values for the heart, and the V5 value were significantly lower compared to HT ($p < 0.005$ for all). However, the Dmax value for PTV was significantly lower in TH compared to HTb ($p < 0.005$).

Table 2 shows the dosimetric parameters for the ipsilateral lung, heart, contralateral breast, esophagus, and spinal cord. Table 3 shows the dosimetric comparisons of the THb and TH plans of right and left the intact breast. The greatest differences were found in the dosimetric parameters of the heart and the ipsilateral lung.

Table 2. Comparison of dosimetric parameters for the OARs THb and TH plans for 17 patients

Parameter	Tomoblock		TomoHelical		P value
	Median	Range	Median	Range	
Ipsilateral lung					
Dmean	4,9	1,79-8,09	10,95	4,39-26,65	0,01
v5	20,14	4,8-30,9	58,9	22,2-98,0	0
v20	3,23	0-11,53	18,7	0-35,0	0,002
Heart					
Dmean	5,67	2,84-12,58	7,25	4,32-10,99	0,004
V5	36,44	10,35-65,11	65,1	26,10-989,7	0
V25	0,2	0-5,3	2,25	0-7,7	0,064
V30	0	0-3,22	0,17	0-4,2	0,262
Spinal Cord					
Dmin	0,24	0,1-2,48	0,28	0,1-3,17	0,088
Dmax	7,95	1,68-30,01	9,7	2,37-26,57	0,959
D2	5,1	1,34-21,8	7,5	2,3-21,8	0,156
Contralateral Breast					
Dmean	4,39	1,76-7,84	5,29	1,65-7,54	0,136
V5	21,1	0,33-656,1	41,1	0-71,2	0,001
Osephagus					
Dmean	5,43	1,32-8,8	5,29	1,65-7,54	0,831
Vx, volume (%) receiving x dose (Gy) or higher; Dmax, maximum dose; Dmean, mean dose; D2, the					

Table 3. Comparison of dosimetric parameters of THb and TH plans of the right and left-sided intact breast

| | Right-sided (n=8) | | | | | Left-sided (n=9) | | | | |
| | THb | | TH | | | TH | | THb | | |
Parameter	Median	Range	Median	Range	P value	Median	Range	Median	Range	P value
PTV										
Dmean	50.66	49,12-51,2	50.68	49,93-50,9	1	50.76	50,65-50,94	50.68	50,42-50,8	0.192
Dmin	26.89	17,50-37,19	35.88	28,9-41,58	0.012	35.65	24,32-38,41	21.3	19,5-35,7	0.017
Dmax	57.43	54,81-59,82	55.26	53,66-58,1	0.012	55.55	54,98-56,75	57.2	54,61-61,2	0.05
V95	95.53	91,91-99,06	96.17	91,46-97,8	0.575	97.14	94,56-98,64	96.35	92,38-98,7	0.123
V107	3.02	0,64-12,85	0.28	0-1,36	0.017	0.93	0,25-1,78	2.55	0,01-14,65	0.036
D2	53.80	52,97-	52.81	51,56-	0.017	53.1	51,04-	53.72	50,75-55,9	0.374

		54,52		53,3			53,43			
D50	50.86	49,32-51,4	50.87	50,38-51,0	0.779	50.68	50,01-51,07	50.88	50,62-51,1	0.123
D95	47.83	46,15-49,3	48	45,8-48,98	0.779	48.58	46,2-49,4	48.43	45,66-48,7	0.76
D98	45.37	45,16-48,19	45.94	43,45-47,1	1	49.44	49,13-49,95	50.68	50,01-510	0.008
HI	0.14	0,10-0,31	0.12	0,09-0,18	0.56	0.16	0,08-0,23	0.18	0,11-0,33	0.215
CI	0.96	0,90-0,98	0.96	0,88-0,98	0.741	0.95	0,90-0,98	0.93	0,89-0,97	0.073
Sided lung										
Dmean	4.23	3,38-6,92	11.22	6,26-26,63	0.012	9.77	4,39-13,19	5.38	1,79-8,09	0.017
V5	17.21	14,13-34,3	61.95	37,8-98	0.012	56.22	22,2-74,5	28.9	4,8-38,9	0.012
V20	3.98	1,02-8,73	18.76	7,73-35	0.012	15.2	0-23,8	1.73	0-11,53	0.036
Heart										
Dmean	5.05	2,84-8,11	7.17	4,96-9,05	0.012	8.09	4,32-10,99	5.93	4,32-12,58	0.093
V5	33.17	10,35-65,11	65.9	32,8-71,12	0.012	59.65	26,1-98,7	42.3	19,8-63,1	0.012
V25	0.00	0,00-5,08	0.95	0-3,45	0.753	3.2	0-7,7	0.2	0-5,3	0.025
V30	0.00	0,00-3,22	0	0-1,25	0.715	1.3	0-4,2	0	0-3,1	0.058
Spinal Cord										
Dmin	0.20	0,10-2,48	0.26	0,1-2,39	0.204	0.34	0,13-3,17	0.55	0,12-1,13	0.233
Dmax	5.93	1,97-17,65	6.33	2,97-14,17	0.889	11.91	2,37-26,57	10.59	1,68-30,01	0.889
D2	4.17	1,7-12,89	5.22	2,45-11,34	0.327	8.97	2,3-21,8	6.79	1,34-21,8	0.237
Contralateral breast										
Dmean	3.54	1,76-4,39	4.85	1,65-7,54	0.05	5.55	4,46-6,49	5.45	3,08-7,84	0.953
V5	14.70	0,33-22,33	43.16	0-58,90	0.017	41.1	22,8-71,2	29.8	9,3-65,1	0.017
Esophagus										
Dmean	4.85	1,63-7,77	4.85	1,65-7,54	0.779	5.55	4,46-6,49	6.67	1.32-8,8	0.441

PTV, Planning target volume; Dmin, minimal dose; Dmean, mean dose; D2, the dose to 2% of the volume; D50, the dose to 50% of the target volume; Dmax, maximum dose; Vx, volume % receiving x dose (Gy) or higher.

4. Discussion

Helical tomotherapy (TH) and IMRT plans ensure superior target dose homogeneity and better normal tissue sparing in breast cancer RT. However, an increase in the doses delivered to low-dose regions is known to cause an increased rate of radiation-induced secondary malignancies [7,11,12]. Therefore, we aimed to compare these TH and THb in terms of achieving homogeneous dose distribution for the target volume for better local control and sparing healthy tissues to prevent life-threatening complications (heart disease and lung pneumonitis) as well as secondary malignancies.

Both techniques provided adequate coverage of the PTV, which was consistent with previous studies [13]. Moreover, all the TH and IMRT plans achieved higher PTV coverage compared to conventional plans (Prescription of V47.5Gy of PTVs>95%). On the other hand, TH and conventional

IMRT led to greater target dose homogeneity compared to 11-field (11FBT) and 11FBT IMRT [14,15]. TomoDirect (TD), Elektra Volumetric Modulated Arc Therapy (E-VMAT), and Varian RapidArc (RA) plans were generated for whole breast irradiation and these plans achieved better target coverage (V95%) compared to Field-in-field (FinF) (97.7-98.3% *vs.* 96.6%) [16]. In our study, the mean V95 value was higher in THb than in TH (95.63% *vs.* 95.09%); however, no significant difference was established.

The conformity index (CI) and homogeneity index (HI) are two analysis tools of a treatment plan. The technique with segmental fields allowed us more homogeneity dose distribution compared to the standard two tangential fields [17]. They found that the mean HI values were 1.08 and 1.09 and mean CI values were 1.38 and 1.43, respectively [17]. We found that the mean HI value was 0.21 in THb and 0.23 in TH and the mean CI value was 0.93 in THb and 0.96 in TH. However, no significant difference was found between the CI and HI values in both THb and TH ($p>0.05$). Mean V107 value for PTV was $0.2\% \pm 0.1$ in HT, and HT led to higher conformity and homogeneity compared to HTb [18]. Moreover, the V107 value was more favorable in TH compared to THb (0.68% vs. 2.55%). The volumetric-arc therapy (VMAT) plans were more inhomogeneous than the TH and TD plans [19].

The clinical benefit of radiotherapy in the treatment of breast cancer must be balanced against the documented risk of early and late toxicity [20]. Adverse effects after breast irradiation have been reported in heart disease, pneumonitis, and pulmonary fibrosis [21]. Increasing irradiated volume leads to pulmonary complications [22]. Moreover, the irradiated volume in an organ depends on the radiation technique used in the treatment [23]. A study showed the TD plans reduced the ipsilateral lung volume and the mean dose and also provided acceptable target dose homogeneity in the patients. However, TH is superior to TD when added nodal irradiation [24]. Moreover, the TH technique, compared to other techniques, decreases the doses delivered to the contralateral OAR while increasing the doses to low-dose regions [18]. In our study, the Dmean, V5 (volume of lung receiving at least 5 Gy), and V20 (volume of lung receiving at least 20 Gy) values for the ipsilateral lung in THb were significantly lower than those in TH in all the 17 patients ($p=0.01$, 0.00, 0.02, respectively). These findings can be attributed to the addition of complete block in the posterior aspect of the ipsilateral lung and the rotational delivery of TH.

Radiotherapy of breast cancer and other thoracic irradiations induce an ionizing radiation dose to the heart. Irradiation of the heart, associated with cardiovascular risk and the cancer treatment-induced cardiotoxicity, leads to increased risk of cardiovascular mortality. The high risk of cardiac events is related to the dose received by the heart and the irradiated cardiac volume. However, the limitation of cardiac irradiation is that it requires a priority in the planning of thoracic irradiations [25]. A previous study showed a low rate of ischemic cardiac disease for both radiation modalities in the women treated for breast cancer [26]. On the other hand, another study suggested that photon radiation therapy cannot achieve an MHD of <5Gy [27]. On the other hand, a previous study indicated that the relationship between the cardiac dose and late complications became prominent when 20% of the cardiac volume gained a dose of greater than 30 Gy [28]. In our study, the irradiated cardiac volume (V5) was significantly greater in TH compared to THb (65.10% vs. 36.44%; $p=0.00$). These rates suggest that these techniques do not pose a meaningful risk in terms of late cardiac complications.

Another important factor in the treatment of breast cancer is the contralateral breast. To avoid an increased risk of second cancer and the adverse effects such as fibrosis in the unaffected breast, the mean dose in this breast should be kept as low as possible. In our study, no significant difference was found between the two techniques with regards to the mean doses delivered to the contralateral breast. Moreover, the Dmean value was 4.39 Gy in THb as opposed to 5.29 Gy in TH ($p > 0.05$).

5. Conclusion

When all the deterministic values are considered, the THb technique appears to be more useful than the TH technique, as the former causes the heart, lung and contralateral breast receive lower doses while adequately covering the PTV. In particular, the low-dose regions in the irradiated contralateral lung is decreased to a very low value in THb, in which complete block is administered in the lower portion of the contralateral lung. Moreover, these low-dose regions may cause secondary malignancy. In conclusion, the complete block may be standardized in helical irradiations of breast cancer.

References

[1] Karlson , P., "Postoperative radiotherapy after DCIS: Useful for whom", *The Breast*, 34, 43-46, 2017.

[2] Dian, C., Lin, L., Chunyan, D., Miya, Y., Maohui, X., Jiaquan, C., Fang, Z., "Conservative surgery plus axillary radiotherapy vs. modified radical mastectomy in patients with stage I breast cancer", *Clinical Breast Cancer*, 14, 10-13, 2014.

[3] Oresta, G., Edoardo, B., Maria, C., Nicole, R., "Ipsilateral axillary recurrence after breast conservative surgery", *Radiotherapy and Oncolog*y, 122, 37-44, 2017.

[4] Garcia, N. A., Ace, N.B., Diaz, I, Builes, R.R., "Axillary radiotherapy in conservative surgery for early-stage breast cancer", *CRESP*, 94, 331-338, 2016.

[5] Hakan, M. D., Burhanedtin, S.Z., Mahmut, A., "Research on different techniques in breast cancer radiotherapy", *Contemp Oncol Pozn*, 17, 291-297, 2013.

[6] Cavey, M.L., Bayouth, J.E., Endres, E.J., Pena, J.M., Colman, M., Hatch, S., "Dosimetric comparison of conventional and forward-planed intensity-modulated techniques for comprehensive locoregional irradiation of post-mastectomy left breast cancer", *Med Dosim of J Am Assoc Med Dosim*, 30, 107-16, 2005.

[7] Orechia, R., Rojas, D.P., Cattani, F., Ricotti, R., "Hypofractionated post-mastectomy radiotherapy with helical tomotherapy in patients with breast reconstruction: Dosimetric result and acute/intermediate toxicity evaluation", *Med Onco*, 35, 39-45, 2018.

[8] Andrea, M.B., John, A., Jennifer, C., Marianne, R., Marita, M., Gillian, L.B., "A dosimetric comparison of 3 DCRT, IMRT and static tomotherapy with a SIB for large and small breast volume", *Medical Dosimetry*, 39, 163-168, 2014.

[9] Nell, P., "Prescribing, recording, and reporting proton-beam therapy: contents", *J ICRU*, 7, 11-19, 2007.

[10] Hodapp, N., Prescribing, recording and reporting photon-beam intensity-modulated radiation therapy (IMRT)), The ICRU Report 83, *Strahlentheroncol Organ DtschRöntgenges A*, 188, 97-99, 2012.

[11] Goddu, S.M., Chaudhari, S., Mamalui, H.M., Pechenaya, O.L., "Helical tomotherapy planning for left contralateral breast cancer patients with positive lymph nodes: comparison to conventional multiport breast technique", Int J *RadiatOncoBiol Phys*, 73, 1243-1251, 2009.

[12] Coon, A.B., Dickler, A., Kirk, M.C., Liao, Y., "Tomotherapy and multifield IMRT planning reduces cardiac doses in left contralateral breast cancer patients with unfavorable cardiac anatomy", *Int J RadiatOncol*, 78, 104-110, 2010.

[13] Hong, L., Hunt, M., Chui, C., Spirou, S., "Intensity-modulated tangential beam irradiation of intact breast", *Int J RadiatOncolBiol Phy*, 44, 1155-1164, 1999.

[14] Jones, R., Yang, W., Read, P., Sheng K., "Radiation therapy of post-mastectomy patients with positive nodes using fixed beam tomotherapy", *RadiotherOncol J EurSocTherRadiolOnco*, 100, 247-252, 2011.

[15] Reynders, T., Tournel, K., Conınck, P.D., Heyman, S., "Dosimetric assessment of static and helical tomotherapy in the clinical implementation of breast cancer tumors", *Radiotherapy and Oncology*, 93, 71-79, 2009.

[16] Koivumaki, T., Fogliata, A., Zeverino, M., Boman, E., Sierpowska, J., "Dosimetric evaluation of modern radiation therapy techniques for left breast in deep inspiration breath hold", *PhysMedica PM Int J*, 45, 82-87, 2018.

[17] Petrova, D., Smickovska, S., Lazeravska, E., "Conformity index and homogeneity index in whole breast irradiation", *Open Access Maced J Med Sci*, 5, 736-739, 2017.

[18] Haciismailoğlu, E., Colak, F., Canyılmaz, E., Dirican, B., Gürdallı, S., "Dosimetric comparison of left-side whole breast irradiation 3DCRT, forward planed IMRT, inverse planned IMRT, helical tomotherapy, and volumetric arc therapy", *PhysMedica PM Int J*, 31, 360-367, 2015.

[19] Qi, X.S., Liu, T.X., Liu, A.K., Newman, F., "Left-sided breast cancer irradiation using rotational and fixed field radiotherapy", *Med Dosim off J Am Assoc Med Dosim*, 39, 227-234, 2014.

[20] Overgaard, M., Jensen, M.B., Overgaard, J., "Post-operative radiotherapy in a high-risk postmenopausal woman with breast cancer patients given adjuvant tamoxifen", *Danish Breast Cancer Cooperative Group. Lancet*, 353, 1641-1648, 1999.

[21] Landberg, T., "The role of radiotherapy in breast conserving treatment", *Acta Oncol*, 34, 675-680, 2017.

[22] Lind, P.A., Wenberg, B., Gagliardi, G., Fornander, T., "Pulmonary complications following different radiotherapy techniques for breast cancer", *Breast Cancer Res Treat,* 68, 199-210, 2001.

[23] Wobb, C.L., Shah, C., Jawad, M.S., Wallace, M., "Comparison of chronic toxicities between brachytherapy based accelerated partial breast irradiation and whole breast irradiation using intensity-modulated radiotherapy", *The Breast*, 24, 739-744, 2015.

[24] Farhan, F., Esmati, E., Maddah, S.A., Shahriarian, S.H., "Ultrasound-guided boost irradiation of tumor cavity after lumpectomy in breast cancer", *Int J Radiat. Res*, 13, 325-329, 2015.

[25] Vandendorpe, B., Vernat, B.S., Ramiandrisoa, F., Bazire, L., Kirova, Y.M., "Doses to organs at risk in conformational radiotherapy and stereotaxic irradiation", *The Heart Cancer/Radiotherapie*, 21, 626-635, 2017.

[26] James, M., Swadi, S., Yi, M., Johansson, L., Robinson, B., Dixit, A., "Ischaemic heart disease following conventional and hypofractionated radiation treatment in a contemporary breast cancer series", *J Med Imaging Radiat Oncol*, 62, 425-431, 2018.

[27] Vega, R.B.M., Ihsak, O., Raldow, A., "Establishing cost-effective allocation of proton therapy for breast irradiation", *Int J Radiat Oncol Biol*, 91, 11-15, 2016.

[28] Gagliardi, G., Laz, I., Ottolenghi, A., Rutqvist, L.E., "Long term cardiac modality after radiotherapy of breast minimizing lung involvement", *Radiother Oncol*, 76, 319-325, 2005.

THE INVESTIGATION OF VARIATIONS IN OPTICAL PROPERTIES DEPENDING ON SINTERING TEMPERATURE OF Ni:ZNO NANO POWDERS

Handan Aydın

Department of Metallurgy and Materials Engineering, Engineering Faculty, Munzur University, Tunceli, Turkey- Orcid: https://orcid.org/0000-0002-0141-9773

Corresponding author: handanaydin23@gmail.com

Abstract: *In this study, Ni:ZnO nano powders were produced by the sol-gel calcination method to investigate and improve the interaction between sintering temperature and optical properties. ZnO based nano-ceramic materials with superior properties which can be used in several scientific researches and high technology applications and can be easily synthesized were produced by this method. The effect of Ni doping on the optical properties of ZnO nanopowders was investigated through spectrophotometric measurements. The optical band gaps of the samples were calculated from the diffuse reflectance curves using Kubelka-Munk function. It was observed that E_g values of the samples changed depending on the Ni dopant and sintering temperature. As a result of the investigations, it was determined that Ni doping and different sintering temperature have significant effects on the optical properties of ZnO nano powders, and the produced samples can be used in high temperature conductive electrode applications, optoelectronic devices, and sensor production.*

1. Introduction

Semiconductor ZnO has become one of the most popular materials for electrical and optical applications over time. It is a promising material for many optoelectronic applications such as ultraviolet lasers, light-emitting diodes, p–n junction devices, thin-film transistor, solar cells, acoustic devices, chemical, and biological sensors. For applications of the transparent and conducting electrode in solar cells and thin-film transistor, the development of low-resistive ZnO films with high transparency is crucial. Due to its large binding energy (60 meV), wide band gap (3.37 eV) and easy facilitate synthesis and assembly methods, the utilization of ZnO has covered various fields such as electric transistors [2], photovoltaic devices [3] and chemical sensors [4]. Nowadays, the nanostructure ZnO materials such as ZnO nanowires [5], nanoparticles [6], and nanotetrapods [7] have attracted the wide attention since their large surface area and enhanced quantum confinement that leads to novel electrical and optical

properties for device application. Studies have shown that the surface of ZnO nanocrystals can play an important role in carrier transport. The unbounded oxygen chemisorbed on the nanocrystal surface serves as traps for charge carriers, thus, increasing the interfacial potential and lowering carrier mobility [1]. However, in order to enhance the versatility of ZnO to meet the different requirements of the application, structural modifications have usually been utilized, among which metal ion doping is the most well known and effective approach.

Spintronics (spin-based electronics) based on diluted magnetic semiconductor oxides, is currently an active area of research because spin-based multifunctional electronic devices have several advantages over the conventional charge-based devices regarding data-processing speed, nonvolatility, and higher integration densities [16]. Diluted magnetic semiconductors (DMSs), i.e., semiconductors with a dilute concentration of magnetic dopants are expected to be promising materials for spin-based multifunctional devices. An ideal DMS must satisfy certain conditions, such as high Curie temperature (TC) and the easy incorporation of p- and n-type carriers. Besides the need for materials with high Curie temperature along with high magnetic moments, the critical point is to assure those dopant atoms are uniformly dissolved into the host lattice and that the resulting ferromagnetism (FM) indeed originates from the doped matrices [16,17].

The sol-gel method has advantages such as low cost, easy to handle, safe, and the non-vacuum method, to prepare ZnO materials over conventional synthesis methods such as magnetic sputtering, chemical vapor deposition, and hydrothermal reaction [18]. Moreover, it is easy to realize the incorporation of the dopant using a one-route process simply by modulating the ingredient of the precursors. In this communication, synthesis of nanopowders based on Ni-doped ZnO via the sol-gel calcination method is introduced. Up to our knowledge, there are a few works on the characterization of sol-gel synthesized Ni-doped ZnO nanopowders especially optical band gap calculations based on the measured diffused reflectance. In addition, the diffused reflectance was used to determine the optical constants of Ni-doped ZnO nanopowders.

2. Experimental

2.1. Preparation of Samples

In order to form solutions of ZnO containing Ni in different atomic ratios with the sol-gel method, Nickel(II) acetate tetrahydrate ($Ni(OCOCH_3)_2.4H_2O$) at different atomic ratios (0%, 0.1%, 0.5%, 1%, and 2%) was added into zinc acetate ($ZnCH_3COO)_2.2H_2O$). All solutions were prepared as 1M, 10 ml. The starting materials with calculated substance quantities were weighed and placed in the test tubes containing the solvent (2-methoxyethanol ($CH_3OCH_2CH_2OH$)). These mixtures were stirred at 800 rpm for 10 min. by the magnetic stirrer at room temperature and then stirred in an ultrasonic mixer for 5 min. to ensure better dissolution. For Ni doping, Nickel(II) acetate tetrahydrate ratios calculated according to the starting material were determined. It was stirred again under the same conditions by adding a dopant source. Monoethanolamine was then added as a stabilizer and the stirring process was repeated under the same conditions. Finally, the solution was stirred at 60 0C for 2 h to obtain the gel form. The production process of the samples is given in Fig. 1.
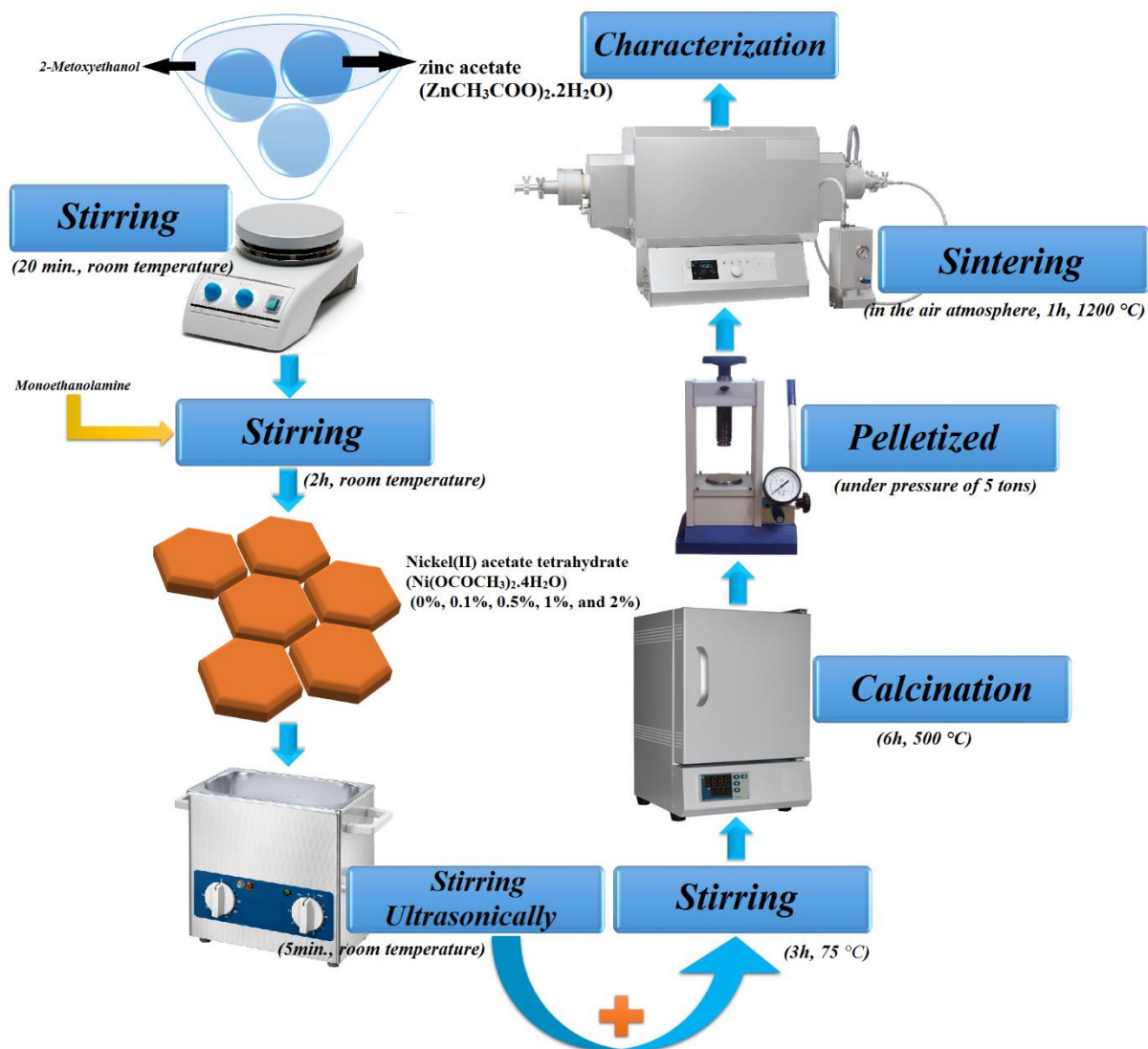
Figure 1. The preparation process of samples

2.2. Characterization Techniques

The optical properties of the prepared nano powders was characterized by spectrophotometer. Measurements of diffuse reflectance (R-λ) of the samples were taken at 200-1200 nm wavelength with a Shimadzu UV-VIS-NIR 3600 spectrophotometer. All measurements were made at room temperature.

3. Results and Discussions

3.1. The reflectance measurements of samples sintered at different temperatures

If the item exposed to the light beam is a semiconductor, many optical phenomena such as absorption, reflection, and transmission occur by the interaction of photons with the material. With this method, the optical characterization of the samples was conducted. Optical characterization of undoped and Ni-doped ZnO thin films obtained with the sol-gel method was carried out at 200-1200 nm scanning zone and room temperature.
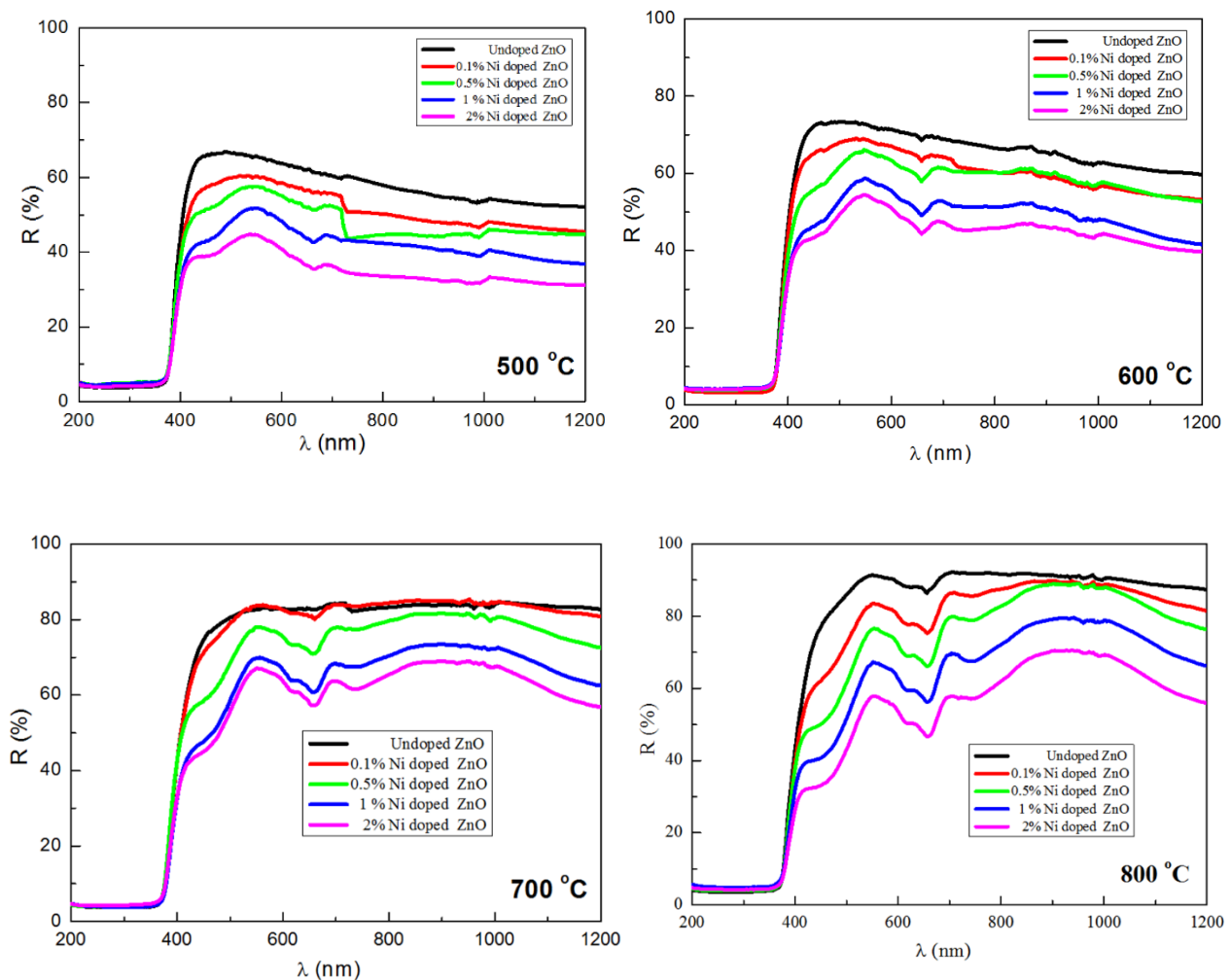
Figure 2. The reflectance graphs of samples sintered at 500, 600, 700 and 800 °C

Fig. 2. shows the reflection spectra of undoped and Ni-doped ZnO samples. As seen in Fig. 2., the reflection curves of the samples showed a decline at about 400 nm wavelength. This decline varied with Ni dopant. This confirmed that the optical band gaps of the films changed with Ni dopant. While the reflection values of the samples decreased at visible region wavelengths, they increased at high wavelengths beyond the visible region. This was associated with the increased interaction of the photons with electrons, atoms or crystal molecules and increased back reflections depending on increasing energy. Furthermore, the reflection values of the samples decreased with Ni dopant. This was associated with the increase in the number of grain boundaries causing optical scattering due to the reduction of the crystal size depending on the doped Ni. Since the grain boundary scattering increased with the increasing number of grain boundaries, the optical reflection values of the samples were thought to decrease.
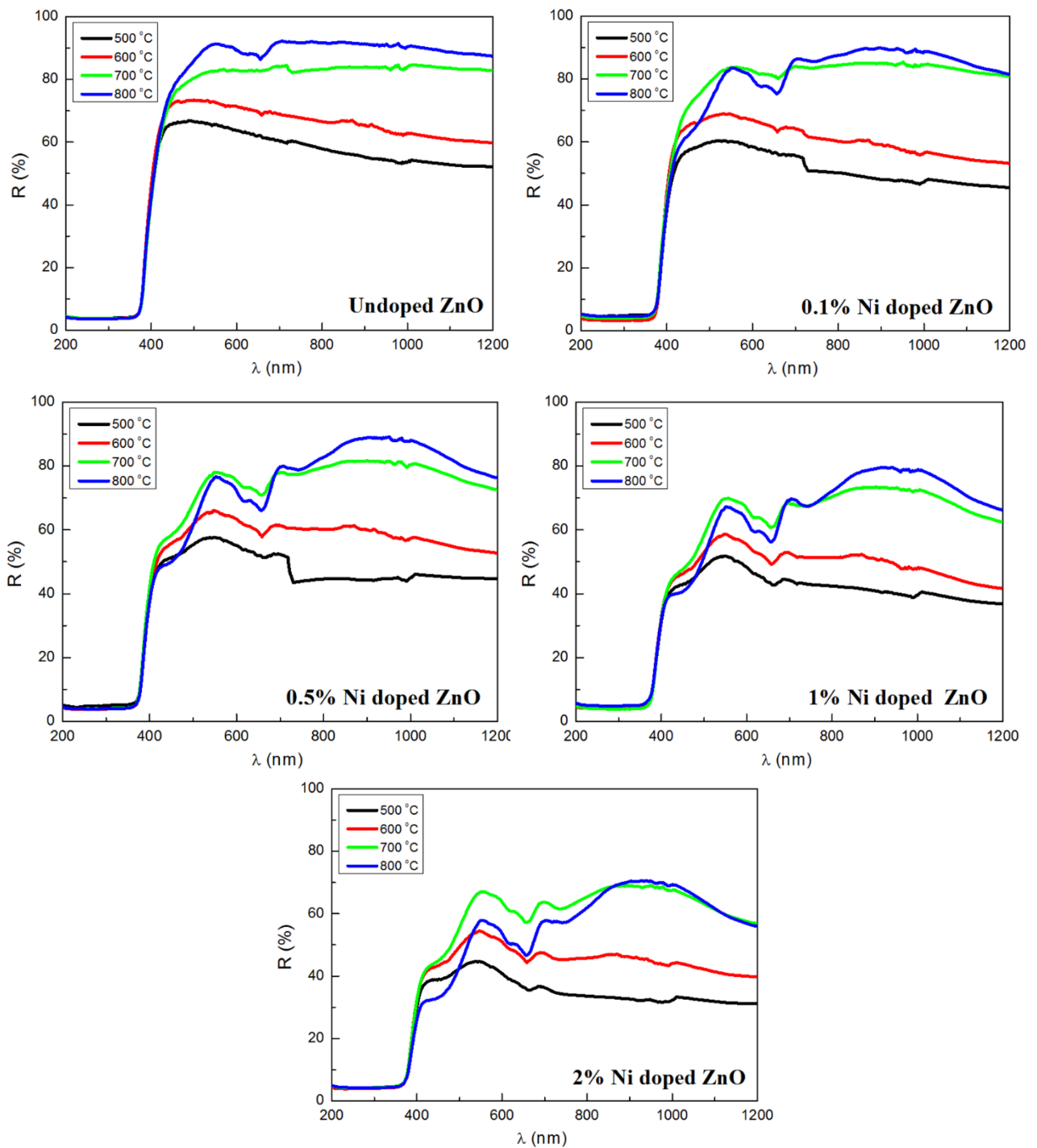
Figure 3. The comparison of reflectance values of samples with different sintering temperature with the same additive ratio

Fig. 3. shows the diffuse reflectance curves obtained from the ZnO-based nano-electroceramics at different temperature. As can be seen from the reflection spectra given in Fig. 2, optical reflections also increased with the increasing sintering temperature. The lowest reflection values were observed in undoped ZnO sample. The reflection curves of the samples show that the optical reflection increased

with increasing wavelength but decreased when shifting to short wavelengths. This was caused by the fact that the photons less interacted with electrons, atoms or crystal molecules and the back reflection decreased since the energy of photons decreased.

3.2. Determination of forbidden energy ranges of samples

In order to determine E_g values of undoped and Ni-doped ZnO nano electroceramics, diffuse reflectance spectra given in Fig. 2 were used based on The Kubelka-Munk theory. With this method, reflectance values can be converted into absorption values by means of the Kubelka-Munk function. Kubelka-Munk function is defined by [19]:

$$F(R) = \frac{(1-R)^2}{2R} \tag{1}$$

Where R is diffuse reflectance and $F(R)$ is the Kubelka-Munk function corresponding to the absorbance value. $F(R)$ value is converted to the absorption coefficient by the following equation [20] :

$$\alpha = \frac{F(R)}{t} = \frac{Absorbance}{t} \tag{2}$$

Where t is the sample thickness. In this case, the equation used for determining the optical band gaps of the samples can be written as follows [21]:

$$\left(\frac{F(R)h\nu}{t}\right) = A \cdot (h\nu - E_g)^n \tag{3}$$

Where A is an energy-independent constant, $h\nu$ is the photon energy, E_g is the optical band gap and n is ½ (for direct transitions). With the help of sample thicknesses, $(\alpha h\nu)^{1/n}$ graphs of the samples against $h\nu$ were plotted. Energy value of the point where the line corresponding to the linear part of the graph intersects with *the h*ν axis at *(αhν)*^{n} *= 0* gives the value of the optical band gap of that material. If the value of *n* is 2, then the material has an indirect band gap, if n is ½, then the material has a direct band gap. When *n* was replaced with ½ in the obtained graphs, the best linearity was obtained. Thus, it was determined that the samples had the direct band pass. Fig. 4 shows $h\nu$-$(\alpha h\nu)^2$ graphs of the samples. Table.1 shows the optical band gap values calculated with the help of these curves.
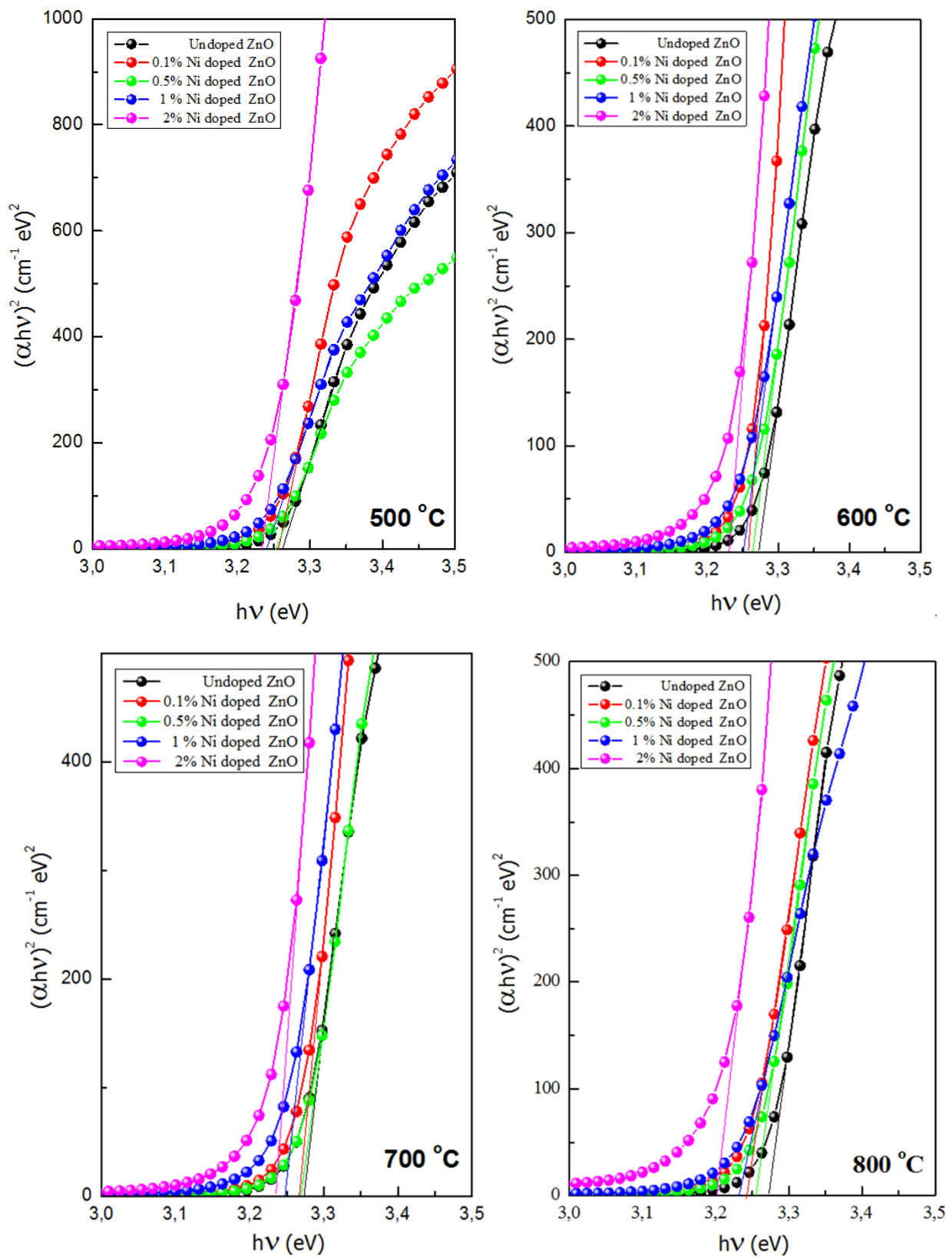
Figure 4. The plots of $(\alpha h\nu)^2$ vs. the photon energy of the undoped and Ni-doped ZnO nanoceramics sintered at 500, 600, 700 and 800 °C

Table 1. E_g values of the undoped and Ni-doped ZnO nanoceramics sintered at 500, 600, 700 and 800 °C

	E_g at 500 °C (eV)	E_g at 600 °C (eV)	E_g at 700 °C (eV)	E_g at 800 °C (eV)
Undoped	3.27	3.28	3.28	3.28
0.1% Ni	3.26	3.26	3.27	3.24
0.5% Ni	3.25	3.27	3.27	3.26
1% Ni	3.23	3.25	3.25	3.23
2% Ni	3.21	3.23	3.24	3.20

As it is seen in Table 1, the optical band gap of the samples significantly decreased with increasing Ni ratio. In addition, when the temperature increases, the forbidden energy ranges decrease. This is because the carrier concentration increased with increasing Ni ratio [22]. The sample having the lowest optical band gap was 2% Ni-doped ZnO at 800 °C. The obtained optical band gap values were compatible with the theoretical values in the literature and Eg values of ZnO-based materials synthesized with different methods [23]. The variation of the forbidden energy ranges depending on the sintering temperature is shown in Fig. 5.
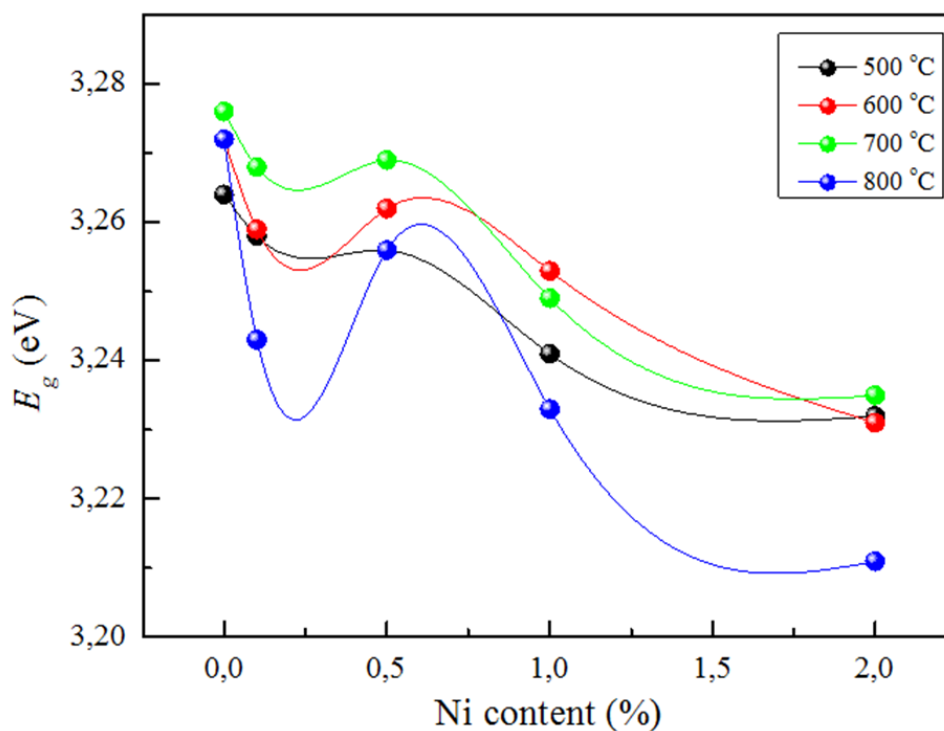
Figure 5. The change of the E_g with temperature

References:

[1] .   Aydin, C., Abd El-Sadek, M. S., Zheng, K. B., Yahia, I. S., Yakuphanoglu, F. "Synthesis, diffused reflectance and electrical properties of nanocrystalline Fe-doped ZnO via sol-gel calcination technique", *Optics and Laser Technology*, 48, 447-452, 2013.

[2] .   Aydın, H., Yakuphanoglu, F., Aydın, C.," Al-doped ZnO as a multifunctional nanomaterial: Structural, morphological, optical and low-temperature gas sensing properties", *Journal of Alloys and Compounds*, 773, 802-811, 2019.

[3] .   Aydin, H., Aydin, C., Al-Ghamdi, A. A.; Farooq, W. A., Yakuphanoglu, F., "Refractive index dispersion properties of Cr-doped ZnO thin films by sol-gel spin coating method", *Optik*, 127, 1879-1883, 2016.

[4] .   Aydin, C, "Synthesis of Pd: ZnO nanofibers and their optical characterization dependent on modified morphological properties", *Journal of Alloys and Compounds*, 777, 145-151, 2019.

[5] .   Aydın, C, "Synthesis of SnO2:rGO nanocomposites by the microwave-assisted hydrothermal method and change of the morphology, structural, optical and electrical properties", *Journal of Alloys and Compounds*, 771, 964-972, 2019.

[6] .   Aydin, H., Gündüz, B., Aydin, C., "Surface morphology, spectroscopy, optical and conductivity properties of transparent poly(9-vinylcarbazole) thin films modified with graphene oxide", *Synthetic Metals*, 252, 1-7, 2019.

[7] .   Aydin, C., Aydin, H., Taskin, M., Yakuphanoglu, F., "A Novel Study: The Effect of Graphene Oxide on the Morphology, Crystal Structure, Optical and Electrical Properties of Lanthanum Ferrite Based Nano Electroceramics Synthesized by Hydrothermal Method", *Journal of Nanoscience and Nanotechnology*, 19, 2547-2555, 2019.

[8] .   Aydin, C., "The functionalization of morphological, structural and optical properties of Fe doped SnO2 nanocrystals synthesized by the sol-gel method", *Journal of Materials Science: Materials in Electronics*, 29, 20087-20096, 2018.

[9] .   Aydin, C, "Tin Oxide-Based Nano Electroceramics Obtained from Sol– Gel Process: The Modified of the Structural and Opto-Electrical Properties with the Al Doping", *Journal of Nanoelectronics and Optoelectronics*, 13, 1460-1467, 2018.

[10] .   Aydın, C, "Variation of structural and electrical properties of gallium nitride-based nanomaterials with nickel dopant at different atomic ratios", *Ceramics International*, 44, 17473-17478, 2018.

[11] .   Aydin, C., Khusayfan, N. M., Al-Ghamdi, A. A., El-Tantawy, F., Farooq, W. A., Yakuphanoglu, F., "Facile synthesis, electrical and optical properties of Cu-doped GaN nanorods by sol-gel technique", *Journal of Sol-Gel Science and Technology*, 78, 68-75, 2016.

[12] . Aydin, H., El-Nasser, H. M., Aydin, C., Al-Ghamdi, A. A., Yakuphanoglu, F., "Synthesis and characterization of nanostructured undoped and Sn-doped ZnO thin films via sol-gel approach", *Applied Surface Science*, 350, 109-114, 2015.

[13] . Aydin, H., Tataroglu, A., Al-Ghamdi, A. A., Yakuphanoglu, F., El-Tantawy, F., Farooq, W. A., "A novel type heterojunction photodiodes formed junctions of Au/LiZnSnO and LiZnSnO/p-Si in series", *Journal of Alloys and Compounds*, 625, 18-25, 2015.

[14] . Orhan, A., Aydin, C., Aydin, H., Al-Ghamdi, A. A., El-Tantawy, F., Yakuphanoglu, F., "Synthesis and optical properties of iron-doped gallium nitride nanostructures by sol-gel method", *Microsystem Technologies-Micro-and Nanosystems-Information Storage and Processing Systems*, 21, 1219-1224, 2015.

[15] . Guler, O., Guler, S. H., Yo, F., Aydin, H., Aydin, C., El-Tantawy, F., Duraia, E. M., Fouda, A. N., "Electrical and Optical Properties of Carbon Nanotube Hybrid Zinc Oxide Nanocomposites Prepared by Ball Mill Technique", *Fullerenes Nanotubes and Carbon Nanostructures*, 23, 865-869, 2015.

[16] . Aydin, H, "Electrical and Optical Properties of Titanium Dioxide-Carbon Nanotube Nanocomposites", *Journal of Nanoelectronics and Optoelectronics*, 9, 608-613, 2014.

[17] . Aydin, H., Tataroğlu, A., Al-Ghamdi, A. A., Yakuphanoglu, F., El-Tantawy, F., Farooq, W. A., "A novel type heterojunction photodiodes formed junctions of Au/LiZnSnO and LiZnSnO/p-Si in series", *Journal of Alloys and Compounds*, 625, 18-25, 2015.

[18] . Aydın, C., Benhaliliba, M., Al-Ghamdi, A. A., Gafer, Z. H., El-Tantawy, F., Yakuphanoglu, F., "Determination of optical band gap of ZnO: ZnAl2O4 composite semiconductor nanopowder materials by optical reflectance method", *Journal of Electroceramics*, 31, 265-270, 2013.

[19] . Aydın, C., El-Nasser, H. M., Yakuphanoglu, F., Yahia, I. S., Aksoy, M., "Nanopowder synthesis of aluminum doped cadmium oxide via sol-gel calcination processing", *Journal of Alloys and Compounds*, 509, 854-858, 2011.

[20] . Benhaliliba, M., Benouis, C. E., Yakuphanoglu, F., Tiburcio-Silver, A., Aydin, C., Hamzaoui, S., Mouffak, Z., "Detailed investigation of submicrometer-sized grains of chemically sprayed (Sn1−xAlx, O2) (0≤x≤0.085) thin films", *Journal of Alloys and Compounds*, 527, 40-47, 2012.

[21] . Aydin, C., Al-Hartomy, O. A., Al-Ghamdi, A. A., Al-Hazmi, F., Yahia, I. S., El-Tantawy, F., Yakuphanoglu, F., "Controlling of crystal size and optical band gap of CdO nanopowder semiconductors by low and high Fe contents", *Journal of Electroceramics*, 29, 155-162, 2012.

[22] . Aydın, C., Mansour, S. A., Alahmed, Z. A., Yakuphanoglu, F., "Structural and optical characterization of sol-gel derived boron doped Fe2O3 nanostructured films". *Journal of Sol-Gel Science and Technology*, 62, 397-403, 2012.

[23] . Aydin, H., Mansour, S. A., Aydin, C., Al-Ghamdi, A. A., Al-Hartomy, O. A., El-Tantawy, F., Yakuphanoglu, F., "Optical properties of nanostructure boron doped NiO thin films", *Journal of Sol-Gel Science and Technology*, 64, 728-733, 2012.

ENDOPARASITIC FAUNA OF SOME COMMERCIALLY IMPORTANT FISH SPECIES FROM MENZELET DAM LAKE (KAHRAMANMARAŞ, TURKEY)

Mikail ÖZCAN[1] * orcid:0000-0001-9032-0697 *Yasemin YILMAZ[1]* orcid:0000-0002-3720-0298

Elif DONAT[1] orcid:0000-0002-7540-868X *Damla KILAVUZ[1]* orcid:0000-0002-5314-6885

Meltem TUNCEL[1] orcid:0000-0002-5161-3232

[1]Kahramanmaraş Sütçü Imam University, Faculty of Agriculture, Department of Fisheries

Kahramanmaraş-TURKEY.

*Corresponding Author: mikailozcan@ksu.edu.tr

Abstract: *This study aims to determine the endoparasitic fauna of seven species of freshwater fish from Menzelet Dam Lake in Kahramanmaraş, Turkey. Cyprinus carpio, Barbus rajanorum, Alburnus sp., Capoeta angorae, Capoeta barroisi, Leuciscus cephalus and Luciobarbus pectoralis caught in the Dam Lake were examined in terms of internal parasites. Neoecinorhynchus rutili (Acanthocephala: Neoechinorhynchidae) and Ligula intestinalis (Cestoda: Pseudophyllidea) endoparasites were found. Parasites were stained and pictures were taken under a microscope. The distribution of parasites is presented according to ecological terms.*
Key words: *Menzelet Dam Lake, Fish, Neoechinorhynchus rutili, Ligula intestinalis*

1. Introduction

The fact that Turkey has a large inland water potential with variable ecological aspects allows for the cultivation of a variety of fish. The decline of fish species with an economic value in our seas due to pollution by the discharge of domestic and industrial wastewater and ignorant hunting have made it necessary to protect and improve the existing fish stocks in inland waters. Fish diseases are one of the factors that negatively affect fishing in our country's lakes and ponds. Diseases caused by parasites constitute a large part of fish diseases [1].

Fish take first place in aquaculture in terms of protein and vitamin values they contain. Juvenile or adult fish farmed in the natural environment or in culture in order to meet the need for protein are infected by parasites through direct contact with parasitic fishes or by means of nutrients. As known, parasitism cases can lead to decreased fertility, weakness or even death in the host organism. For this reason, studies aiming to detect parasitic fauna of fish in natural environments are of great importance in terms of taking measures for coping and protecting against parasites [2].

Approximately 10,000 parasite species live in fish and of these parasite species, 27% include Crustacea, 18% Protozoa, 15% Monogenea, 17% Trematoda, 10% Cestoda, 7% Nematoda, 4% Acanthocephala and 1% include Huridinea groups [3].

Commercially important fish species in Menzelet dam lake are *Silurus glanis, Cyprinus carpio, Barbus rajanorum, Capoeta capoeta, Capoeta barroisi* and *Leuciscus cephalus* [4].

This study was carried out to determine the internal parasitic fauna of *Cyprinus carpio, Barbus rajanorum, Alburnus sp., Capoeta angorae, Capoeta barroisi, Leuciscus cephalus* and *Luciobarbus pectoralis* species from Menzelet Dam Lake (Kahramanmaraş).

2. Material and Methods

1113 fish (36 *Cyprinus carpio,* 449 *Barbus rajanorum,* 60 *Alburnus sp.,*78 *Capoeta angorae,* 332 *Capoeta barroisi,* 150 *Luciobarbus pectoralis* and 8 *Leuciscus cephalus*) caught in Menzelet Dam Lake (Fig. 1) with gill nets between January and August of 2013 were transported alive in plastic buckets to the Fish Diseases Laboratory in the Department of Aquaculture of Agricultural Faculty in Kahramanmaraş Sütçü Imam University and examined parasitological after being anaesthetized with 2-phenoxyethanol. The mean weight and total lenght of samples ranged 25,51cm and 198,84 g for *Cyprinus carpio;* 25,93 cm and 210,99 g for *Barbus rajanorum;* 12,87 cm and 26,09 g for *Alburnus sp;* 17,80 cm and 55,73g for *Capoeta angorae;* 30,55 cm and 301,01g for *Capoeta barroisi;*18,47 cm and 46,03 g for *Luciobarbus pectoralis*; 26,9 cm and 235 g for *Leuciscus cephalus.* The internal examinations of the fish were performed by autopsy technique [5]. The abdomen of the fish was cut from the anus to the isthmus and the stomach and intestines were transferred into petri-dishes containing physiological water. The parasites that were found were stained with aceto-carmine after going through alcohol series and their indefinite sections were prepared. Inspection, detection, preparation, and diagnosis of parasites were identified by using Bauer [6], Bykhovskaya-Pavlovskaya [7], Cheng [8], Chubb et al. [9], Reinhenbach-Klinke [10], Hoffman [11], Kennedy [12] and Ekingen [13]. According to Bush et al. [17] prevalence, mean intensity and mean abundance was calculated by the following formulas.

Prevalence =Number of parasitic fishes / Total number of fishes x 100

Average density = Total number of parasites / Number of parasitic fish

Average abundance = Total number of parasites / Total number of fish
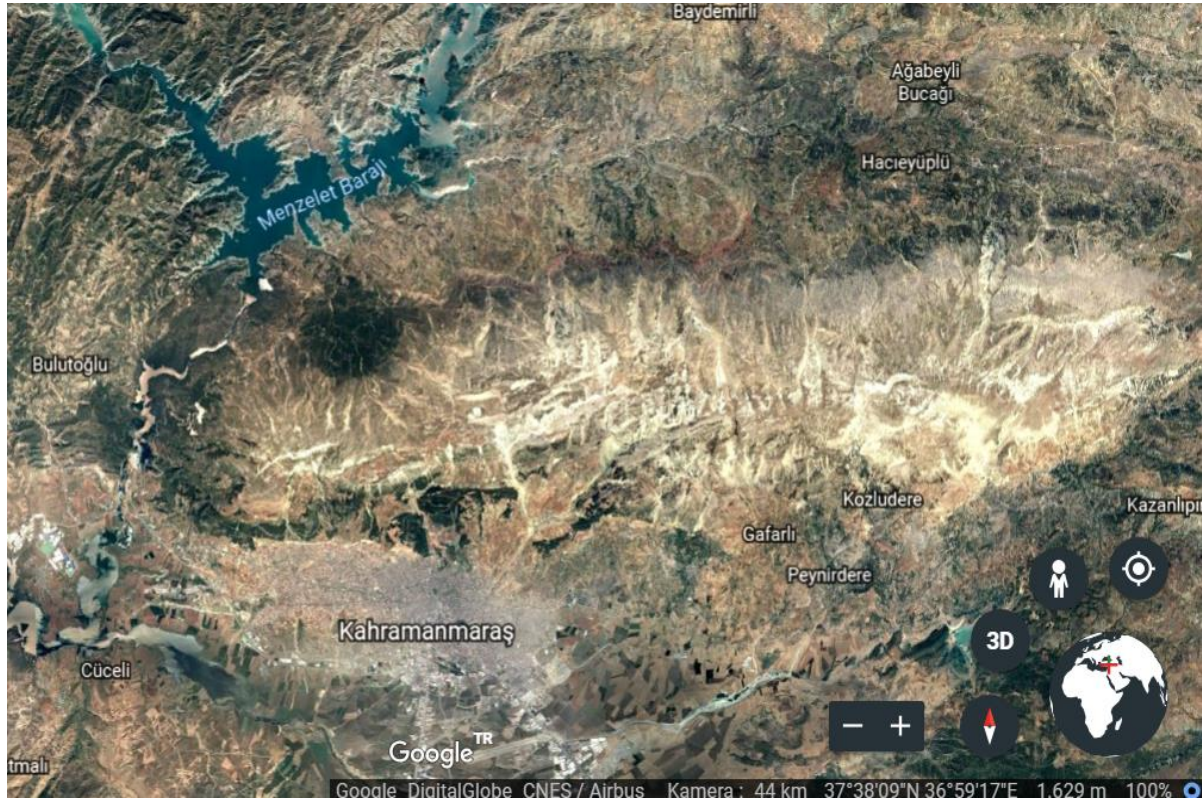
Figure 1. Locations of sampling sites in Menzelet Dam Lake

3. Results

In this study, 1113 fish samples of 7 species were examined. 2 species of parasites (1 acanthocephalan and 1 cestoda species) were found in 490 of these fishes examined and a total of 14614 parasite samples were detected. Both parasite species were found in other all fish species except *C. barroisi*. In *C. barroisi,* only *N. rutili* was determined. While the most common among the parasite species infecting the fish is *Neoechinorhynchus rutili* (Fig. 2) (14575) and *Ligula intestinalis* plerocercoid (Fig. 3) (39) have been the least common (Tab. 1).

Ligula intestinalis is a pseudophyllidean cestode that in its plerocercoid stage infests freshwater fish species. These are tapeworms that are effective in both marine and freshwater environments. Their bodies are segmented. They are hermaphrodites and their digestive and excretory systems are relatively well developed. Their need for invertebrates as intermediate hosts is possible the reason why they are less prevalent in aquaculture environments [16].

Figure 2. *Neoechinorhynchus rutili* (Scale: 100 μm-0,1mm)

N. rutili is an acanthocephalan worm. Their body is small and cylindrical. Their proboscis is short and there are 6 hook lines on the proboscis with 3 hooks on each. Their anterior hook is more elongated [16]. Parasites were found in the small intestines of fish. Hemorrhage was observed in areas where the parasites were widespread.
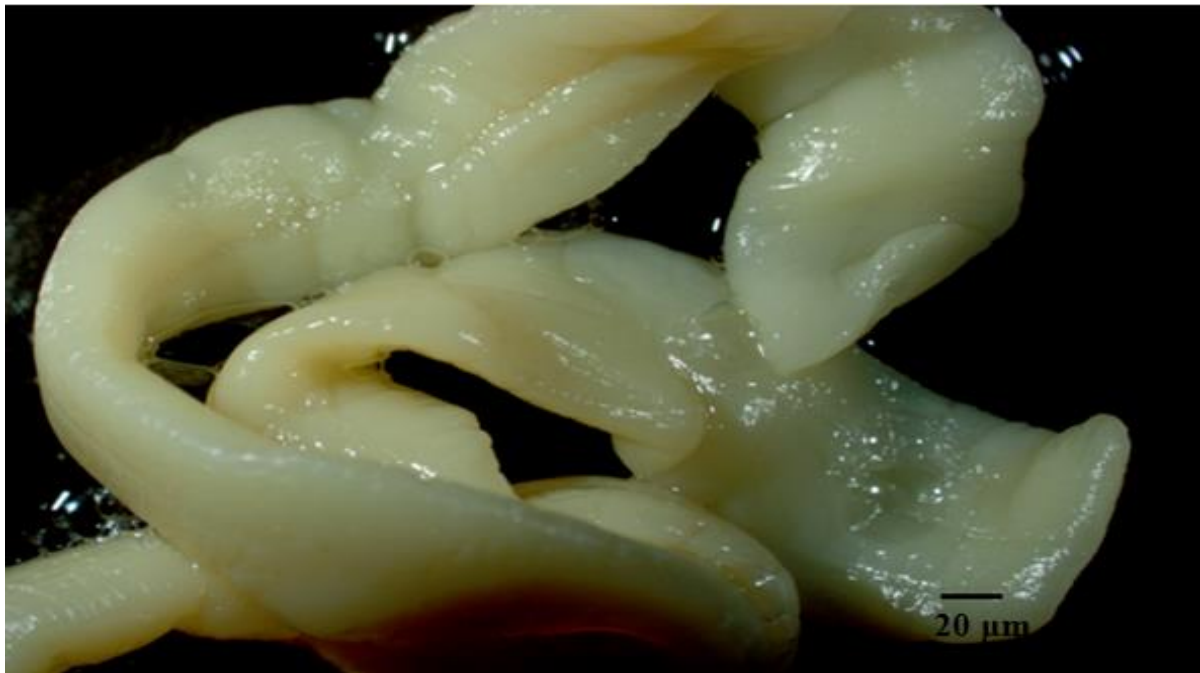
Figure 3. Plerocercoid of *Ligula intestinalis* (Scale: 100 μm-0,1mm)

Table 1. Distribution of parasites according to fish species

Fish species	Number of fish examined	Number of fish infested	Parasite species	Location	Number of parasites	Prevalence (%)
Cyprinus carpio	36	5	*Neoechinorhynchus rutili*	Intestine	4	13.88
			Ligula intestinalis	Intestine	2	
Alburnus sp,	60	18	*Neoechinorhynchus rutili*	Intestine	3	30
			Ligula intestinalis	Intestine	27	
Barbus rajanorum	449	118	*Neoechinorhynchus rutili*	Intestine	693	26.28
			Ligula intestinalis	Intestine	2	
Capoeta angorae	78	11	*Neoechinorhynchus rutili*	Intestine	22	14.10
			Ligula intestinalis	Intestine	1	
Capoeta barroisi	332	319	*Neoechinorhynchus rutili*	Intestine	13799	96.08
Luciobarbus pectoralis	150	15	*Neoechinorhynchus rutili*	Intestine	52	10
			Ligula intestinalis	Intestine	5	
Leuciscus cephalus	8	4	*Neoechinorhynchus rutili*	Intestine	2	50
			Ligula intestinalis	Intestine	2	
Total	1113	490			14614	

1113 fishes (44.02%) of 490 fishes infected with at least one parasite were detected. Prevalence of parasites in fish species; as of *Cyprinus carpio,* 13.88%, *Barbus rajanorum* 26.28%, *Alburnus sp.* 30%, *Capoeta angorae* 14.10%, *Capoeta barroisi* 96.08%, *Luciobarbus pectoralis* 10% and *Leuciscus cephalus* 50% was calculated (Fig.4). Parasites at that study together with the rates of detection as follows: as endoparasites *Neoechinorhynchus rutili*; 99.73%, *Ligula intestinalis*; 0.26%.
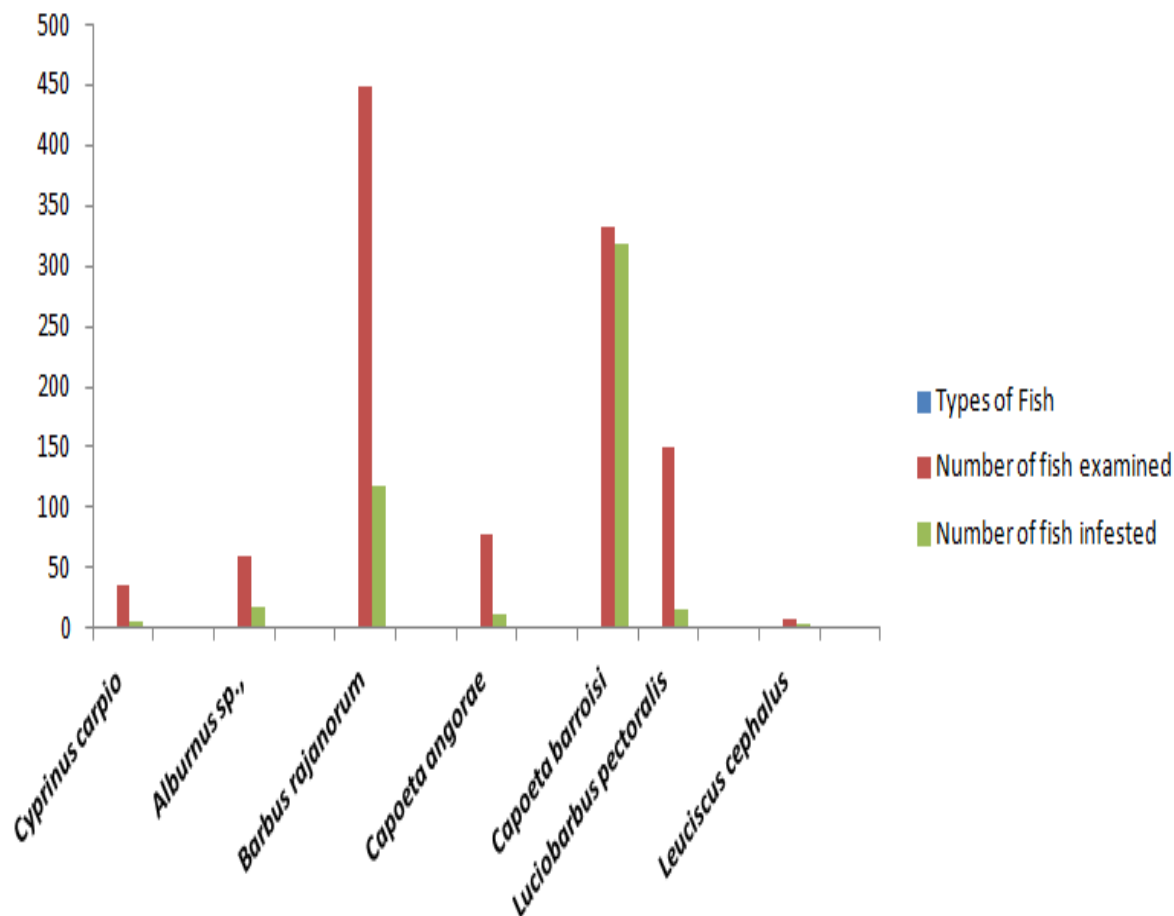
Figure 4. Prevalence (%) of parasites according to fish species

Prevalence, mean density and mean abundance rates tabulated separately for each parasite species (Table 2).

Table 2. Intensity, prevalence, and abundance of parasites in captured fish species

Fish species	Prevalence (%)		Mean density		Mean abundance	
	Neoechinorhynchus rutili	*Ligula intestinalis*	*Neoechinorhynchus rutili*	*Ligula intestinalis*	*Neoechinorhynchus rutili*	*Ligula intestinalis*
Cyprinus carpio	11,11	5,55	0,8	0,4	0,11	0,05

Alburnus sp,	5	45	0,166	1,5	0,05	0,45
Barbus rajanorum	154,34	0,44	5,872	0,016	1,54	0,004
Capoeta angorae	28,20	1,28	2	0,09	0,28	0,01
Capoeta barroisi	4156,32	0	43,25	0	41,56	0
Luciobarbus pectoralis	34,66	3,33	3,46	0,33	0,34	0,03
Leuciscus cephalus	25	25	0,5	0,5	0,25	0,25

4. Discussion and Conclusion

In this study, *Cyprinus carpio, Barbus rajanorum, Alburnus sp., Capoeta angorae, Capoeta barroisi, Leuciscus cephalus* and *Luciobarbus pectoralis* species caught in Menzelet Dam Lake in Kahramanmaraş were examined in terms of internal parasites and the locations of parasites, the amounts of infested fish and the number of parasites were calculated. The identification of *Neoechinorhynchus rutili* and *Ligula intestinalis* species found as a result of parasitological examination of fish was carried out according to Bykhouskaya – Poulovskaya [7], Hoffman [11], Kennedy [12] and Ekingen [13].

The fish studied in the study was found at least one parasite 44.02% (490/1113). *Leuciscus cephalus* was the highest infestation rate in 50% and *Luciobarbus pectoralis* was the least in 10%.

Unfortunately, the information on the spread of parasites in our country's fish, their life cycles and the economic losses caused by these is still not sufficient, although it was mentioned many years ago [14]. Massive deaths take place in acute parasitic diseases and declining growth in fish in chronic cases, and problems occur in marketing. In addition to this, the money spent on the treatment and the expenses of feeding the fish as a result of the fish not being able to benefit from the feed is making the situation worse.

Parasites need other living organisms in some or all of their lives in accordance with their biological evolution. They carry on their parasitic life cycles on top of or within these living organisms called hosts. They constantly affect the host's metabolism and vital functions during this life cycle. The parasites living in the digestive tract also disrupt the host's secretory function. All these effects lead to diseases and sometimes kill the host [15]. This study was conducted by taking into account that it is necessary to carry out a parasitological screening for fish species which are found in our region in order to prevent the parasitic diseases causing economic losses in fishing.

The presence of common parasites in these fish in the same environment has resulted in a more careful protective system in the aquaculture system.

Acknowledgments

References

[1] Dörücü, M., Kan, N.İ., Öztekin, Z., "Keban Baraj Gölü'nden avlanan bazı balık türlerinde iç parazitlerin incelenmesi", *Journal of FisheriesSciences*, 2(3), 484-488, 2008.

[2] Oğuz, M.C., "Mudanya kıyılarında yakalanan bazı teleost balıklarda kayıt edilen Nematodlar", *Türkiye Parazitoloji Dergisi*, 20 (3-4): 467-477, 1996.

[3] Cengizler, İ., "*Balık Hastalıkları*", Çukurova Üniversitesi Su Ürünleri Fakültesi Yayınları, Adana, 2000.

[4] Alp, A., Büyükçapar, H.M., Eren, A., "Menzelet Baraj Gölü (Kahramanmaraş) Balıkçılığı ve Ekonomik Olarak Avlanan Balık Türleri", *KSÜ Fen ve Mühendislik Dergisi,* 6(2), 142-153, 2003.

[5] Çolak, A., "*Balık Hastalıkları El kitabı*", Cumhuriyet Üniversitesi Fen-Edebiyat Fakültesi Yayınları, No:1, Esnaf matbaası, Sivas, 1982.

[6] Bauer, O.N., "*Key to the Parasites of Freshwater Fishes in the Fauna of the U.S.S.R*". Leningrad, 1987.

[7] Bykhovskaya – Pavlovskaya, A.V., "*Key to Parasites of Freshwater Fishes of the U.S.S.R.II, III., Transl*". by Birrow, A.,Cale, Z.S., Israel Program for scientific translations, Jerusalem, 1964.

[8] Cheng, C.T., "*General Parasitology*". Academic Press Inc, London, 1973.

[9] Chubb, J.C., Pool, D.W., Veltkamp, C.J., "A Key to the Species of Cestodes (Tapeworms) Parasitic in British and Irish Freshwater Fishes". *J Fish Biol,* 31: 517-543, 1987.

[10] Reichenbach-Klinke, H.H., "*Krankheiten und Schädigungen der Fischer, Gustav Fischer Verlag*". Stuttgart. 1966.

[11] Hoffman, G.L., "*Parasites of North American Freshwater Fishes*". University of California Pres, Berkeley and Los Angeles, 1967.

[12] Kennedy, C.R., "A checklist of British and Irish fresh water fish parasites with notes on their distribution". *Journal of Fish Biology*, 6, 613-644,1974.

[13] Ekingen, G., "*Tatlı su balık parazitleri*". Fırat Üniversitesi, Su Ürünleri Y.O. yayınları no:1, F.Ü.Basımevi, Elazığ, 1983.

[14] Güralp, N., "*Helmintoloji*". Ankara Üniversitesi, Veteriner Fakültesi Yayınları, 1981.

[15] Williams, H.M., Jones, A., "*Parasitic Worms of Fish*". 1st Edn., Taylor and Francis, Bristol, UK., 1994.

[16] Dörücü, M., İspir, Ü., "Keban Baraj Gölü'nden Avlanabilen Balık Türlerinde İç Paraziter Hastalıkların İncelenmesi". *F. Ü. Fen ve Mühendislik Bilimleri Dergisi*, 17 (2), 400-404, 2005.

GENERATING NUMERICAL SERIES VIA FUNCTIONS

Nurettin Pirinccioglu (ORCID: 0000-0002-5348-0349)

Dicle University, Department of Physics, Diyarbakır/Turkey

Corresponding author: npirinc@dicle.edu.tr

Abstract: *Series are the sum of the pattern of numbers or functions. One can produce a series in different ways. This is a study of the construction of series with differentiation of some functions.*

Keywords: Series, functions, numerical

1. Introduction

The basic definition of series is the sum of the pattern of numbers or functions. One can also define a decimal expansion as an infinite series. For example, e can be expressed as an infinite series in the following form

$$e = 2{,}71828247\ldots = 2 + 7/10 + 1/10^2 + 8/10^3 + \ldots \; . \tag{1}$$

Series are used in most areas of mathematics. Besides to their inevitability in mathematics, series are also widely used in other areas of sciences such as physics, computer science, statistics, and finance. One can generate series in different ways. Functions are also can be determined with infinite series; Fourier, and Taylor series. On the other hand, one may determine series with function as well.

The use of series in mathematics and physics is well known. Some well-known types of series are arithmetic, geometric, power, and harmonic series. Our aim in this study is not to discuss series, but rather to derive some series with a different method. This method will be discussed in the next section. In this section, we give some basic information about the most used series [1], [2].

It is known that a power series of a variable x can be identified as follows

$$\sum_{n=1}^{\infty} a_n x^n \; . \tag{2}$$

Here a_n are coefficients to be determined. This series specially are used to solve partial differential equations. A geometric series can be produced via the following equation

$$\sum_{n=1}^{\infty} \frac{1}{2^n} . \tag{3}$$

Another well-known type of series, which is known as the harmonic series, can be constructed as follows

$$\sum_{n=1}^{\infty} \frac{1}{n} . \tag{4}$$

Also, basically, an arithmetic series can be defined in the following form

$$\sum_{n=1}^{\infty} n. \tag{5}$$

In the next two sections, we generate some series by a functional operation. Finally, we end the study by writing a short conclusion section.

2. Definition and basic examples

In this section, we see how series can be obtained from functions and their derivatives. For example, a function of a variable x may be expressed as follows

$$f(x) = x^n, \tag{6}$$

where n indicates a constant. After taking the first derivative of this function and multiplying it with x, the result is obtained as

$$f_1(x) = nx \frac{df(x)}{dx} = nf(x). \tag{7}$$

Then, taking the derivative of the equation (7) and multiplying it again with x, we obtain the following result

$$f_2(x) = n^2 f(x). \tag{8}$$

Carrying on these steps to the last equation, we reach

$$f_3(x) = n^3 f(x). \tag{9}$$

Consequently, the mth step gives the mth term as

$$f_m(x) = n^m f(x). \tag{10}$$

Collecting all terms for $f(1)$, the result is obtained in the form of well-known infinite geometric series

$$\sum_{n=1}^{\infty} n^m . \tag{11}$$

For the case $n = 1/2$, it is seen that the result transforms into the convergent geometric series (3)

$$\sum_{m=1}^{\infty} \frac{1}{2^m} . \tag{12}$$

From the equation (6), one can get a finite series with a different decimal approximation. For example, if $f(x) = x$, the value of $f(1)$ is 1, and $\frac{d}{dx}f(1)$ is also equal to 1. Collecting two terms yields

$$f(1) + \frac{1}{1!}\frac{d}{dx}f(1) = 1 + 1 = 2^1 . \tag{13}$$

Also, this approximation gives 2^2 for the function $f(x) = x^2$.

$$f(1) + \frac{1}{1!}\frac{d}{dx}f(1) + \frac{1}{2!}\frac{d^2}{dx^2}f(1) = 1 + 2 + 1 = 2^2 \tag{14}$$

For $f(x) = x^3$, gives $1 + 3 + 3 + 1 = 2^3$, and finally for $f(x) = x^a$, we get

$$f(1) + \frac{1}{1!}\frac{d}{dx}f(1) + \frac{1}{2!}\frac{d^2}{dx^2}f(1) + \cdots .... + \frac{1}{a!}\frac{d^a}{dx^a}f(1) = 2^a . \tag{15}$$

To produce the arithmetic series, one can start with the case

$$f(x) = x^c \tag{16}$$

where c implies a constant. Taking the first derivative and performing the multiplication again with x/c, it leads us to the same equation as given in (16).

$$f(x) = 1x^c. \tag{17}$$

Adding 1 to the coefficient of the former equation and dividing this by that coefficient we get

$$f_1(x) = 1\frac{2}{1}x^c \tag{18}$$

Subsequently, the next term is

$$f_2(x) = 2\frac{3}{2}x^c \tag{19}$$

After the nth steps, the nth term becomes

$$f_n(x) = n\frac{n+1}{n}x^c . \tag{20}$$

Now, collecting all the coefficients of the x^c, the result transforms into an infinite arithmetic series (5) which is written as

$$\sum_{n=1}^{\infty} n . \tag{21}$$

In order to produce the harmonic series, one can also start with equation (6). Taking the first derivative and performing a multiplication again with x/c, it gives us the same conclusion as given in the equation (6).

$$f(x) = x^c \tag{22}$$

Moreover, taking the derivative of the last function and adding 1 to the inverse coefficient of the previous function, one gets the 1st term as

$$f_1(x) = \frac{1}{1+1}x^c = \frac{1}{2}x^c . \tag{23}$$

And, the second one is

$$f_2(x) = \frac{1}{2+1}x^c = \frac{1}{3}x^c .$$ (24)

After the nth step, the nth term becomes

$$f_n(x) = \frac{1}{n+1}x^c$$ (25)

Again, collecting all coefficients of the x^c, the result is an infinite harmonic series (4) which is defined as

$$\sum_{n=1}^{\infty}\frac{1}{n} .$$ (26)

3. Logarithmic, exponential, and trigonometric functions

Logarithmic case:

A logarithmic function can be defined as follows

$$f(x) = lnx .$$ (27)

Next, the corresponding series obtained as follows

$$f(1) + \frac{1}{1!}\frac{d}{dx}f(1) + \frac{1}{2!}\frac{d^2}{dx^2}f(1) + \cdots .... + \frac{1}{n!}\frac{d^n}{dx^n}f(1) + \cdots .. =$$

$$1 - \frac{1}{2} + \frac{1}{3} - \frac{1}{4} + \cdots ..... = \sum_{n=1}^{\infty}(-1)^{n+1}\frac{1}{n}$$ (28)

Exponential case:

In the case of $f(x) = e^x$, a series becomes

$$f(0) + \frac{1}{1!}\frac{d}{dx}f(0) + \frac{1}{2!}\frac{d^2}{dx^2}f(0) + \cdots .... + \frac{1}{n!}\frac{d^n}{dx^n}f(0) + \cdots .. =$$

$$1 + \frac{1}{1!} + \frac{1}{2!} + \frac{1}{3!} + \frac{1}{4!} + \cdots ..... = \sum_{n=1}^{\infty}\frac{1}{(n-1)!}$$ (29)

Trigonometric case:

A sinusoidal function can be defined as follows

$$f(x) = sinx .$$ (30)

Therefore, the corresponding series is expanded as

$$f(0) + \frac{1}{1!}\frac{d}{dx}f(0) + \frac{1}{2!}\frac{d^2}{dx^2}f(0) + \cdots .... + \frac{1}{n!}\frac{d^n}{dx^n}f(0) + \cdots .. =$$

$$\frac{1}{1!} - \frac{1}{3!} + \frac{1}{5!} - \frac{1}{7!} + \cdots ..... = \sum_{n=1}^{\infty}(-1)^{n-1}\frac{1}{(2n-1)!} \tag{31}$$

Correspondingly, the $cosx$ function gives the following expansion

$$f(0) + \frac{1}{1!}\frac{d}{dx}f(0) + \frac{1}{2!}\frac{d^2}{dx^2}f(0) + \cdots .... + \frac{1}{n!}\frac{d^n}{dx^n}f(0) + \cdots .. =$$

$$1 - \frac{1}{2!} + \frac{1}{4!} - \frac{1}{6!} + \cdots ..... = \sum_{n=1}^{\infty}(-1)^{n-1}\frac{1}{(2n-2)!} \tag{32}$$

4. Conclusion

In this study well-known types, some numerical series (geometric, harmonic, and arithmetic) are generated via a new method, which is called as generating function. We believe that this method will give a new aspect to mathematics, physics, and other scientific disciplines for relative purposes. Consequently, it is important to mention here that one can generate most of the series via this method by using a suitable function such as the trigonometric, logarithmic and the exponential functions.

References

[1] Gradshteyn, I., S., Ryzhik, I. M., "Table of Integrals, Series, and Products" Academic Press (1980).

[2] Thomas, G. B., Finney, R. L., "Calculus and Analytic Geometry" **7th Edition**, Addison-Wesley (1988).

THE BINDING ENERGY AND THE TOTAL ENERGY OF A MACROSCOPIC BODY IN THE RELATIVISTIC UNIFORM MODEL

Sergey G. Fedosin* *Orcid: 0000-0003-3627-2369*

Perm State University, Sviazeva str. 22-79, 614088, Perm, Russia

* Corresponding author; fedosin@hotmail.com

Abstract: *The total energy, binding energy, energy of fields, pressure energy and the potential energy of the system consisting of particles and four fields is precisely calculated in the relativistic uniform model. These energies are compared with the kinetic energy of particles. The relations between the coefficients of the acceleration field and the pressure field independent of the system's properties are found, which can be expressed in terms of each other and in terms of the gravitational constant and the vacuum permittivity. A noticeable difference is shown between the obtained results and the relations for simple systems in classical mechanics, in which the acceleration field and pressure field are not taken into account or the pressure is considered to be a simple scalar quantity. The conclusion is substantiated that as increasingly massive relativistic uniform systems are formed, the average density of these systems decreases as compared to the average density of the particles or bodies making up these systems. In this case, the inertial mass of the massive system is less than the total inertial mass of the system's parts.*

Keywords: *Relativistic uniform system, Binding energy, Pressure energy, Potential energy, Kinetic energy*

1. Introduction

By definition, the relativistic energy of the system includes all forms of energy and should be written in a covariant form. In some cases, a constant term in the form of the rest energy of the system's particles must be subtracted from the relativistic energy. Thus we obtain the total energy of the system, which is usually used in classical mechanics when simple problems are solved that do not require the relativistic approach. As a rule, the total energy is divided into two main parts – the kinetic energy and the potential energy.

In large macroscopic systems, several fields can be acting simultaneously, each of them changes the energy of the particles and can also have its own potential energy. This significantly complicates the expressions for the relativistic and total energies and often leads to the fact that different field theories give the expressions for the energy that is different in form. For example, in the general theory of relativity, the gravitational field energy is calculated not directly, but indirectly, with the help of the stress-energy pseudotensor and the spacetime metric obtained previously [1]. This means that the

46

knowledge of the system metric is necessary to determine the energy even in case of an extremely weak field. But even with the known metric, there is some ambiguity in the determination of the relativistic energy and inertial mass of the system and its individual parts [2, 3].

In contrast to this, in the covariant theory of gravitation, there is a stress-energy tensor of the gravitational field, and the metric of any system in the weak field limit turns gradually into the constant metric of Minkowski space, where the gravitational energy no longer depends on the type of the system metric [4]. Similarly, under earthly conditions, the spacetime metric is almost never used to calculate the energy of the bodies' electromagnetic field.

With this in mind, in the framework of the covariant theory of gravitation and the relativistic uniform model we will further determine the total energy and the binding energy of a macroscopic body, which is in equilibrium without rotation and compares the obtained expressions with the results for simple systems in classical mechanics. We will also calculate the individual energy components, including the fields' energy, the pressure energy and the potential energy of the system. Our approach uses the field theory in the covariant notation so that the results obtained for the flat spacetime can be easily adjusted for the curved spacetime with the corresponding metric, if necessary.

The thermodynamic properties of the considered physical system of particles and fields have previously been studied by Chernikov using the methods of the relativistic kinetic theory of gases and statistical physics [5]. For the case of a self-gravitating system with charged particles, there is a special name – the Vlasov plasma. Vlasov used the additional idea of a self-consistent field [6] and pointed to the constraints of the Boltzmann's model with pair collisions, which did not take into account the action of the electromagnetic and gravitational fields at a distance. However, our approach is based not on the kinetic theory, but on the vector field theory, and instead of the general theory of relativity, we use the covariant theory of gravitation. In addition, we describe the interaction of particles by means of the fields with the proper four-potentials, and this applies both to the pressure field and to the particles' acceleration field. Thus, obtaining the average values of physical quantities is not associated either with the distribution functions, the phase space or the Liouville's theorem, but with averaging the physical quantities directly in the equations, arising from the principle of least action.

Despite the fact that the approximation of the constant invariant mass density in the presence of sufficiently strong gravitational fields is a certain constraint, this approach is justified, as it gives an accurate description and can be applied to a number of macroscopic systems, such as the observable Universe, cosmic gas clouds and even neutron stars. In addition, the suggested approach can also be adjusted for the case of non-uniform mass density, as it was done in [7] for white dwarfs and the Sun, which is the main-sequence star.

2. Relativistic and kinetic energy

In [8] within the framework of the covariant theory of gravitation, the formula was found to calculate the relativistic energy of a physical system of particles and fields associated with these particles. At the same time, the electromagnetic and gravitational fields, the acceleration field and the pressure field were taken into account, and the role of the stress-energy tensor of the matter was played by the stress-energy tensor of the acceleration field. A similar formula for the energy was presented in the general field concept for a macroscopic system in [9, 10].

With the help of this formula in [4] the energy of the equilibrium system with continuously distributed randomly moving matter was calculated, taking into account the energy of the fields, in the explicit form with an accuracy up to the terms that do not contain the square of the speed of light in the denominators. Taking into account the corrections, made in [11], the energy is equal to:

$$E_r = M c^2 \approx m c^2 \gamma_c^2 - \frac{7 \eta m^2 \gamma_c^2}{10 a} - \frac{3 G m^2 \gamma_c^2}{5 a} + \frac{3 q^2 \gamma_c^2}{20 \pi \varepsilon_0 a} + m \wp_c \gamma_c - \frac{2 \sigma m^2 \gamma_c^2}{5 a} . \tag{1}$$

Expression (1) for the energy differs noticeably from the energy accepted in classical mechanics. The main difference arises from the acceleration field and the pressure field, which is considered as unique and independent vector fields that have stress-energy tensors determined in a covariant way.

In Eq. (1) it is assumed that the system has a spherical form with the radius a; the mass m and the charge q of the system are obtained by multiplying the mass density ρ_0 and the charge density ρ_{0q} by the volume of the fixed sphere, while ρ_0 and ρ_{0q} are the invariant densities of the particles that make up the sphere, measured in the reference frames associated with the particles. Within the relativistic uniform model, these densities are assumed to be constants. Due to the random motion of matter, the global vector potentials and the corresponding solenoidal vectors of the system's fields are considered equal to zero, so that the contribution of the solenoidal vectors into the energy according to Eq. (1) is neglected.

At the center of the sphere, the velocity of the particles is v_c and the Lorentz factor of the particles equals $\gamma_c = \dfrac{1}{\sqrt{1 - v_c^2 / c^2}}$, where c is the speed of light. Each field is characterized by its own coefficient: η is the acceleration field coefficient, G is the gravitational constant, ε_0 is the vacuum permittivity, σ is the pressure field constant. The quantity $\wp_c$ in Eq. (1) represents the scalar potential of the pressure field at the center of the sphere, and the mass M is the relativistic invariant inertial mass of the system.

The kinetic energy of motion of this system's particles was found in [12] by three methods – by the virial theorem, by subtracting the rest energy of the particles from the relativistic energy of their motion and using the generalized three-momenta of the system's particles. All these methods give the same result:

$$E_k \approx m c^2 \gamma_c^2 - \frac{3 \eta m^2 \gamma_c^2}{5 a} - m c^2 \gamma_c + \frac{3 \eta m^2 \gamma_c}{10 a} \approx \frac{m v_c^2 \gamma_c}{2} - \frac{3 \eta m^2 \gamma_c}{10 a} \approx \frac{27 \eta m^2 \gamma_c}{20 \sqrt{14} a} . \tag{2}$$

Expressions (1) and (2) are the initial point for determining the components of the total energy and the binding energy of the system under consideration. The numerical coefficient $\dfrac{27}{20 \sqrt{14}}$ in Eq. (2) is the consequence of the solution of the quadratic equation for the velocity v_c at the center of the sphere and is a property of the relativistic uniform system. As a result, similar numerical coefficients can be found in some other energy components.

3. The total energy components

According to [13], the Lorentz factor of the particles, moving randomly inside the sphere, depends on the current radius r:

$$\gamma' = \frac{c\gamma_c}{r\sqrt{4\pi\eta\rho_0}}\sin\left(\frac{r}{c}\sqrt{4\pi\eta\rho_0}\right) \approx \gamma_c - \frac{2\pi\eta\rho_0 r^2\gamma_c}{3c^2}. \qquad (3)$$

The Lorentz factor is maximal at the center of the sphere, where the particles are moving at the highest velocity. We use the reference frame K' that is associated with the center of the sphere so that all the results will refer to the sphere, which is stationary relative to the observer. If necessary, the energies and momenta of individual fields and the entire system can be converted into the laboratory reference frame K by means of the corresponding Lorentz transformations at a known velocity of the sphere's motion in K.

Formula (3) was obtained by solving the wave equation for the scalar potential ϑ of the acceleration field in the same way as the potentials of the electromagnetic or gravitational fields are calculated inside the sphere. In this case in the Minkowski space the acceleration field potential becomes proportional to the Lorentz factor: $\vartheta = \gamma'c^2$.

The physical reason for the radial dependence in Eq. (3) is the need to maintain a balance of the acting forces. Thus, the gravitational force tends to compress the matter, and the pressure of the moving particles resists such compression. Indeed, the gravitational field strength inside the uniform system of a spherical form is proportional to the current radius and is directed towards the center of the sphere. The volumetric density of the gravitational force is proportional to the field strength and the mass density of the matter. As the observation point moves from the surface to the center along the radius, the total thickness and the mass of the observed spherical layer increase, as well as the total gravitational force from this layer towards the center. The gravitational pressure is balanced by the dynamic pressure of the particles, which according to the kinetic theory is two-thirds of the kinetic energy of the particles per unit volume. Consequently, the closer to the center, the greater is the pressure of particles in the matter.

Gravitation also forms some spherical boundary of the system with the radius a so that the particles do not on average go beyond this radius. If N charged particles were closed inside a sphere with a rigid boundary, then in the equilibrium state and in the absence of mass forces we could expect the uniform mass density, the same velocity and the constant Lorentz factor of the particles at each point of the system, which would depend only on the temperature. However, there is no rigid boundary in our model, and the proper gravitational and electromagnetic forces penetrating into any point of the system act as the mass forces. Thus, it turns out that the velocity of particles and their Lorentz factor are maximal at the center of the system under consideration and decrease with increasing current radius.

We will take into account now that as a consequence of the relativistic effect of length contraction the moving particles in the special theory of relativity must be considered as if they have a reduced volume and increased density. Indeed, ρ_0 is the mass density in the reference frames associated with the particles, γ' is the Lorentz factor of the moving particles, and $\rho_b = \rho_0\gamma'$ gives the mass density of these particles from the viewpoint of an observer, who is stationary relative to the sphere.

For the motion of particles, there should be some voids between them. In order to calculate the volume of the sphere, it is necessary, to sum up, the volumes of all the typical particles moving inside

the sphere, as well as the volumes of the voids between them. Suppose now that the sizes of the typical particles are much larger than the voids between the particles, and the volume of the voids is substantially less than the total volume of the particles. In this case, we can use the approximation of continuous medium, so that the unit of the mass of matter inside the sphere will be given by the approximate expression $dm \approx \rho_0 \gamma' dV$, where dV is the volume element of the fixed sphere.

The question whether it is acceptable to increase the sizes of typical particles up to the limit necessary for using the approximation of continuous medium can be answered as follows. In the gravitational field, the acceleration of particles depends neither on the mass nor on the density of particles, which follows from the equivalence principle in the general theory of relativity and from the equation of motion in the covariant theory of gravitation. For the electric forces, the acceleration is proportional to the ratio of densities $\dfrac{\rho_{0q}}{\rho_0}$ and does not depend on the mass of particles. The same applies to the motion velocity, Lorentz factor, kinetic energy, and other quantities, which are determined not by the mass of particles, but by their density ρ_0. Thus, with a given density, we can choose the mass and, consequently, the sizes of typical particles within the limits we need.

The standard formula to calculate the kinetic energy all of the N particles of the system has the form:

$$E_k = \sum_{i=1}^{N} (\gamma_i - 1) m_i c^2 .$$

The mass m_i and the Lorentz factor γ_i of the particles were substituted in [12] with $dm = \rho_0 \gamma' dV$ and γ', respectively, and the sum for the particles was substituted with the integral over the sphere volume. This led to relation (2) for the kinetic energy of the particles, which also contains the expression for the total rest energy of the sphere's particles from the viewpoint of the observer associated with the sphere:

$$W_b = m_b c^2 = \rho_0 c^2 \int \gamma' r^2 \sin\theta \, dr \, d\theta \, d\phi \approx mc^2 \gamma_c - \frac{3\eta m^2 \gamma_c}{10a} . \tag{4}$$

The average rest mass of one particle is obtained by dividing the total rest mass m_b by the number N of particles in the system.

In order to obtain the total energy of the system, we need to subtract the energy W_b from the relativistic energy in Eq. (1):

$$E_t = E_r - W_b .$$

On the other hand, according to Eq. (2):

$$E_k \approx mc^2 \gamma_c^2 - \frac{3\eta m^2 \gamma_c^2}{5a} - W_b .$$

After eliminating W_b from these equations, taking into account Eq. (1) and collecting similar terms, we obtain the expression for the total energy:

$$E_t = E_k - \frac{3Gm^2\gamma_c^2}{5a} + \frac{3q^2\gamma_c^2}{20\pi\varepsilon_0 a} + m\wp_c\gamma_c - \frac{2\sigma m^2\gamma_c^2}{5a} - \frac{\eta m^2\gamma_c^2}{10a}.$$ (5)

The total energy should consist of the kinetic and potential energies, $E_t = E_k + W_p$, therefore the potential energy of the system will be as follows:

$$W_p = -\frac{3Gm^2\gamma_c^2}{5a} + \frac{3q^2\gamma_c^2}{20\pi\varepsilon_0 a} + m\wp_c\gamma_c - \frac{2\sigma m^2\gamma_c^2}{5a} - \frac{\eta m^2\gamma_c^2}{10a}.$$ (6)

As we can see, the potential energy in Eq. (6) contains the energy of the particles in the gravitational and electromagnetic fields and in the pressure field, as well as the energy of these fields themselves, with the addition of the acceleration field energy.

To simplify expression (6) we will use the definition of the scalar potential of the pressure field in [14], according to which the potential at the center of the sphere is $\wp_c = \dfrac{p_{0c}\gamma_c}{\rho_0}$, which means that it is defined by the pressure p_{0c} in the reference frame K_p of the moving particle. On the other hand, the scalar potential of the pressure field from the viewpoint of the observer in K' equals $\wp_c = \dfrac{p_c}{\rho_c}$, where p_c is the pressure, $\rho_c = \rho_0\gamma_c$ is the mass density at the center of the sphere for this observer. Consequently, $p_c = p_{0c}\gamma_c^2$ and the pressure in the system due to the particles' motion increases more rapidly, in proportion to the square of the Lorentz factor, as compared to the mass density, which increases in proportion to the Lorentz factor.

If the radiation pressure is not taken into account, for the pressure in the reference frame K_p of the particle and for the pressure at the center of the sphere in the reference frame K' we can write the following:

$$p_{0c} = \frac{\rho_0 kT_{0c}}{\mu m_u}, \qquad\qquad p_c = \frac{\rho_c\gamma_c kT_{0c}}{\mu m_u} = \frac{\rho_c kT_c}{\mu m_u},$$

where μ is the parameter, which represents the number of nucleons per unit of relativistic ionized gas, m_u is the atomic mass unit, k is the Boltzmann constant, and the temperature at the center of the sphere T_{0c} in the reference frame K_p during the transition from K_p into K' is transformed to the temperature $T_c = \gamma_c T_{0c}$.

Taking this into consideration, the scalar potential $\wp_c = \dfrac{p_c}{\rho_c}$ can be expressed in terms of the temperature T_c at the center of the sphere:

$$\wp_c = \frac{kT_c}{\mu m_u}.$$ (7)

In [12] the square of the particles' velocity at the center of the sphere was estimated:

$$v_c^2 \approx \frac{3\eta m}{5a}\left(1+\frac{9}{2\sqrt{14}}\right).$$

(8)

In the derivation of Eq. (8) the value of the acceleration field coefficient η was not recorded, as well as the mass of the system's particles. Real bodies can contain several types of particles with different masses at the same time, such as atoms, ions, electrons, and individual nucleons. It is convenient to assume that the coefficient η refers to the particles with effective mass $\bar{m}=\mu m_u$. In this case, we can write for the mass density ρ at an arbitrary point of the sphere the following:

$$\rho \approx n_n m_u = n_p \bar{m} = n_p \mu m_u,$$

where n_n is the concentration of nucleons, n_p is the concentration of particles with the effective

mass $\bar{m}$, contributing to the pressure, so that $p = \dfrac{\rho kT}{\mu m_u} = n_p kT$.

We will multiply relation (8) for v_c^2 by $\dfrac{\bar{m}}{2}$ and equate it to $\dfrac{3kT_c}{2}$, which gives the equality between the kinetic energy of one particle with the mass $\bar{m}$ and the kinetic temperature at the center of the sphere:

$$\frac{\eta m \bar{m}}{5a}\left(1+\frac{9}{2\sqrt{14}}\right)=kT_c.$$

Let us substitute the left-hand side of this equation in Eq. (7) instead of kT_c and take into account the definition $\bar{m}=\mu m_u$:

$$\wp_c = \frac{\eta m}{5a}\left(1+\frac{9}{2\sqrt{14}}\right).$$

(9)

According to [13], for the scalar potential of the pressure field inside the sphere, the following relation holds:

$$\wp = \wp_c - \frac{\sigma c^2 \gamma_c}{\eta} + \frac{\sigma c^3 \gamma_c}{r\eta\sqrt{4\pi\eta\rho_0}}\sin\left(\frac{r}{c}\sqrt{4\pi\eta\rho_0}\right) \approx \wp_c - \frac{2\pi\sigma\rho_0 r^2 \gamma_c}{3}.$$

(10)

If we pass from the Lorentz factors to the squares of velocities in Eq. (3), we will obtain:

$$v'^2 \approx v_c^2 - \frac{4\pi\eta\rho_0 r^2\gamma_c}{3}.$$

By multiplying this equation by $\dfrac{\bar{m}}{3k}$ we pass on to the relation for the temperatures inside the sphere:

$$T \approx T_c - \frac{4\pi \eta \bar{m} \rho_0 r^2 \gamma_c}{9k}.$$

Let us go ahead and multiply the last equation by $\dfrac{k}{\mu m_u}$. Taking into account the definition $\bar{m} = \mu m_u$ and Eq. (7) we have:

$$\wp \approx \wp_c - \frac{4\pi \eta \rho_0 r^2 \gamma_c}{9}.$$

From a comparison of this relation with Eq. (10) we arrive at the fact that

$$\sigma = \frac{2\eta}{3}. \tag{11}$$

We will now use the relation between the field coefficients, which was obtained in [7] using the equation of motion:

$$\eta + \sigma = G - \frac{\rho_{0q}^2}{4\pi\varepsilon_0 \rho_0^2} = G - \frac{q^2}{4\pi\varepsilon_0 m^2}. \tag{12}$$

Combination of Eqs. (11) and (12) gives the following for the coefficients of the pressure field and the acceleration field:

$$\eta = \frac{3}{5}\left(G - \frac{\rho_{0q}^2}{4\pi\varepsilon_0 \rho_0^2}\right), \qquad \sigma = \frac{2}{5}\left(G - \frac{\rho_{0q}^2}{4\pi\varepsilon_0 \rho_0^2}\right). \tag{13}$$

Let us now substitute Eq. (11) into Eq. (9):

$$\wp_c = \frac{3\sigma m}{10a}\left(1 + \frac{9}{2\sqrt{14}}\right). \tag{14}$$

In view of Eq. (14), we will sum up all the terms with the pressure in Eq. (6):

$$W_{pr} = m\wp_c\gamma_c - \frac{2\sigma m^2 \gamma_c^2}{5a} \approx \frac{\sigma m^2 \gamma_c}{10a}\left(\frac{27}{2\sqrt{14}} - 1\right). \tag{15}$$

In view of Eq. (15), for the potential energy in Eq. (6) we obtain:

$$W_p \approx -\frac{3G m^2 \gamma_c^2}{5a} + \frac{3q^2 \gamma_c^2}{20\pi\varepsilon_0 a} + \frac{\sigma m^2 \gamma_c}{10a}\left(\frac{27}{2\sqrt{14}} - 1\right) - \frac{\eta m^2 \gamma_c^2}{10a}. \tag{16}$$

Relation (12) can be used to eliminate the coefficient η in Eq. (16) and to express the potential energy of the system in terms of the corresponding energies of the gravitational and electromagnetic fields and the pressure field:

$$W_p \approx -\frac{7Gm^2\gamma_c^2}{10a} + \frac{7q^2\gamma_c^2}{40\pi\varepsilon_0 a} + \frac{27\sigma m^2\gamma_c}{20\sqrt{14}\,a}. \tag{17}$$

We will now express all the terms in Eq. (16) in terms of the acceleration field coefficient η using Eqs. (12) and (11):

$$W_p \approx -\frac{\eta m^2\gamma_c}{30a}\left(35 - \frac{27}{\sqrt{14}}\right). \tag{18}$$

Hence we see that the potential energy of a relativistic uniform system that is in equilibrium condition is always negative.

Substituting Eq. (2) into Eq. (18) gives the following:

$$W_p \approx -\frac{2}{3}\left(\frac{35\sqrt{14}}{27} - 1\right)E_k. \tag{19}$$

Accordingly, the total energy is equal to:

$$E_t = E_k + W_p \approx -\frac{5}{3}\left(\frac{14\sqrt{14}}{27} - 1\right)E_k. \tag{20}$$

Despite the fact that in Eq. (19) the absolute value of the potential energy is much greater than the kinetic energy, the virial theorem is satisfied in the system under consideration. It was shown in [12], where the nonzero virial of the system and the forces acting on the particles were explicitly calculated. In particular, the average energy, associated with these forces, in view of Eq. (2) is equal to:

$$-\left\langle \sum_{i=1}^{N} \mathbf{F}_i \cdot \mathbf{r}_i \right\rangle \approx \frac{3\eta m^2\gamma_c^2}{5a} - \frac{3\eta^2 m^3\gamma_c^2}{14a^2c^2} \approx \frac{4\sqrt{14}}{9}E_k.$$

We can also transform the pressure energy in Eq. (15), using Eq. (11), and compare it with the kinetic energy in Eq. (2):

$$W_{pr} \approx \frac{2}{3}\left(1 - \frac{2\sqrt{14}}{27}\right)E_k. \tag{21}$$

The entire energy, associated with the pressure, appears almost 2 times less than the kinetic energy of the particles' motion.

Most cosmic bodies are neutral, we can neglect their electromagnetic fields and can assume that $\rho_{0q} = 0$. In this case, according to Eq. (13) $\eta = \frac{3G}{5}$, and the potential energy in Eq. (18) is equal to:

$$W_p \approx -\frac{Gm^2\gamma_c}{50\,a}\left(35-\frac{27}{\sqrt{14}}\right) \approx -\frac{0.56Gm^2\gamma_c}{a}\ .$$

In the classical uniform model, the body's matter is compressed by the gravitational forces, which are opposed by the internal pressure force, while the pressure is considered to be a scalar quantity. It is assumed that the main contribution to the potential energy is made by the gravitational energy, which equals the value

$$U_g \approx -\frac{0.6Gm^2}{a}\ .$$

We see that the potential energy W_p in the relativistic uniform model is very close in value to the gravitational energy U_g. This explains why in the classical model for estimating the potential energy of the system it is sufficient to calculate only the total gravitational energy of the system and there is no need to take into account neither the pressure field energy nor the acceleration field energy.

4. The binding energy

By definition, the binding energy of the physical system is obtained by subtracting the relativistic energy E_r in Eq. (1) from the total rest energy of the particles W_b in Eq. (4):

$$\Delta E = W_b - E_r\ . \tag{22}$$

Taking into account the definition of the total energy $E_t = E_r - W_b$, in view of Eq. (20), we find for the binding energy the following:

$$\Delta E = -E_t = -E_k - W_p \approx \frac{5}{3}\left(\frac{14\sqrt{14}}{27}-1\right)E_k \approx 1.57\,E_k\ . \tag{23}$$

For comparison, in simple systems, where there are only potential forces in the absence of pressure, due to the virial theorem $\Delta E \approx E_k$.

In our physical system of closely interacting particles and fields in addition to the electromagnetic field, we also take into account the contributions from the gravitational field, the acceleration field, and the pressure field. In such a system, according to Eq. (19), the potential energy of the fields W_p is negative and it is much greater in its absolute value than the kinetic energy E_k in comparison to simple systems. This leads to the increased binding energy, which is required to separate the system's particles from each other and to scatter them to infinity. Thus it is expected that during the formation of a bound relativistic uniform system with charged particles under the action of the gravitational field, taking into account the contributions from the acceleration field and the pressure field, the system must emit the energy, which is equal to the binding energy $\Delta E \approx 1.57\,E_k$.

Among all the energies it's most convenient to calculate the energies of the gravitational and electromagnetic fields, which go beyond the limits of the system to infinity. The sum of the energies of these external fields, taking into account Eqs. (12) and (11), is equal to:

$$E_{og} + E_{oe} \approx -\frac{Gm^2 \gamma_c^2}{2a} + \frac{q^2 \gamma_c^2}{8\pi \varepsilon_0 a} = -\frac{\eta m^2 \gamma_c^2}{2a} - \frac{\sigma m^2 \gamma_c^2}{2a} = -\frac{5\eta m^2 \gamma_c^2}{6a}. \tag{24}$$

From Eq. (4) the relation follows:

$$m\gamma_c \approx m_b + \frac{3\eta m^2 \gamma_c}{10ac^2} \approx m_b + \frac{3\eta m_b^2}{10ac^2 \gamma_c}.$$

Similarly, in [4] the charge q was associated with the charge q_b of the sphere, which was found by the observer in K':

$$q\gamma_c \approx q_b + \frac{3\eta m_b q_b}{10ac^2 \gamma_c}.$$

Applying this to Eq. (24), we find:

$$E_{og} + E_{oe} = -\frac{Gm_b^2}{2a} + \frac{q_b^2}{8\pi \varepsilon_0 a}. \tag{25}$$

In Eq. (25) the energy of the gravitational and electromagnetic fields outside the sphere is expressed in terms of the total rest mass m_b of the particles inside the sphere and the total charge of the particles q_b. From Eq. (25) we see that the mass m_b is actually equal to the gravitational mass m_g, which is responsible for the gravitation outside the body.

Comparing Eq. (24) with the kinetic energy in Eq. (2) and the binding energy in Eq. (23) gives the following:

$$E_{og} + E_{oe} \approx -\frac{50\sqrt{14}\,\gamma_c}{81} E_k \approx -\frac{10\sqrt{14}\,\gamma_c}{\left(14\sqrt{14} - 27\right)} \Delta E. \tag{26}$$

With the help of Eq. (26) we can easily estimate the binding energy ΔE, if we know the mass, charge, and radius of the system, using which in Eqs. (24) and (25) we can calculate the sum of the energies $E_{og} + E_{oe}$ outside the system. Although cosmic bodies with the same masses and sizes can differ in their state of matter, the binding energy of these bodies in Eq. (23), according to Eq. (26), will be the same. Indeed, the phase transformations of matter, arising from the energy transfer inside the system with the constant radius and mass, should not influence the energy of the external fields and the total binding energy of the system.

5. Estimation of the energy of fields

In this section, we will consider the question about what contribution into the relativistic energy and the total energy is made by the energy E_f, associated with the system's fields. The energy E_f is calculated with the help of the volume integrals of the fields' tensor invariants, for which it is necessary to know the strengths and solenoidal vectors of the fields. As part of the relativistic energy of the system in Eq. (1), the energy E_f according to [4] equals:

$$E_f = \frac{3Gm^2\gamma_c^2}{5a} - \frac{3q^2\gamma_c^2}{20\pi\varepsilon_0 a} - \frac{\sigma m^2\gamma_c^2}{10a} - \frac{\eta m^2\gamma_c^2}{10a} .$$

In this expression, we will take into account Eqs. (12), (11), (24), (2), (26) and (23):

$$E_f = -E_{og} - E_{oe} \approx \frac{50\sqrt{14}\,\gamma_c}{81} E_k \approx \frac{10\sqrt{14}\,\gamma_c}{\left(14\sqrt{14} - 27\right)} \Delta E \approx -\frac{10\sqrt{14}\,\gamma_c}{\left(14\sqrt{14} - 27\right)} E_t . \qquad (27)$$

According to Eq. (27), the energy E_f of all the four fields is approximately $2.31\gamma_c$ times greater than the kinetic energy of the particles E_k and $1.47\gamma_c$ times greater than the binding energy ΔE, which is equal in its absolute value to the total energy of the system E_t. In addition, in Eq. (27) $E_f = -E_{og} - E_{oe}$, that is, the energy E_f is up to a sign equal to the sum of the energies of the gravitational and electromagnetic fields outside the sphere. Hence it follows that the sum of the energies of all the fields inside the sphere is equal to zero.

We will now calculate the sum of the particles' energies E_{gep} in the gravitational and electromagnetic fields and in the pressure field. According to Eq. (1) we have the following:

$$E_{gep} = -\frac{6Gm^2\gamma_c^2}{5a} + \frac{3q^2\gamma_c^2}{10\pi\varepsilon_0 a} + m\wp_c\gamma_c - \frac{3\sigma m^2\gamma_c^2}{10a} .$$

Using Eqs. (12), (14), (11), (2) and (24) we find:

$$E_{gep} \approx -\frac{2\eta\,m^2\gamma_c}{a}\left(1 - \frac{9}{20\sqrt{14}}\right) \approx -\frac{2}{3}\left(\frac{20\sqrt{14}}{9} - 1\right) E_k \approx \frac{12}{5\gamma_c}\left(1 - \frac{9}{20\sqrt{14}}\right)(E_{og} + E_{oe}) .$$

Comparison with Eq. (27) gives us the following:

$$E_{gep} \approx -\frac{12}{5\gamma_c}\left(1 - \frac{9}{20\sqrt{14}}\right) E_f , \qquad (28)$$

that is, the energy E_f, associated with the fields, in its absolute value is over 2 times less than the sum of the particles' energies E_{gep} in the gravitational and electromagnetic fields and in the pressure field. Note that all the conclusions are made in the weak field approximation, while the Lorentz factor γ_c of the particles at the center of the sphere does not differ significantly from unity.

As it was shown in [12], although the global vector potentials of the fields inside the sphere with the particles are equal to zero, there are also proper vector potentials of the fields inside the particles due to their motion. These vector potentials are part of the generalized momentum, with the help of which we can estimate the kinetic energy of the system's particles. Because of the proper vector potentials, during the particles' motion, the corresponding solenoidal fields emerge, which make an additional contribution to the energy of the particles' fields E_f.

What can be the value of this contribution? Due to the motion, the energy of the fields becomes dependent on the velocity, however, the total energy of the fields inside the body vanishes. If we assume that the same is true for each particle filling the sphere in the model under consideration, then the proper scalar and vector potentials of the fields inside the particles do not result in the total energy of the fields. At the same time the global scalar potentials of the fields, that are the scalar superposition of the external

scalar potentials of individual particles, give the corresponding field strengths, with the help of which we can calculate the energy of the fields E_f inside and outside the sphere.

In contrast to this, the global vector potentials of the fields are the vector superposition of the external vector potentials of individual particles, and they are equal to zero due to the randomness of motion of the set of system's particles. This implies the equality of all the global solenoidal vectors to zero, and thus they do not contribute to the energy of the fields.

6. Conclusion

Our analysis of the energy for the system of a spherical form shows that in real massive bodies there are noticeable deviations of the total, kinetic and potential energies from the expressions for the energies of simple systems, interacting only by means of gravitational and electromagnetic forces at a distance. This is due to the additional contributions from the acceleration field and the pressure field.

Taking into account Eqs. (23) and (19-20), the binding energy and the total energy can be expressed in terms of the kinetic energy of the particles or the potential energy of the system:

$$\Delta E = -E_t \approx \frac{5}{3}\left(\frac{14\sqrt{14}}{27}-1\right)E_k \approx -\frac{5\left(14\sqrt{14}-27\right)}{70\sqrt{14}-54}W_p,$$

$$W_p \approx -\frac{2}{3}\left(\frac{35\sqrt{14}}{27}-1\right)E_k \approx -2.57E_k,$$

(29)

Relations (29) that we obtained can be compared to the standard expression for simple systems and the corresponding virial theorem in classical mechanics:

$$\Delta E = -E_t = -E_k - W_{pc} = -0.5W_{pc}, \qquad W_{pc} = -2E_k, \qquad (30)$$

where the classical potential energy is expressed as the sum over all the particles in terms of the radius vectors of the particles and the forces acting on the particles from the potential fields:

$$W_{pc} = \left\langle \sum_{i=1}^{N} \mathbf{F}_i \cdot \mathbf{r}_i \right\rangle.$$

In contrast to Eq. (30), in [12] we obtained the following expression for the virial theorem:

$$E_k \approx -\frac{9}{4\sqrt{14}}\left\langle \sum_{i=1}^{N} \mathbf{F}_i \cdot \mathbf{r}_i \right\rangle. \qquad (31)$$

From Eqs. (29) and (31) it follows that taking into account the acceleration field and the pressure field in the system under consideration leads to a change from the classical value -0.5 to approximately -0.61 of the binding energy's share relative to the potential energy, and to a corresponding change in the value from -0.5 to approximately -0.6 of the kinetic energy's share relative to the energy associated with the action of the potential forces. In addition, Eqs. (29) and (31) imply the inequality of the potential energy and the energy associated with the forces acting on the particles, so that

$$W_p \neq \left\langle \sum_{i=1}^{N} \mathbf{F}_i \cdot \mathbf{r}_i \right\rangle.$$

The binding energy of the system, according to the Eq. (26), can be expressed in terms of the sum of energies of the gravitational and electromagnetic fields outside the body:

$$\Delta E \approx -\frac{1}{5\gamma_c}\left(7-\frac{27}{2\sqrt{14}}\right)(E_{og}+E_{oe}). \tag{32}$$

The unique relation between the total, kinetic and potential energies and the binding energy in the system under consideration can be obtained due to the fact that we use the effective mass of the particles $\bar{m}=\mu m_u$, which is associated with the system's state of matter by means of the parameter μ (the number of nucleons per one particle of relativistic gas). This leads to relations between the coefficients of the acceleration field and the pressure field in Eq. (11) and to relations between these coefficients and the gravitational constant and the vacuum permittivity in Eqs. (12-13), which allows us to compare the values of the energies.

In the last section, we estimated the contribution of the energy E_f , which is made by the fields into the relativistic energy E_r , and we compared it with the energy E_{gep} in the gravitational and electromagnetic fields, as well as in the pressure field in relation (28). Using Eqs. (2) and (4) we obtain the relation:

$$mc^2\gamma_c^2-\frac{3\eta m^2\gamma_c^2}{5a}\approx W_b+E_k.$$

Taking this into account, from Eqs. (1) and (26-28) for the relativistic energy of the system we find the following:

$$E_r = Mc^2 \approx mc^2\gamma_c^2-\frac{3\eta m^2\gamma_c^2}{5a}+E_{gep}+E_f \approx W_b+E_k-\frac{1}{5}\left(7-\frac{27}{5\sqrt{14}}\right)E_f$$
$$\approx W_b+\frac{1}{5\gamma_c}\left(7-\frac{27}{2\sqrt{14}}\right)(E_{og}+E_{oe}). \tag{33}$$

Expression (33) for the relativistic energy E_r , in view of Eq. (32), corresponds to expression (22) for the binding energy of the system.

Since W_b is the rest energy of the systems' particles according to Eq. (4), and the fields' energy $E_{og}+E_{oe}$ outside the sphere is typically negative due to the prevailing contribution of the gravitational energy over the electromagnetic energy, we can see that the inertial mass M of the system turns out to be less than the total invariant mass of the particles m_b , which is part of the equation $W_b=m_bc^2$. We should also note that the mass m_b is exactly equal to the gravitational mass m_g , according to [4].

After substituting Eq. (25) into Eq. (33) we arrive at the relation, which is only slightly different from relation (31) in [4]:

$$Mc^2 \approx m_bc^2-\frac{1}{10\gamma_c}\left(7-\frac{27}{2\sqrt{14}}\right)\left(\frac{Gm_b^2}{a}-\frac{q_b^2}{4\pi\varepsilon_0 a}\right). \tag{34}$$

Hence it follows that the introduction of the charge q_b into the system typically increases the inertial mass M , at least this holds exactly at the constant mass m_b . And conversely, since $m_b=m_g$, a decrease

in the gravitational mass m_g of the system is possible with increasing of the charge q_b. To see this, it suffices to solve Eq. (34) as a quadratic equation for m_b, and to fix the inertial mass M while q_b is changing:

$$m_b = m_g \approx M + \frac{1}{10\gamma_c}\left(7 - \frac{27}{2\sqrt{14}}\right)\frac{GM^2}{ac^2} - \frac{1}{10\gamma_c}\left(7 - \frac{27}{2\sqrt{14}}\right)\frac{q_b^2}{4\pi\varepsilon_0 ac^2}.$$

In the classical uniform system of a spherical shape with stationary particles the total gravitational energy summed up with the total electric energy is equal to the following: $E_g + E_e = -\frac{3Gm_b^2}{5a} + \frac{3q_b^2}{20\pi\varepsilon_0 a}$. Consequently, Eq. (34) can be written as follows:

$$Mc^2 \approx m_b c^2 + \frac{1}{6\gamma_c}\left(7 - \frac{27}{2\sqrt{14}}\right)\left(E_g + E_e\right).$$

As we can see, the inertial mass M of the relativistic uniform system differs from the rest mass of the particles m_b by approximately half of the total mass-energy of the gravitational and electric fields of the classical uniform system, whereas the presence of the electric field increases the mass M in contrast to the action of the gravitational field.

Now let us imagine that for an external observer the sphere with the particles has the invariant inertial mass M, the volume V, and the corresponding mass density $\rho_s : M = \rho_s V$. Let us substitute Eq. (4) into Eq. (33) and take into account Eq. (24) and relation $m = \rho_0 V$. This gives the following:

$$E_r = Mc^2 = \rho_s V c^2 \approx \rho_0 V c^2 \gamma_c \left[1 - \left(\frac{22}{15} - \frac{9}{4\sqrt{14}}\right)\frac{\eta m}{ac^2}\right]. \tag{35}$$

In [12] we found expression (8) for the squared velocities of the particles at the center of the sphere, with the help of which we can estimate the Lorentz factor:

$$\gamma_c = \frac{1}{\sqrt{1 - v_c^2/c^2}} \approx 1 + \frac{v_c^2}{2c^2} + \frac{3v_c^4}{8c^4} \approx 1 + \frac{3\eta m}{10ac^2}\left(1 + \frac{9}{2\sqrt{14}}\right) + \frac{27\eta^2 m^2}{200a^2 c^4}\left(1 + \frac{9}{2\sqrt{14}}\right)^2.$$

Substituting the expression for γ_c into Eq. (35), after reduction by Vc^2 we find:

$$\rho_s \approx \rho_0 \gamma_c \left[1 - \left(\frac{22}{15} - \frac{9}{4\sqrt{14}}\right)\frac{\eta m}{ac^2}\right] \approx \rho_0 \left[1 - \left(\frac{7}{6} - \frac{18}{5\sqrt{14}}\right)\frac{\eta m}{ac^2}\right]. \tag{36}$$

Hence it follows that $\rho_s < \rho_0$, i.e., as more increasingly massive relativistic uniform systems are formed, the average density of these systems decreases as compared to the average density of the particles and bodies that make up these systems.

Let us assume that this conclusion holds true for neutron stars, mostly consisting of nucleons only with a small admixture of atomic nuclei and a certain number of electrons, which give a small contribution into the total mass. We will assume that the mass density ρ_0 in Eq. (36) represents the

density of the nucleons' matter, and ρ_s is the average density of a neutron star, and we will use Eq. (13) for the case of an uncharged star with zero charge density ρ_{0q}. This gives the following:

$$\rho_s \approx \rho_0 \left[1 - \frac{3}{5} \left(\frac{7}{6} - \frac{18}{5\sqrt{14}} \right) \frac{Gm}{ac^2} \right]. \tag{37}$$

Substituting here instead of m the mass of a typical star of 1.35 solar masses, taking as the nucleon density ρ_0 the proton density of 6×10^{17} kg/m³ with the proton radius of 8.73×10^{-16} m according to [15], and using the estimate of the star density in the form $\rho_s = \frac{3m}{4\pi a^3}$, we find the corresponding radius of the neutron star: $a \approx 10.3$ km. This radius supposes tight packing of neutrons in the matter of the star and by the order of magnitude is in reasonable agreement with the observational data. However, it should be noted that in the star there are gaps between the nucleons. Therefore, in Eq. (37) for ρ_0 we should substitute not the mass density of the proton, but a smaller quantity. This leads to decreasing of ρ_s so that the radius $a \approx 10.3$ km places the lower limit on the radius of the neutron star.

In the theory of infinite nesting of matter, nucleons are similar in their properties to neutron stars, and for these objects, the ratio of the central density to the average density is approximately 1.5 according to [7, 15]. Thus, in the first approximation nucleons and neutron stars are close enough in their properties to relativistic uniform systems. In addition, it should be noted that these objects consist of particles, for which it is necessary at least to take into account the energy of the proper spin rotation and the energy of strong interaction. Consequently, our analysis with respect to such relativistic objects needs clarification, starting with the introduction of additional terms into the Lagrangian and finishing with taking into account the metric in the equations, arising from the principle of least action. These calculations have not yet been made, but we can rely on the equation derived by Tolman, Oppenheimer, and Volkoff in the framework of the general theory of relativity [16].

From Eqs. (37) and (33) it follows that as a certain large relativistic uniform system is formed from a number of small relativistic uniform systems, the average mass density of the system decreases as compared to the average density of its parts, while the inertial (invariant) mass of the large system is less than the sum of inertial (invariant) masses of the system's parts. At the same time, the relativistic energy density and the binding energy density decrease in the transition to increasingly more massive objects. From a qualitative point of view, the density decrease can be explained by the presence of gaps between the individual parts of the system with reduced mass density. From a quantitative point of view, the decrease in the average density of the system can be derived from the contributions of the particles' energy in the potentials of the system's proper fields with addition from the fields' energy, found through the strengths and solenoidal vectors of the fields.

In this regard, we note that the strengths and solenoidal vectors of the fields are the temporal and spatial rates of change of the field potentials, as they are calculated using the partial derivatives of the scalar and vector potentials. Therefore, in case of the known dependencies of the field potentials on time and coordinates, the full description of the system can be easily achieved and the main dependencies, including the equation of motion and the stress-energy tensor [14], can be easily found. In contrast to this, if only the strengths and solenoidal vector of the fields are given, in order to determine the potentials we need to perform integration and to take into account the initial conditions. And such integration, as is known, is much more difficult than differentiation. An additional advantage of the use of potentials in the field physics is the fact that they are calculated in the standard way using the corresponding wave equations [4], [13].

References

[1] Landau, L.D., Lifshitz, E.M., *The Classical Theory of Fields,* (Vol. 2, 4th ed.) Butterworth-Heinemann, 1975.

[2] Denisov, V.I., Logunov, A.A., "The inertial mass defined in the general theory of relativity has no physical meaning", *Theoretical and Mathematical Physics*, 51(2), 421-426, 1982.

[3] Khrapko, R.I., "The Truth about the Energy-Momentum Tensor and Pseudotensor", *Gravitation and Cosmology*, 20(4), 264-273, 2014.

[4] Fedosin, S.G., "Relativistic Energy and Mass in the Weak Field Limit", *Jordan Journal of Physics*, 8(1), 1-16, 2015.

[5] Chernikov, N.A., "Derivation of the equations of relativistic hydrodynamics from the relativistic transport equation", *Physics Letters*, 5(2), 115-117, 1963.

[6] Vlasov, A.A., "On Vibration Properties of Electron Gas", *J. Exp. Theor. Phys.* (in Russian), 8(3), 291, 1938.

[7] Fedosin, S.G., "Estimation of the physical parameters of planets and stars in the gravitational equilibrium model", *Canadian Journal of Physics*, 94(4), 370-379, 2016.

[8] Fedosin, S.G., "About the cosmological constant, acceleration field, pressure field and energy", *Jordan Journal of Physics*, 9(1), 1-30, 2016.

[9] Fedosin, S.G., "The Concept of the General Force Vector Field", *OALib Journal*, 3, 1-15, 2016, e2459.

[10] Fedosin, S.G., "Two components of the macroscopic general field", *Reports in Advances of Physical Sciences*, 1(2), 1750002, 9 pages, 2017.

[11] Fedosin, S.G., "The Gravitational Field in the Relativistic Uniform Model within the Framework of the Covariant Theory of Gravitation". *International Letters of Chemistry, Physics and Astronomy*, 78, 39-50, 2018.

[12] Fedosin, S.G., "The virial theorem and the kinetic energy of particles of a macroscopic system in the general field concept", *Continuum Mechanics and Thermodynamics*, 29(2), 361-371, 2016.

[13] Fedosin, S.G., "The Integral Energy-Momentum 4-Vector and Analysis of 4/3 Problem Based on the Pressure Field and Acceleration Field", *American Journal of Modern Physics*, 3(4), 152-167, 2014.

[14] Fedosin, S.G., "The procedure of finding the stress-energy tensor and vector field equations of any form", *Advanced Studies in Theoretical Physics*, 8, 771-779, 2014.

[15] Fedosin, S.G., "The radius of the proton in the self-consistent model", *Hadronic Journal*, 35(4), 349-363, 2012.

[16] Oppenheimer, J.R., Volkoff, G.M., "On Massive Neutron Cores", *Physical Review*, 55(4), 374-381, 1939.

DOSIMETRIC INVESTIGATION OF RADIOTHERAPY OF SMALL SIZE TUMORS IN RADIOSURGERY DEVICES

[1]Duygu TUNÇMAN GENÇ*, [2]Eda MUTLU, [3]Murat OKUTAN, [4]Bayram DEMİR

[1]Altınbaş University, Vocational School of Health Services, Medical Imaging Techniques Department, İstanbul. ORCID:0000-0002-0929-0441

[2] Altınbaş University, Vocational School of Health Services, Radiotherapy Department, İstanbul. ORCID:0000-0002-3972-7309

[3]Istanbul University, Oncology Institute, Medical Physics Department, İstanbul. ORCID: 0000-0002-2276-631X

[4]Istanbul University, Science Faculty, Physics Department, İstanbul. ORCID: 0000-0001-6815-6384

* Corresponding author; duygu.tuncman@altinbas.edu.tr

Abstract: *In stereotactic radiotherapy, high radiation doses were delivered to tumors using small fields in 1-5 fractions. It is very important to make sure the accuracy of dose and position of given dose in stereotactic radiotherapy. In this study, dosimetric measurements of small sized brain tumors irradiated in CONE- based linear accelerator (linac) and the volumetric arc therapy (VMAT) linac modalities were performed with EBT3 film. 1,2 and 3 cm diameter tumors were virtually created in Cyberknife head and neck phantom. Gafchromic EBT3 film was placed into the phantom to evaluate the accuracy of the doses given. The phantom was irradiated with Gafchromic EBT3 film according to treatment plans created in the treatment planning system of two separate devices for each tumor size. Conformity Index (CI) and Homogeneity Index (HI) were calculated for the quality of created treatment plans. The dose distributions calculated in the film and the TPS were compared. When the CI and HI values were examined, the CI and HI values of the cone-based linac device were close to 1. The EBT3 measurement results indicate that all SRT treatment modalities achieved accurate doses. According to results, if a critical organ, such as the brainstem, is located near the tumor and the situation requires a steep dose gradient, the cone-based linac should be used for SRT therapy. This study has shown that on CONE-based linac or VMAT-based linac devices can be used instead of each other in small-area irradiations.*

Keywords*: Stereotactic radiosurgery, Cyberknife, Linac, VMAT, Film dosimetry.*

1. Introduction

The main purpose of radiotherapy; to give the least dose to the critical organs around the tumor and to give the maximum dose to the tumor. Many modern radiotherapy techniques have been developed for this purpose. Stereotactic Radio Surgery (SRC) which is preferred in clinics in recent years is one of the modern radiotherapy techniques developed. SRC is (tumor diameter <4 cm) high-dose irradiation with a single fraction of small targets on the brain. If this application is applied in multiple fractions (not

in a single fraction), it is called Stereotactic Radiotherapy (SRT). The same procedure is referred to as Stereotactic Body Radiotherapy (SBRT) if it is applied to the tumor placed at a small area in any part of the body as hypofraction. Higher conformity treatment is provided with SRT and SBRT compared to normal radiotherapy applications [1]. SRT and SBRT have very speed dose gradient between the critical organs and tumor. Due to the fact that the treatment area is less than 4 cm, there are a number of problems in small-field irradiation. Because for small fields, the accuracy of Treatment Planning Systems (TPS) is more difficult than large treatment fields. There are problems such as the detector used to measure the dose received by the irradiated target is not small enough for the small area, the area size is not large enough to provide lateral electronic balance, sharp dose change and partial blocking of the source. These problems come as dosimetric effects on the absorbed dose in the central axis, in the dose profile taken in the axial section and in the stored dose at a certain x point [2-3].

SRS or SRT treatments can be performed with many treatment devices. Different treatment devices have different output dose characteristics, which may affect the radiation doses received by normal tissues surrounding the tumor [4].

We aimed to compare the SRT treatment doses of the cone-based linac and VMAT linac treatment modalities and evaluate the differences between doses calculated according to treatment planning systems and measured radiation doses. In this study; 1, 2 and 3 cm diameter virtual tumor volumes were irradiated in two stereotactic radiosurgery devices.

2. Material and Method

Scannings using Philips Big Bore Brilliance 4D CT was applied to obtain images of the Cyberknife head and neck phantom. The images were sent to Multiplan 4.5.3 TPS and Ecplise 8.9. TPS. As a small area in the study, 1, 2 and 3 cm diameter GTV volumes were virtually created in Cyberknife head and neck phantom. Different treatment plans were designed by the treatment planning systems according to the size of the tumors as shown in Figures1 and 2.

The accelerator used for the cone-based linac was a 6 MV Accuray Cyberknife treatment device. Cone diameters of 5-10, 10-20, and 12,5-25 mm were used for 1, 2 and 3 cm target, respectively.

The arc-therapy method was used for 6 MV VMAT linac plans. The beam angles were as follows: counter-clockwise from 179.9^0 -180.1^0 with a collimator angle of 45^0, a couch angle of 0° and clockwise from 180.1^0- 179.9^0 with a collimator angle of 315°, a couch angle of 0°.

In all treatment plans, a dose of 500 cGy was delivered to the tumors, and the conditions were optimized to maintain %100 dose coverage on the tumor.
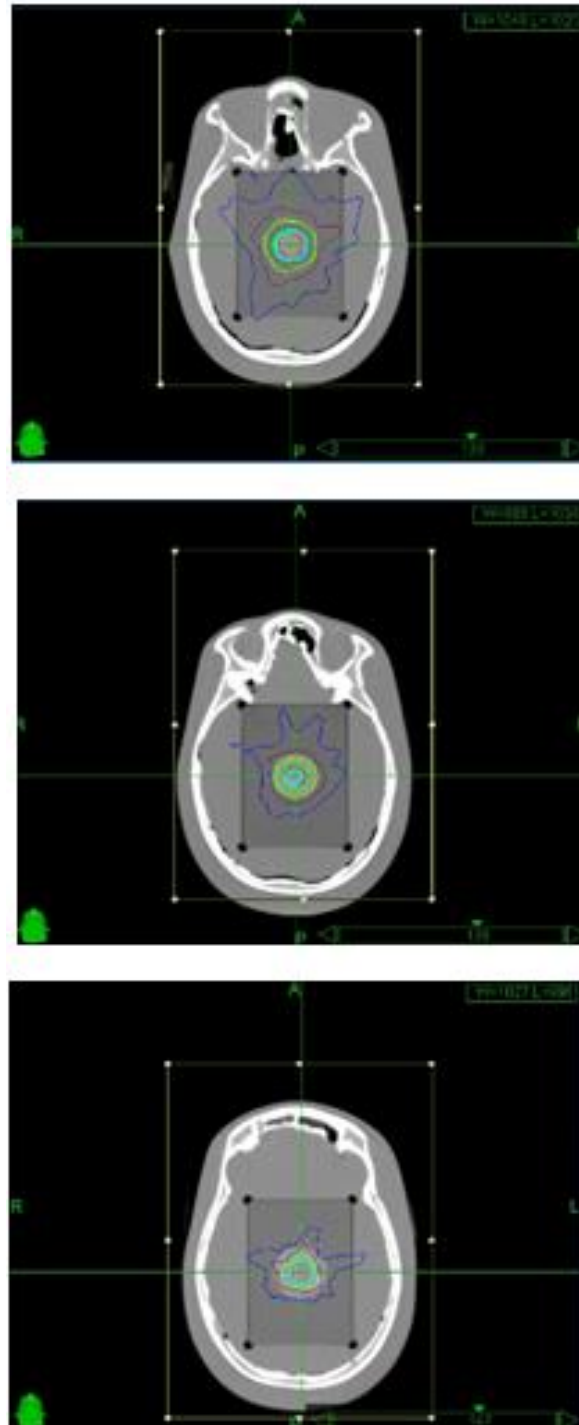
Figure 1. The treatment plan for a 1,2 and 3 cm tumors in Multiplan TPS
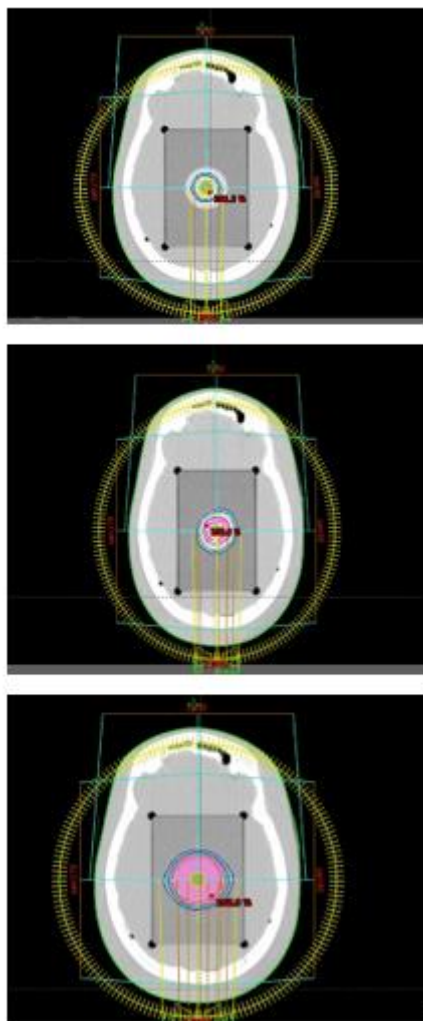
Figure 2. The treatment plan for a 1,2 and 3 cm tumors in Eclipse TPS

Gafchromic EBT3 films were used to measure the radiation dose. The measurements were repeated for three times for each tumor location and each treatment device. The films for the irradiations were cut in accordance with the phantom dimensions (6.3 x 9 cm) and placed in the 3. part of the RW4 solid water phantom in 1 cm thickness as shown in Figure 3.

Figure 3. The positioning of the films to be irradiated in the Cyberknife phantom

Phantom was positioned as in routine patient irradiation position according to the treatment plan. PTW Verisoft was used to evaluate the profile changes in superior-inferior (S–I) directions on the films as shown in Figures 4, 5 and 6. Moreover, isodose curves generated from irradiated films were plotted in S-I rotation for each tumor dimension.
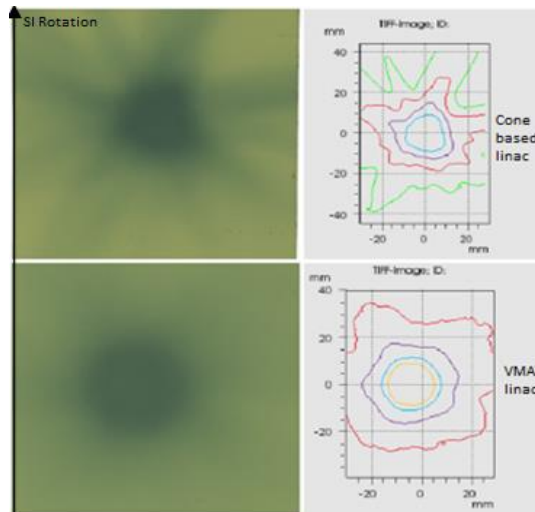
Figure 4. Films irradiated by Cone based linac and VMAT linac devices of the one-cm tumor and their isodose curves.
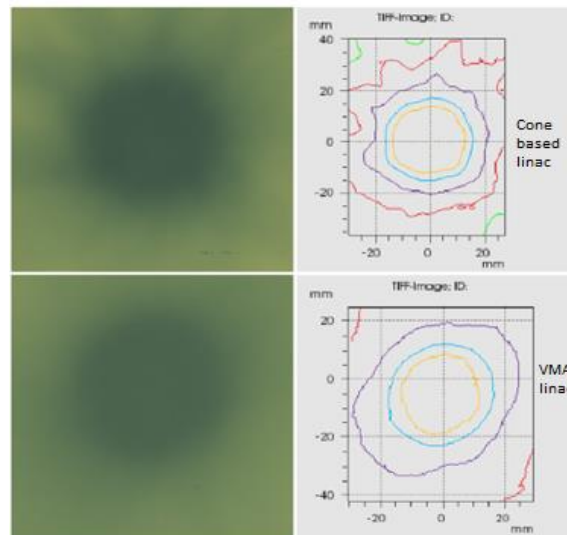
Figure 5. Films irradiated by Cone based linac and VMAT linac devices of the two-cm tumor and their isodose curves
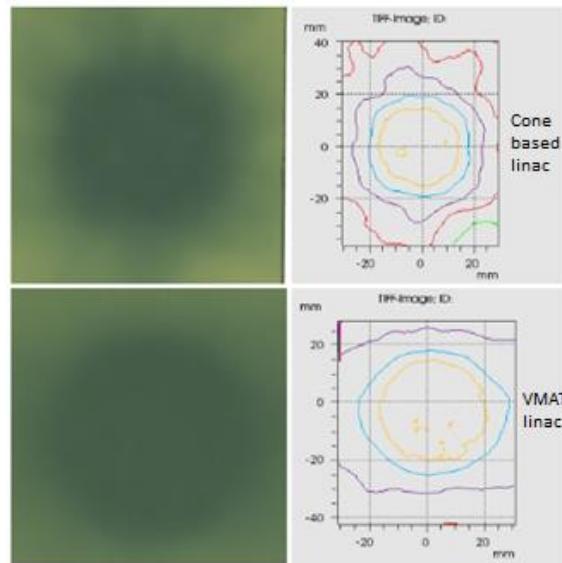
Figure 6. Films irradiated by Cone based linac and VMAT linac devices of the three-cm tumor and their isodose curves

Besides, the homogeneity index (HI) and conformity index (CI) were used to compare the quality of the treatment plans in this study. The HI was used to describe the homogeneity of the dose within the tumor [5].

HI = MD/PD

where MD is the maximum dose within the tumor and PD is the 100% prescription dose. The HI of a perfect treatment plan should be 1.

The CI is defined as

CI= (TV_{PIV})^2 /TV x PIV

where PIV refers to the volume covered by the 100% prescription dose curve, TV is the tumor volume, and TV_{PIV} is the tumor volume covered by PIV. The CI of a perfect treatment plan should be 1 [6].

3. Results
3.1 CI and HI values calculated in treatment planning systems

CI and HI values calculated by Ecplise TPS and Multiplan TPS for each tumor dimension are shown in Table 1.

Table 1. CI and HI values calculated by Ecplise TPS and Multiplan TPS for each tumor dimension

	Multiplan TPS	Ecplise TPS
1 cm tumor		
CI	0,98	0,5
HI	1,18	1,01
2 cm tumor		

CI	0,998	0,53
HI	1,12	1,04
3 cm tumor		
CI	0,999	1,21
HI	1,10	1,06

3.2 Dose profiles for tumor irradiation in all three dimensions from treatment planning systems and scanned films

Dose profiles for 1 cm tumor from treatment planning systems and scanned films are shown in Figure 7.

3.2.1. 1 cm tumor
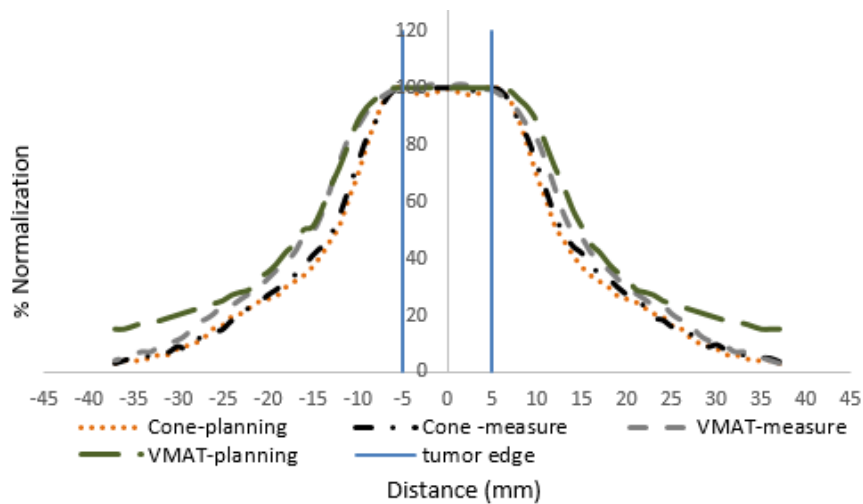
Figure 7. Dose profiles for 1 cm tumor from treatment planning systems and scanned films. All doses were normalized to the dose of the center of the fields.

3.2.2. 2 cm tumor

Dose profiles for 2 cm tumor from treatment planning systems and scanned films are shown in Figure 8.
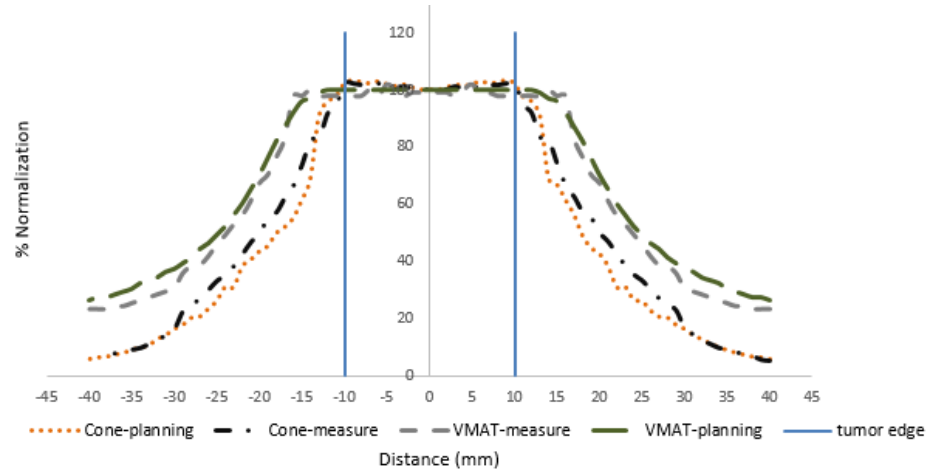
Figure 8. Dose profiles for 2 cm tumor from treatment planning systems and scanned films. All doses were normalized to the dose of the center of the fields.

3.2.3. 3 cm tumor

Dose profiles for 3 cm tumor from treatment planning systems and scanned films are shown in Figure 9.
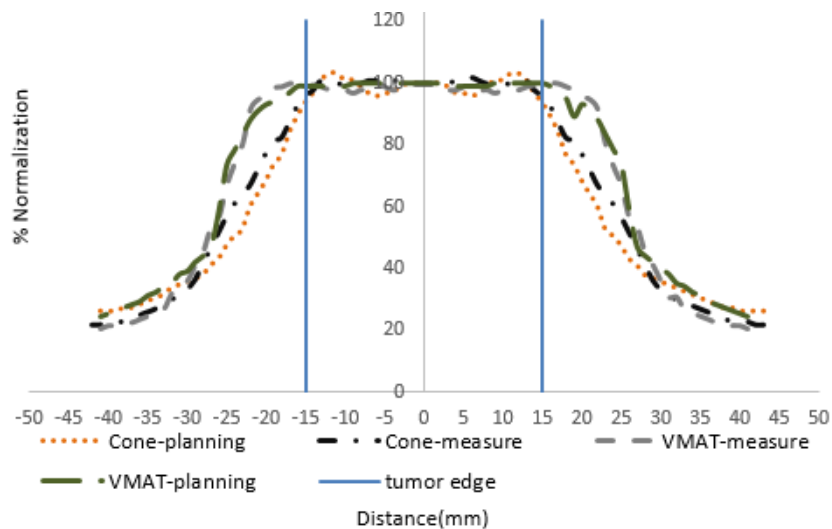
Figure 9. Dose profiles for 3 cm tumor from treatment planning systems and scanned films. All doses were normalized to the dose of the center of the fields.

3. Discussion

In stereotactic radiotherapy, it is important that the dose reaches the target correctly. This is achieved by delivering the dose in the TPS as planned. Therefore, it is necessary to check the accuracy

of the given dose of the treatment plan. In this study, three virtual intracranial tumors with 1, 2 and 3 cm diameters were examined [7-8].

In our study, HI values for VMAT were calculated as 1.01, 1.04 and 1.06 for tumors with 1, 2 and 3 cm diameters, respectively. Similarly, HI values for cone-based linac were calculated as 1.18, 1.12 and 1.10 for tumors 1, 2 and 3 cm, respectively. Both treatment modalities are compatible with each other compared to HI values. CI values in VMAT were calculated as 0.5, 0.53 and 1.21 for tumors with 1, 2 and 3 cm diameters, respectively. CI values for cone-based linac were calculated as 0.98, 0.998 and 0.999 for tumors of 1, 2 and 3 cm, respectively. Regardless of the tumor diameter, the cone-based linac device has more conformal irradiation for all tumors than VMAT because the radiation field of the cone-based linac device is similarly compatible with tumor sizes [9].

In research of Shih- Ming Hsu et. al study, the cone-based linac, FFF-VMAT linac, and tomotherapy modalities were evaluated by measuring the differences between the doses delivered during brain SRT and experimentally assessing the accuracy of the output radiation doses through clinical measurements. The average HI values of the cone -based linac, the FFF-VMAT linac, and tomotherapy were 1.20, 1.21, and 1.23, respectively. The average CI for the cone-based linac, the FFF-VMAT linac, and tomotherapy were 0.90, 0.73, and 0.65, respectively. In this study, among the three treatment modalities studied, the cone-based linac had the best conformity and the best dose gradient for all tumors sizes and locations [9].

Q.-R. Jackie Wu et al. in his conformity measurement study for the Gamma knife stereotactic radiosurgery technique, conformity index evaluation was performed for tumors of different sizes of 0.3, 1.0, 3.0, 10.0 and 30.0 cm^3. They developed a different parameter called conformity distance index (CDI) for conformity calculations of treatment. According to the study, CI was 0.61 for 1 cm^3 tumor, while CDI value was 0.93; CI was 0.71 for 3 cm ^{3}, while CDI was found 0.95. Q.-R. Jackie Wu et al. indicated that the low conformity index value would be related to the complex geometry of the target and target volume. The CDI recommended by Q.-R. Jackie Wu et. al is defined as the average distance between the target and the prescribed isodose line. The proposed CDI has provided more consistent and accurate measurement for all target sizes and shapes. They emphasize that CDI is a more useful index for stereotactic radiosurgery [10].

The results measured with EBT3 film for tumors 1, 2 and 3 cm are consistent with the planned values in TPS as shown in Figures 7, 8 and 9 because the difference between the profiles obtained from the planned and measured values is less than 4%. Film measurement results show that both treatment modalities have reached the correct doses. SBRT is the irradiation of small tumor in several fractions using high doses. For this reason, the dose given to the tumor should be compatible with the prescribed dose.

When Figures 7, 8 and 9 are examined, it is shown that the dose gradient of CONE based LINAC device is higher than VMAT. This is a positive finding for critical organs that will take place near the target volume. The faster the dose gradient outside the volume, the very important it is for the protection of critical organs. For example, in the presence of a critical organ such as the brainstem, a cone-based

treatment device may be preferred in the surroundings of their irradiated area such as Shih-Ming Hsu et al.

According to results from this study; Stereotactic radiotherapy can be performed with a cone-based linac device and VMAT-based linac devices. However, the cone-based linac had the best conformity and dose gradient for tumors of all sizes and locations. If a critical organ, such as the brainstem, is located near the tumor and the situation requires a steep dose gradient, the cone-based linac should be used for SRT therapy.

References

[1] Yazıcı, G., Cengiz, M., *et al.,"*Stereotaktik Vücut Radyoterapisi", *Hacettepe Tıp Dergisi*, 42, 74-81, 2011.

[2] Çağıran Kılçıksız, S., Ermiş, E., *et al.,"*Görüntü Eşliğinde Stereotaktik Radiotherapy", *Okmeydanı Tıp Dergisi*, 29, 3-9, 2013.

[3] Baş, H., Sterotaktik Radyocerrahi için Küçük alanlarda 6 MV Foton Dozimetrisi, Ankara Üniversitesi, Fen Bilimleri Enstitüsü, Yüksek Lisans Tezi, 2005.

[4] Kayalılar, N., Cyberknife ve gamma knife tedavilerinde hedef hacim ve normal doku dozlarının karşılaştırılması, Acıbadem Üniversitesi, Sağlık Bilimleri Enstitüsü, Yüksek Lisans Tezi, 2012.

[5] Feuvret, L., Noel, G., *et al.,"*Conformity Index: A Review", *Int J. Radiation Oncology Biol. Phys.,* 64(2), 333-342, 2006.

[6] Feuvret, L., Noel, *G., et al., "*Conformal Index and Radiotherapy", *CancerRadiother.*, 8,2108-19, 2004.

[7] Das, I., J., Ding, G., *X., et al.,* "Small fields: Nonequilibrium radiation dosimetry", *Medical Physics,* 35(1), 206-215, 2007.

[8] http://amos3.aapm.org/abstracts/pdf/77-22581-312436-91466.pdf

[9] Hsu, Shih-Ming, Lai, Yuan-Chin, *et al., "*Dosimetric comparison of different treatment modalities for stereotactic radiotherapy", *Radiation Oncology,*155(12), 1-11, 2017.

[10] Jackie Wu, Q-R., Wessels, B.W., e*t al., "*Quality of coverage: Conformity measures for stereotactic radiosurgery", *Journal of Applied Clinical Medical Physics*, 4(4), 374-381,2003.

INTERNATIONAL ENGINEERING, SCIENCE AND EDUCATION GROUP	

SOLVING INTEGRO-DIFFERENTIAL EQUATIONS USING EXPONENTIALLY FITTED COLLOCATION APPROXIMATE TECHNIQUE (EFCAT)

FALADE K.I

Department of Mathematics, Faculty Computing and Mathematical Sciences,
Kano University of Science and Technology, P.M.B 3244 Wudil Kano State Nigeria.
ORCID: 0000-0001-7572-5688

Corresponding author: faladekazeem2013@gmail.com

Abstract: *In this paper, we present and employ Exponentially Fitted Collocation Approximate Technique (EFCAT) to solve linear Volterra and Fredholm integro-differential equations.The collocated-perturbed Integro-differential equations were transformed into square matrix form which eventually solves using MAPLE 18 software. To demonstrate the applicability of the present method four examples is considered. It is observed that the present technique is in good agreement with the analytical solution and available methods in the literature.*

Keywords*: Volterra and Fredholm integro-differential equations, exponentially fitted collocation approximate technique, analytical solution, Maple 18 software.*

1. Introduction

Integro-differential equations find special applicability within scientific and mathematical disciplines. It plays an important role in many branches of mathematical sciences and their applications in the theory of engineering, physics, mechanics, chemistry, astronomy, biology, economics, potential theory, and electrostatics. The theory and application of integrodifferential equations are important roles in engineering and applied sciences. The existence and uniqueness of the solutions of integrodifferential equations usually discussed in terms of their kernel have been established in [1]. The integro-differential equations are usually difficult to solve analytically thus, it requires suitable numerical techniques to obtain analytic-numeric solutions of Integro-differential equations. Therefore, several authors have proposed and applied different methods to obtain the solution of both linear and nonlinear IDEs such as, Adomian decomposition [2], Homotopy perturbation method [3], variation iteration method [4], Chebyshev polynomial collocation [5], The Taylor expansion approach [6], Bessel or Chebyshev polynomial approach are used to solve integro-differential equations in [7] and just mention a few.

Generally, integro-differential equations are difficult to solve, thus this present work is to apply a technique proposed in [8] to solve linear Volterra and Fredholm integro-differential equations, which promise to be a reliable, easy, fast and accurate numerical technique to obtain numerical solution of linear Volterra and Fredholm integro-differential equations. We obtain derivative of power series of function $y(x)$ and substitute into the linear integro differential equation. Slightly perturbation and collocation are carried out which eventually transform to square matrix form and MAPLE 18 software is used to obtain the unknown constants.

In this paper, we considered pth order general integro-differential equation of the form:

$$\begin{cases} \dfrac{d^p y}{dx^p} + \alpha(x)\dfrac{d^{p-1}y}{dx^{p-1}} + \beta(x) + \dfrac{d^{p-2}y}{dx^{p-2}} + \cdots + y(x) \\ = g(x) + \psi(x)\displaystyle\int_a^b \gamma(t,x)\, y(t)dt \qquad x \in [a,b] \qquad (1) \end{cases}$$

subject to initial conditions

$$\begin{cases} y(a) = A \\ \dfrac{dy}{dx}(a) = B \\ \dfrac{d^2 y}{dx^2}(a) = C \\ \quad . \\ \quad . \\ \quad . \\ \dfrac{d^{p-1}y}{dx^{p-1}}(a) = H \end{cases} \qquad (2)$$

Where $\alpha(x), \beta(x), g(x), \psi(x)$ are continuous function on interval $[a,b]$, $\gamma(t,x)$ is a kernel and A,B,C,…..H are constants.

1.1 Defınıtıon of Chebyshev Polynomıals

The chebyshev polynomials of the first kind can be defined by the recurrence relation given by
$$T_0(x) = 1 \quad , \quad T_1(x) = 2x - 1$$

Thus, we have
$$T_{N+1}(x) = 2(2x-1)T_N(x) - T_{N-1}(x) \qquad N \geq 1 \quad (3)$$

Table 1. The First ten (10) Chebyshev Polynomials

$T_N(x)$	Chebyshev Polynomials
$T_0(x)$	1
$T_1(x)$	$2x - 1$
$T_2(x)$	$8x^2 - 8x + 1$
$T_3(x)$	$32x^3 - 48x^2 + 18x - 1$
$T_4(x)$	$128x^4 - 258x^3 + 160x^2 - 32x + 1$
$T_5(x)$	$512x^5 - 1280x^4 + 1120x^3 - 400x^2 + 50x - 1$
$T_6(x)$	$2048x^6 - 6144x^5 + 6912x^4 - 3584x^3 + 640x^2 - 72x + 1$
$T_7(x)$	$8172x^7 - 28672x^6 + 39424x^5 - 26880x^4 + 9408x^3 - 1568x^2 + 98x - 1$
$T_8(x)$	$32768x^8 - 131072x^7 + 212992x^6 - 180224x^5 - 84480x^4 - 21504x^3 + 2688x^2 - 128x + 1$
$T_9(x)$	$131072x^9 - 589824x^8 + 1105920x^7 - 1118208x^6 + 658944x^5 - 228096x^4 + 44352x^3 - 4320x^2 + 162x - 1$
$T_{10}(x)$	$52488x^{10} - 2621440x^9 + 5570560x^8 - 6553600x^7 + 4659200x^6 - 2050048x^5 + 549120x^4 - 84480x^3 + 6600x^2 - 200x + 1$

2. Methodology

In this study, we consider the power series of the form
$$y(x) = \sum_{k=0}^{N} q_k x^k \tag{4}$$

and exponentially fitted approximate solution proposed in [8]

$$y(x) \approx \sum_{k=0}^{N} q_k x^k + \tau_1 e^x \tag{5}$$

Taking the first derivative of equation (4), we obtain

$$\frac{dy}{dx} = \sum_{k=1}^{N} k q_k x^{k-1} \tag{6}$$

Suppose $p = 1$ and substitute equations (4) and (6) into equation (1), leads to

$$\sum_{k=1}^{N} k q_k x^{k-1} + \sum_{k=0}^{N} q_k x^k = g(x) + \psi(x) \left(\int_a^b \gamma(t,x) \sum_{k=0}^{N} q_k t^k dt \right) \tag{7}$$

Expansion of (7), we obtain

$$(q_1 + 2q_2 x + 3q_3 x^2 + \cdots + N q_N x^{N-1}) + (q_0 + q_1 x + q_2 x^2 + q_3 x^3 \ldots + q_N x^N)$$
$$= g(x) + \psi(x) \left(\int_a^b \gamma(t,x)(q_0 + q_1 t + q_2 t^2 + q_3 t^3 \ldots + q_N t^N) dt \right) \tag{8}$$

Collecting the likes terms, we have

$$\left(1 - \psi(x) \int_a^b \gamma(t,x) dt \right) q_0 + \left(1 + x - \psi(x) \int_a^b \gamma(t,x) t\, dt \right) q_1 +$$

$$\left(2x + x^2 - \psi(x) \int_a^b \gamma(t,x) t^2 dt \right) q_2 + \left(3x^2 + x^3 - \psi(x) \int_a^b \gamma(t,x) t^3 dt \right) q_3$$
$$+ \cdots + \left(Nx^{N-1} + x^N - \psi(x) \int_a^b \gamma(t,x) t^N dt \right) q_N = g(x) \tag{9}$$

Slightly perturbe and collocate equation (9), we have

$$\left(1 - \psi(x) \int_a^b \gamma(t_i, x_i) dt \right) q_0 + \left(1 + x_i - \psi(x) \int_a^b \gamma(t_i, x_i) t_i\, dt \right) q_1$$

$$+ \left(2x_i + x_i{}^2 - \psi(x) \int_a^b \gamma(t_i, x_i) x_i{}^2 dt \right) q_2$$

$$+ \left(3x_i{}^2 + x_i{}^3 - \psi(x) \int_a^b \gamma(t_i, x_i) x_i{}^3 dt \right) q_3$$

$$+ \left(Nx_i{}^{N-1} + x_i{}^N - \psi(x) \int_a^b \gamma(t_i, x_i) t_i{}^N dt \right) q_N - T_N(x_i)\tau_1 = g(x_i) \tag{10}$$

Here τ_1 are free tau parameter to be determined [8], $T_N(x_i)$ are the Chebyshev polynomials of degree N define in table 1 and

$$x_i = a + \frac{(b-a)i}{N+2}; \qquad i = 1,2,3 \dots. N+1$$

Hence, equation (10) gives rise to (N+1) algebraic linear system of equations in (N+2) unknown constants. One extra equation is obtained from the initial condition given as

$$y(a) = \sum_{k=0}^{N} q_k x^k + \tau_1 e^a \qquad\qquad (11)$$

Altogether, we obtained (N+2) algebraic linear equations in (N+2) unknown constants. Thus, we put the (N+2) algebraic equations in matrix form as

$$E_1 Q_1 = G_1(x) \qquad\qquad\qquad (12)$$

Where $\quad E_1 =$ is the system of the equation of $N+2$, $\quad Q_1 = (q_0, q_1, q_2, q_3, \dots \dots \dots, q_N, \tau_1\ )^T$

$$G_1(\text{x}) = (g(x_1), \dots \dots g(x_N), A\ )^T$$

MAPLE 18 software is used to obtain the unknown constants $q_0, q_1, q_2, q_3, \dots \dots \dots, q_N$ and τ_1 and substitute into the exponentially fitted approximate solution (5).

Generally, we consider the order $p = 2,3,4,5$ for the equation (1) and repeat the procedures from equations (6) to (11), we obtain the follow:

When $p = 2$ we have

$$E_2 Q_2 = G_2(x) \qquad\qquad\qquad (13)$$

Where $\quad E_2 =$ is the system of the equation of $N+3$, $\quad Q = (q_0, q_1, q_2, q_3, \dots \dots \dots, q_N, \tau_1, \tau_2\ )^T$

$$G_2(\text{x}) = (g(x_1), g(x_2), \dots \dots g(x_N), A\ , B)^T$$

MAPLE 18 software is used to obtain the unknown constants $q_0, q_1, q_2, q_3, \dots \dots \dots, q_N$ and τ_1, τ_2 and substitute into the exponentially fitted approximate solution (5).

When $p = 3$ we have

$$E_3 Q_3 = G_3(x) \qquad\qquad\qquad (14)$$

Where $\ E_3 =$ is the system of the equation of $N+4$, $Q_3 = (q_0, q_1, q_2, q_3, \dots \dots \dots, q_N, \tau_1, \tau_2\ , \tau_3\ )^T$

$$G_3(\text{x}) = (g(x_1), g(x_2), g(x_3), \dots \dots g(x_N), A\ , B, C)^T$$

MAPLE 18 software is used to obtain the unknown constants $q_0, q_1, q_2, q_3, \dots, q_N$ and τ_1, τ_2, τ_3 and substitute into the exponentially fitted approximate solution (5).

When $p = 4$ we have

$$E_4 Q_4 = G_4(\text{x}) \qquad\qquad\qquad (15)$$

Where $\ E_4 =$ is the system of equation of $N+5$, $Q_4 = (q_0, q_1, q_2, q_3, \dots \dots \dots, q_N, \tau_1, \tau_2\ , \tau_3\ , \tau_4)^T$
$$G_4(\text{x}) = (g(x_1), g(x_2), g(x_3), g(x_4) \dots \dots g(x_N), A\ , B, C, D)^T$$

MAPLE 18 software is used to obtain the unknown constants $q_0, q_1, q_2, q_3, \ldots \ldots \ldots, q_N$, $\tau_1, \tau_2. \tau_3, \tau_4$ and substitute into the exponentially fitted approximate solution (5).

When $p = 5$ we have
$$E_5 Q_5 = G_5(x) \qquad\qquad (16)$$

Where $E_5 = $ is the system of equation of N + 6 , $Q_4 = \left(q_0, q_1, q_2, q_3, \ldots \ldots \ldots, q_N, \tau_1, \tau_2, \tau_3, \tau_4, \tau_{5,}\right)^T$

$$G_5(\text{x}) = (g(x_1), g(x_2), g(x_3), g(x_4), g(x_5) \ldots \ldots g(x_N), A, B, C, D, E)^T$$

MAPLE 18 software is used to obtain the unknown constants $q_0, q_1, q_2, q_3, \ldots \ldots \ldots, q_N$, $\tau_1, \tau_2. \tau_3, \tau_4, \tau_5$ and substitute into the exponentially fitted approximate solution (5).

3. Numerical Application
In this section, we implement exponentially fitted collocation approximate technique on first, second, third and fifth orders Volterra and Fredholm Integro-Differential Equations. Four examples are considered to illustrate the accuracy and efficiency of the proposed method.

Example 1. Consider the First-order Volterra integro-differential equation [9]

$$\frac{dy}{dx} + y(x) = (x^2 + 2x + 1)e^{-x} + 5x^2 + 8 - \int_0^x t\, y(t)dt \qquad x \in [0,1] \quad (17)$$
$$\text{Subject to initial condition } y(0) = 10 \qquad\qquad (18)$$

$$\text{Analytical solution } y(x) = 10 - xe^{-x} \qquad\qquad (19)$$

EFCAT technique

Comparing equation (17) with equation (10) and $\psi(x) = -1$

Choosing computational length N=10, we obtain linear system of equation.

$$
\begin{cases}
\left(1 + \frac{1}{2}x_i{}^3\right)q_0 + \left(1 + x_i + \frac{1}{3}x_i{}^3\right)q_1 + \left(2x_i + x_i{}^3 + \frac{1}{4}x_i{}^4\right)q_2 + \\[4pt]
\left(3x_i{}^3 + x_i{}^3 + \frac{1}{5}x_i{}^5\right)q_3 + \left(4x_i{}^3 + x_i{}^4 + \frac{1}{6}x_i{}^6\right)q_4 + \left(5x_i{}^4 + x_i{}^5 + \frac{1}{7}x_i{}^7\right)q_5 + \\[4pt]
\left(6x_i{}^5 + x_i{}^6 + \frac{1}{8}x_i{}^8\right)q_6 + \left(7x_i{}^6 + x_i{}^7 + \frac{1}{9}x_i{}^9\right)q_7 + \left(8x_i{}^7 + x_i{}^8 + \frac{1}{10}x_i{}^{10}\right)q_8 + \\[4pt]
\left(9x_i{}^8 + x_i{}^9 + \frac{1}{11}x_i{}^{11}\right)q_9 + \left(10x_i{}^9 + x_i{}^{10} + \frac{1}{12}x_i{}^{12}\right)q_{10} \\[4pt]
- \begin{Bmatrix} 52488x_i{}^{10} - 2621440x_i{}^9 + 5570560x_i{}^8 - 6553600x_i{}^7 + 4659200x_i{}^6 \\ -2050048x_i{}^5 + 549120x_i{}^4 - 84480x_i{}^3 + 6600x_i{}^2 - 200x_i + 1 \end{Bmatrix}\tau_1 = \\[4pt]
\qquad\qquad (x_{\text{i}}{}^3 + 2x_i + 1)e^{-x_i} + 5x_{\text{i}}{}^3 + 8
\end{cases}
\quad (20)
$$

Collocate equation (20) as follows:
$$x_i = a + \frac{(b-a)i}{N+2}; \quad i = 1,2,3 \ldots \ldots N + 1 \text{ Where } a = 0 \ , \ b = 1 \ , \ N = 10$$
$$x_1 = \frac{1}{12}, x_2 = \frac{2}{12}, x_3 = \frac{3}{12}, x_4 = \frac{4}{12}, x_5 = \frac{5}{12}, x_6 = \frac{6}{12},$$
$$x_7 = \frac{7}{12}, x_8 = \frac{8}{12}, x_9 = \frac{9}{12}, x_{10} = \frac{10}{12}, x_{11} = \frac{11}{12}$$

Consider initial condition (18) and using MAPLE 18 software to obtain twelve (12) unknown constants of equations (20), we obtain the following constants

$$\begin{cases} q_0 = 10.00000000000, q_1 = -0.99999569981 \\ q_2 = 0.999929888700, q_3 = -0.49945051670 \\ q_4 = 0.164233879700, q_5 = -0.03520284380 \\ q_6 = -0.00217697048, q_7 = 0.008870692442 \\ q_8 = -0.00536139901, q_9 = 0.001307283762 \\ q_{10} = -0.00003367108, \tau_1 = -0.00000007663 \end{cases}$$

Substitute the above values into approximation solution (5).The approximate solution of
First-order Volterra integro-differential equation (17) can be written as

$$y(x) \approx \begin{cases} 10.000000000 - 0.99999569981x + 0.999929888700x^2 \\ -0.49945051670x^3 + 0.164233879700x^4 - 0.03520284380x^5 \\ -0.00217697048x^6 + 0.008870692442x^7 - 0.00536139901x^8 \\ 0.001307283762x^9 - 0.00003367108x^{10} - 0.00000007663e^x \end{cases} \qquad (21)$$

Example 2. Consider the Second-order Volterra integro-differential equation [10]

$$\frac{d^2y}{dx^2} = 1 + xe^x - \int_0^x e^{x-t} y(t)dt \qquad x \in [0,1] \qquad (22)$$

Subject to initial conditions

$$\begin{cases} y(0) = 0 \\ \frac{dy}{dx}(0) = 1 \end{cases} \qquad (23)$$

Analytical solution $y(x) = e^x - 1$ (24)

EFCAT technique

Comparing equation (22) with equation (13) and choosing computational length N=8, we have

$$\begin{cases} (e^{x_i} - 1)q_0 + \\ (e^{x_i} - x_i - 1)q_1 + \\ (2e^{x_i} - x_i{}^2 - 2x_i)q_2 + \\ (6e^{x_i} - x_i{}^3 - 3x_i{}^2 - 6)q_3 + \\ (24e^{x_i} - x_i{}^4 - 4x_i{}^3 - 24x_i - 24)q_4 + \\ (120e^{x_i} - x_i{}^5 - 5x_i{}^4 - 60x_i{}^2 - 120x_i - 120)q_5 + \\ (720e^{x_i} - x_i{}^6 - 6x_i{}^5 - 120x_i{}^3 - 360x_i{}^2 - 720x_i - 720)q_6 + \\ (5040e^{x_i} - x_i{}^7 - 7x_i{}^6 - 210x_i{}^4 - 840x_i{}^3 - 2520x_i{}^2 - 5040x_i - 5040)q_7 + \\ (40320e^{x_i} - x_i{}^8 - 8x_i{}^7 - 336x_i{}^5 - 1680x_i{}^4 - 6720x_i{}^3 - 20160x_i{}^2 - 40320x_i - 5040)q_8 \\ \quad - \begin{cases} 32768x_i{}^8 - 131072x_i{}^7 + 212992x_i{}^6 - 180224x_i{}^5 - \\ 84480x_i{}^4 - 21504x_i{}^3 + 2688x_i{}^2 - 128x_i + 1 \end{cases} \tau_1 \\ \quad - \begin{cases} 8172x_i{}^7 - 28672x_i{}^6 + 39424x_i{}^5 - 26880x_i{}^4 + \\ 9408x_i{}^3 - 1568x_i{}^2 + 98x_i - 1 \end{cases} \tau_2 = 1 + x_i e^{x_i} \qquad (25) \end{cases}$$

Collocate equation (25) as follows:

$$x_i = a + \frac{(b-a)i}{N+2}; \quad i = 1,2,3 \dots\dots N + 1 \text{ where } a = 0 , b = 1 , N = 8$$

$$x_1 = \frac{1}{10}, x_2 = \frac{2}{10}, x_3 = \frac{3}{10}, x_4 = \frac{4}{10}, x_5 = \frac{5}{10}, x_6 = \frac{6}{10}, x_7 = \frac{7}{10}, x_8 = \frac{8}{10}, x_9 = \frac{9}{10}$$

Consider initial condition (23) and using MAPLE 18 software to obtain eleven (11) unknown constants in equations (25), thus we obtain

$$\begin{cases} q_0 = 0.000000043736, q_1 = 1.000000044 \\ q_2 = 0.4999999721, \quad q_3 = 0.1666663308 \\ q_4 = 0.04167069796, \quad q_5 = 0.008317273866 \\ q_6 = 0.001420233805, q_7 = 0.000166139345 \\ q_8 = 0.0000411775232, \tau_1 = -0.00000000163 \\ \tau_2 = -0.0000000373624797 \end{cases}$$

Substitute the above values into approximation solution (5). The approximate solution of Second-order Volterra integro-differential equation (22) can be written as

$$y(x) \approx \begin{cases} 0.000000043736 + 1.000000044x + 0.4999999721x^2 + \\ 0.1666663308x^3 + 0.04167069796x^4 + 0.008317273866x^5 + \\ 0.001420233805x^6 + 0.000166139345x^7 + 0.00004117752315x^8 \\ -0.0000000373624797e^x \end{cases} \quad (26)$$

Example 3. Consider the Third-order Volterra integro-differential equation [11]

$$\frac{d^3y}{dx^3} - x\frac{d^2y}{dx^2} = \frac{4}{7}x^9 - \frac{8}{5}x^7 - x^6 + 6x^2 - 6 + 4\int_0^x x^2t^3\, y(t)dt \qquad x \in [0,1] \qquad (27)$$

Subject to initial conditions

$$\begin{cases} y(0) = 1 \\ \frac{dy}{dx}(0) = 2 \\ \frac{d^2y}{dx^2}(0) = 0 \end{cases} \qquad (28)$$

Analytical solution $y(x) = -x^3 + 2x + 1$ \qquad (29)

EFCAT technique

Comparing equation (27) with equation (14) and $\psi(x) = 4$

Choosing computational length N=8, we have linear system of equation

$$\begin{cases} (-x_i{}^6)q_0 + \\ \left(-\frac{4}{5}x_i{}^7\right)q_1 + \left(-2x_i - \frac{2}{3}x_{i_i}{}^8\right)q_2 + \\ \left(-6x_i + 6 - \frac{4}{9}x_i{}^9\right)q_3 + \left(-12x_i{}^3 + 24x_i{}^3 - \frac{1}{2}x_i{}^{10}\right)q_4 + \\ \left(-20x_i{}^4 + 60x_i{}^2 - \frac{4}{9}x_i{}^{11}\right)q_5 + \left(-30x_i{}^4 + 120x_i{}^3 - \frac{2}{5}x_i{}^{12}\right)q_6 + \\ \left(-42x_i{}^6 + 210x_i{}^4 - \frac{4}{11}x_i{}^{13}\right)q_7 + \left(-56x_i{}^7 + 336x_i{}^5 - \frac{1}{3}x_i{}^{14}\right)q_8 + \\ -\begin{Bmatrix} 32768x_i{}^8 - 131072x_i{}^7 + 212992x_i{}^6 - 180224x_i{}^5 \\ -84480x_i{}^4 - 21504x_i{}^3 + 2688x_i{}^2 - 128x_i + 1 \end{Bmatrix}\tau_1 \\ -\begin{Bmatrix} 8172x_i{}^7 - 28672x_i{}^6 + 39424x_i{}^5 - 26880x_i{}^4 \\ +9408x_i{}^3 - 1568x_i{}^2 + 98x_i - 1 \end{Bmatrix}\tau_2 \\ -\begin{Bmatrix} 2048x_i{}^6 - 6144x_i{}^5 + 6912x_i{}^4 - 3584x_i{}^3 + \\ 640x_i{}^2 - 72x_i + 1 \end{Bmatrix}\tau_3 \\ = \left(\frac{4}{9}x_i{}^9 - \frac{8}{5}x_i{}^7 - x_i{}^6 + 6x_i{}^2 - 6\right) \end{cases} \quad (30)$$

Collocate equation (30) as follows:

$$x_i = a + \frac{(b-a)i}{N+2}; \quad i = 1,2,3\ldots\ldots N + 1 \text{ Where } a = 0 \;, b = 1 \;, N = 8$$

$$x_1 = \frac{1}{10}, x_2 = \frac{2}{10}, x_3 = \frac{3}{10}, x_4 = \frac{4}{10}, x_5 = \frac{5}{10}, x_6 = \frac{6}{10}, x_7 = \frac{7}{10}, x_8 = \frac{8}{10}, x_9 = \frac{9}{10}$$

Consider initial condition (28) and using MAPLE 18 software to obtain twelve (12) unknown constants of equations (30), thus we obtain the following constants

$$\begin{cases} q_0 = 1.0000000000000, \quad q_1 = 2.00000000 \\ q_2 = 0.000000000190070, q_3 = -1.0000000000 \\ q_4 = 0.000000000084219129, \quad q_5 = -0.00000000007143969 \\ q_6 = 0.0000000151048311, \quad q_7 = -0.00000000130707181 \\ q_8 = 0.000000000415825808, \tau_1 = -0.000000000030283257 \\ \tau_2 = -0.000000000515148426, \tau_3 = -0.000000000019007089 \end{cases}$$

Substitute the above values into approximate solution (5).The approximate solution of
Third-order Volterra integro-differential equation (27) can be written as

$$y(x) \approx \begin{cases} 1.00000000 + 2.00000000\ x + 0.000000000190070x^2 \\ -1.0000000000x^3 + 0.000000000084219129x^4 \\ -0.00000000007143969x^5 + 0.00000000151048311x^6 \\ + 0.00000000151048311x^6 - 0.00000000130707181x^7 \\ +0.000000000415825808x^8 - 0.000000000019007089e^x \end{cases} \quad (31)$$

Example 4. Consider the Fifth -order Fredholm integro-differential equation

$$\frac{d^5y}{dx^5} - x^2\frac{d^3y}{dx^3} - \frac{dy}{dx} - xy(x) = x^2\cos(x) - x\sin(x) + 4\int_{-1}^{1} y(t)dt \qquad x \in [-1,1] \quad (32)$$

subject to initial conditions

$$\begin{cases} y(0) = 0 \\ \frac{dy}{dx}(0) = 1 \\ \frac{d^2y}{dx^2}(0) = 0 \\ \frac{d^3y}{dx^3}(0) = -1 \\ \frac{d^4y}{dx^4}(0) = 0 \end{cases} \qquad (33)$$

Analytical solution $y(x) = \sin(x)$. (34)

EFCAT technique
Comparing equation (32) with equation (16) and when $\psi(x) = 4$
Choosing computational length N=8, we obtain a linear system of equations

$$\begin{cases}
(-x_i + 8)q_0 + (-x_i{}^2 - 1)q_1 + \left(-x_i{}^3 - 2x_i - \frac{8}{3}\right)q_2 + (-x_i{}^4 - 9x_i{}^2)q_3 + \\
\left(-x_i{}^5 - 28x_i{}^2 - \frac{8}{5}\right)q_4 + (-x_i{}^6 - 65x_i{}^4)q_5 + \left(-x_i{}^7 - 126x_i{}^5 - \frac{5032}{7}\right)q_6 \\
(-x_i{}^8 - 217x_i{}^6 + 5040x_i)q_7 + \left(-x_i{}^9 - 344x_i{}^7 + 20160x_i{}^2 - \frac{8}{7}\right)q_8 \\
\quad -\begin{Bmatrix} 32768x_i{}^8 - 131072x_i{}^7 + 212992x_i{}^6 - 180224x_i{}^5 - \\ 84480x_i{}^4 - 21504x_i{}^3 + 2688x_i{}^2 - 128x_i + 1 \end{Bmatrix}\tau_1 \\
\quad -\begin{Bmatrix} 8172x_i{}^7 - 224x_i{}^5 - 26880x_i{}^4 + \\ 9408x_i{}^3 - 1568x_i{}^2 + 98x_i - 1 \end{Bmatrix}\tau_2 \\
\quad -\begin{Bmatrix} 2048x_i{}^6 - 6144x_i{}^5 + 6912x_i{}^4 - 3584x_i{}^3 \\ +640x_i{}^2 - 72x_i + 1 \end{Bmatrix}\tau_3 \\
\quad -\begin{Bmatrix} 512x_i{}^5 - 128x_i{}^4 + 1120x_i{}^3 - 400x_i{}^2 \\ +50x_i - 1 \end{Bmatrix}\tau_4 \\
\quad -\begin{Bmatrix} 128x_i{}^4 - 258x_i{}^3 + 160x_i{}^2 \\ -32x_i + 1 \end{Bmatrix}\tau_5 = x_i{}^2\cos(x_i) - x_i\sin(x_i)
\end{cases} \quad (35)$$

Collocate equation (35) as follows:

$$x_i = a + \frac{(b-a)i}{N+2}; \quad i = 1,2,3 \ldots\ldots N + 1 \text{ where } a = 0 \text{ , } b = 1 \text{ , } N = 8$$
$$x_1 = \frac{1}{10}, x_2 = \frac{2}{10}, x_3 = \frac{3}{10}, x_4 = \frac{4}{10}, x_5 = \frac{5}{10}, x_6 = \frac{6}{10}, x_7 = \frac{7}{10}, x_8 = \frac{8}{10}, x_9 = \frac{9}{10}$$

Consider initial condition (33) and using MAPLE 18 software to obtain fourteen (14) unknown constants of equations (35), thus we obtain the following constants

$$\begin{cases}
q_0 = 0.001882931290, \quad q_1 = 1.001882931 \\
q_2 = 0.0009414656452, \quad q_3 = -0.1663528448 \\
q_4 = 0.00007845547043, \quad q_5 = 0.003352490348 \\
q_6 = 0.001374368978, \quad q_7 = -0.0000000715278865 \\
q_8 = -0.0000310258822, \tau_1 = 0.0000000328467432 \\
\tau_2 = 0.000001712327853, \tau_3 = 0.000002396932743 \\
\tau_4 = -0.0004291360005, \tau_5 = -0.00188293129
\end{cases}$$

Substitute the above values into approximation solution (5). The approximate solution of Fifth-order Fredholm integro-differential equation (31) can be written as

$$y(x) \approx \begin{cases}
0.001882931290 + 1.001882931x + 0.0009414656452x^2 - \\
0.1663528448x^3 + 0.00007845547043x^4 + 0.003352490348x^5 + \\
0.001374368978x^6 - 0.0000000715278865x^7 - \\
0.0000310258822x^8 - 0.00188293129 \, e^x
\end{cases} \quad (36)$$

3. Numerical results

Table 2: Analytical and Numerical results   Example 1

x	Analytical solution	EFCAT solution	TimothyA. Anake [9]	Absolute Error E_{EFCAT}	Absolute Error $E_{[9]}$
0.0	10.00000000	10.00000000	10.00000000	0.000000000	0.000000000
0.1	9.909516258	9.909516343	9.909518155	0.000000085	0.000000000

0.2	9.836253849	9.836253909	9.836255661	0.000000060	0.000001812
0.3	9.777754534	0.777754572	9.777756147	0.000000038	0.000001613
0.4	9.731871982	9.731871988	9.731873400	0.000000006	0.000001418
0.5	9.696734670	9.696734654	9.696735769	0.000000016	0.000001099
0.6	9.670713018	9.670712980	9.670713761	0.000000038	0.000000743
0.7	9.652390287	9.652390219	9.652390809	0.000000068	0.000000522
0.8	9.640536829	9.640536736	9.640537243	0.000000093	0.000000414
0.9	9.634087306	9.634087186	9.634087439	0.000000120	0.000000133
1.0	9.632120559	9.632120518	9.632120150	0.000000041	0.000000405

Table 3:   Analytical and Numerical results   Example 2

x	Analytical solution	EFCAT solution	Akinboro et al [10]	Absolute Error E_{EFCAT}	Absolute Error $E_{[10]}$
0.0	0.000000000	0.0000000000	0.0000000000	0.0000000000	0.0000000000
0.1	0.105170918	0.1051709175	0.1051709278	0.0000000005	0.0000000098
0.2	0.221402758	0.2214027563	0.2214027799	0.0000000017	0.0000000236
0.3	0.349858808	0.3498588044	0.3498587427	0.0000000036	0.0000000617
0.4	0.491824698	0.4918246921	0.4918247080	0.0000000056	0.0000000100
0.5	0.648721271	0.6487212613	0.6487212399	0.0000000097	0.0000000311
0.6	0.822118800	0.8221187864	0.8221188288	0.0000000012	0.0000000288
0.7	1.013752707	1.013752688	1.0137527320	0.0000000019	0.0000000250
0.8	1.225540928	1.225540903	1.2255410370	0.0000000025	0.0000001090
0.9	1.459603111	1.459603080	1.4596032700	0.0000000031	0.0000001590
1.0	1.718281828	1.718281795	1.7182822950	0.0000000033	0.0000004670

Table 4:   Analytical and Numerical results   Example 3

x	Analytical solution	EFCAT solution	Jalil and Ali [11]	Absolute Error E_{EFCAT}	Absolute Error $E_{[11]}$
0.0	1.000000000	1.000000000	1.000000000	0.0000000000	0.0000000000
0.1	1.199000000	1.199000000	1.199000000	0.0000000000	0.0000000000
0.2	1.392000000	1.392000000	1.392000000	0.0000000000	0.0000000000
0.3	1.573000000	1.573000000	1.573000000	0.0000000000	0.0000000000
0.4	1.736000000	1.736000000	1.736000000	0.0000000000	0.0000000000
0.5	1.875000000	1.875000000	1.875000000	0.0000000000	0.0000000000
0.6	1.984000000	1.984000000	1.984000000	0.0000000000	0.0000000000
0.7	2.057000000	2.057000000	2.057000000	0.0000000000	0.0000000000
0.8	2.088000000	2.088000000	2.088000000	0.0000000000	0.0000000000
0.9	2.071000000	2.071000000	2.071000000	0.0000000000	0.0000000000
1.0	2.000000000	2.000000000	2.000000000	0.0000000000	0.0000000000

Table 5:   Analytical and Numerical results   Example 4

x	Analytical solution	EFCAT solution	Absolute Error E_{EFCAT}
-1.0	-0.8414709840	-0.8353290012	0.0061419836
-0.8	-0.7173560909	-0.7154055909	0.0019505000
-0.6	-0.5646424734	-0.5641959781	0.0004464953

-0.4	-0.3894183423	-0.3893619029	0.0000564394
-0.2	-0.1986693308	-0.1986676467	0.0000016841
0.0	0.0000000000	0.0000000000	0.0000000000
0.2	0.1986693308	0.1986678220	0.0000015088
0.4	0.3894183423	0.3893730997	0.0000452426
0.6	0.5646424734	0.5643229354	0.0003195380
0.8	0.7173560909	0.7161143586	0.0012417323
1.0	0.8414709848	0.8380103627	0.0034606221
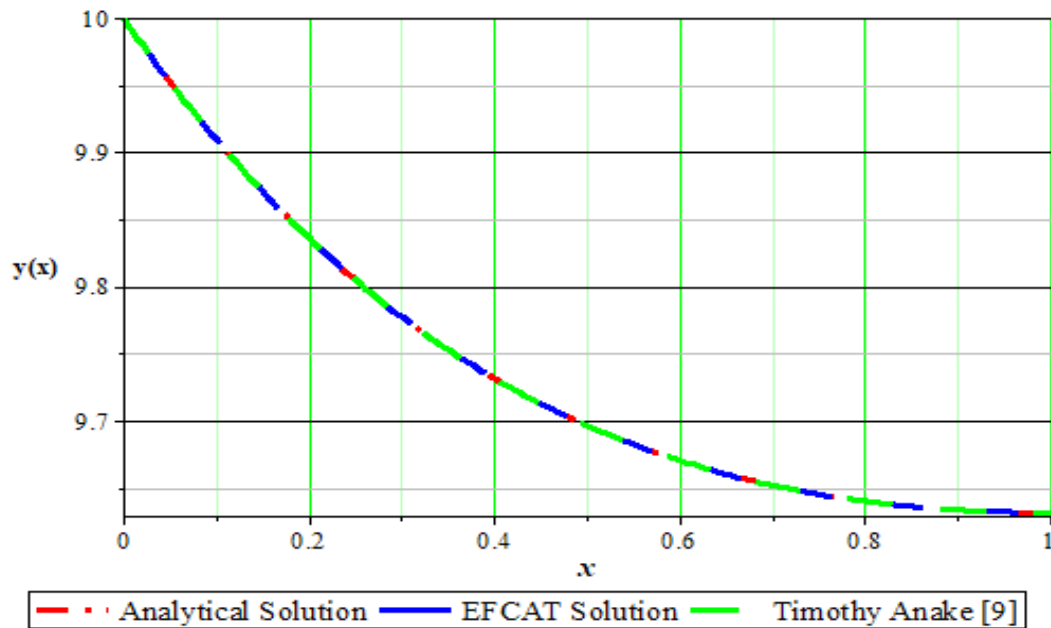
Figure 1. First-order Volterra Integro-differential equation   Example 1
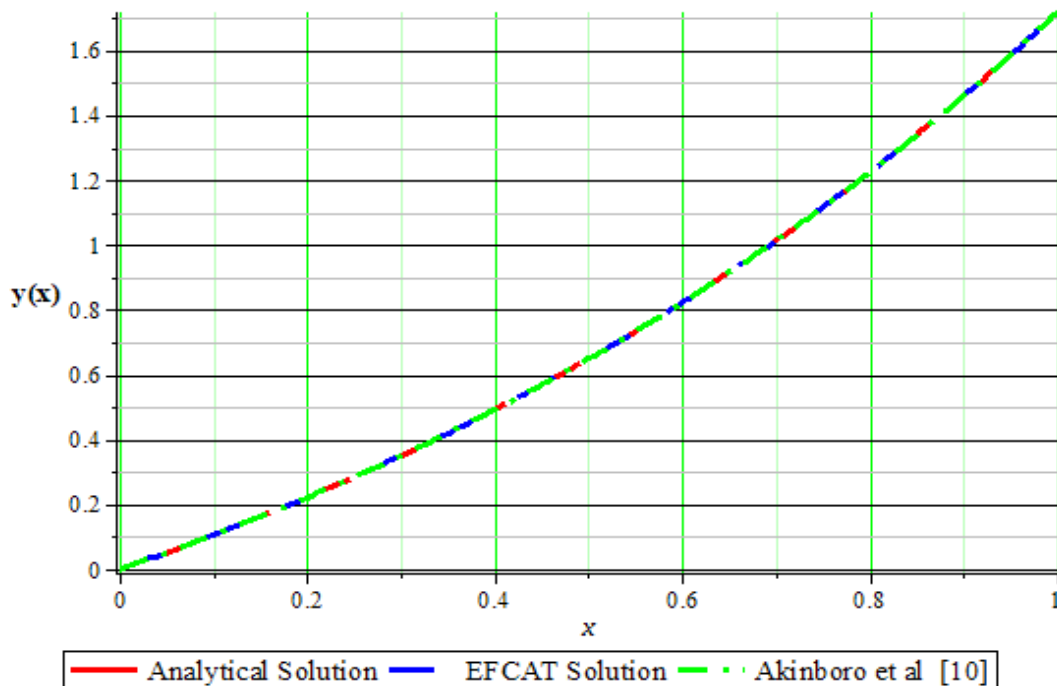
Figure 2. Second-order Volterra Integro-differential equation   Example 2

83
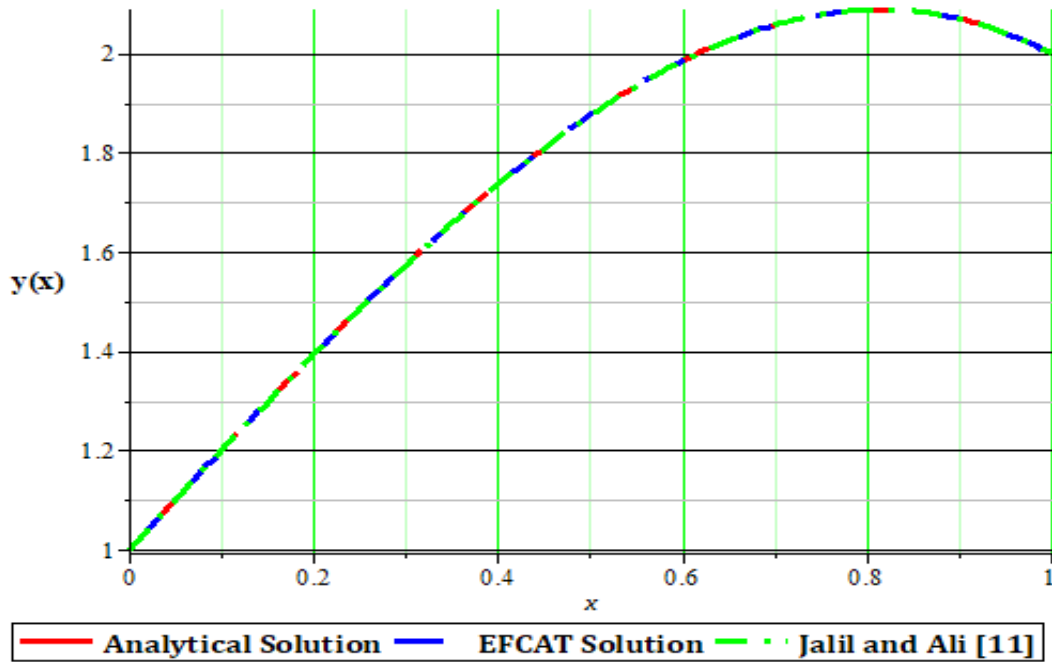
Figure 3. Third-order Volterra Integro-differential equation   Example 3
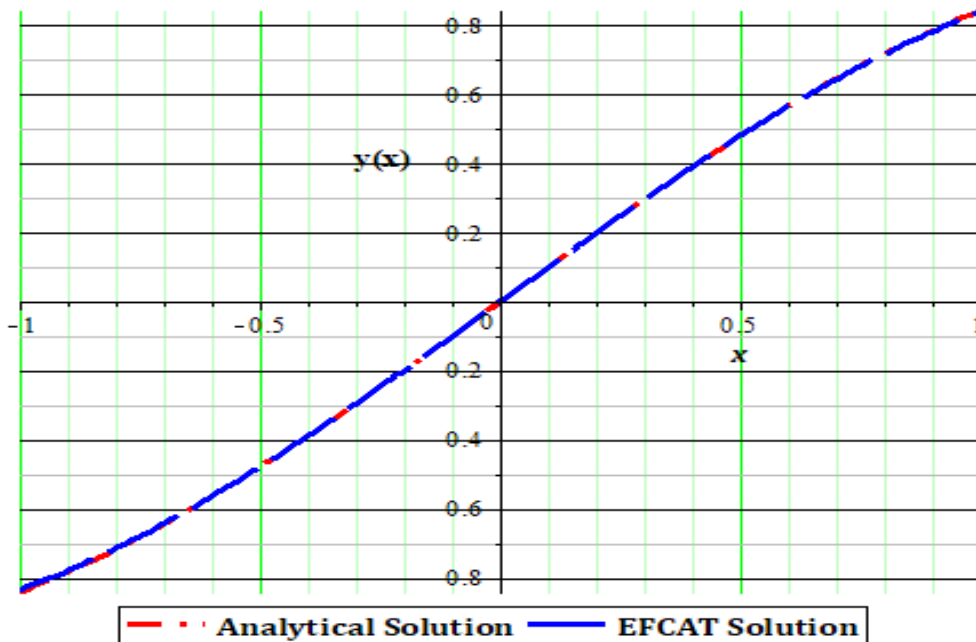
Figure 4. Fifth-order Fredholm Integro-differential equation   Example 4

5. Conclusion

The proposed technique has been successfully applied to find numerical solution of the $1^{st}, 2^{nd},$ $3^{rd},$ and 5th–orders Volterra and Fredholm integro-differential equations. In order to investigate the accuracy of the method, four examples were considered and the numerical solutions were compared to

the analytical solution and some existing methods available in the literature. The comparison of absolute errors (table 2, table 3, table 4 and table 5) of the results obtained by the present method with analytical solution and existing method give close or same results obtained by [9],[10],[11]. Moreover, the method is efficient and reliable for the numerical solutions of integro-differential equations of Volterra and Fredholm type as illustrated in all examples consider. We conclude that the proposed technique is a promising tool to solve higher order integro-differential equations and many applied problems in mathematical physics.

Acknowledgment

References

[1] P. Linz, *Analytic and Numerical Methods for Volterra Equations*, SIAM, Philadelphia, Pa, USA, Pp 132-139, 1985.

[2] G. Adomian, *Solving Frontier problems of physics: The decomposition method*, Kluwer Pp 123-134, 1994.

[3] J.H. He, "Homotopy perturbation technique", *Computation Meth. Appl. Mech. Eng.*, 178, 257-262 1999.

[4] J.H. He, "Approximate analytical solution for seepage flow with fractional derivatives in porous media", *Computer. Meth. Appl. Mech. Engn.*, 167, 57-68, 1998.

[5] O.A. Taiwo, K.I. Falade and A. K. Bello "Application of Collocation Methods for the numerical solution of Integro – Differential Equations by Chebyshev Polynomials", *Intern. Journal of Biological and Physical Sciences,* 16, 12 – 20, 2011.

[6] R. Kanwall, K. Liu. "A Taylor expansion approach for solving integral equations". *International Journal of Mathematical Education in Science and Technology*, 20, 411–414, 1989.

[7] S. Yuzbasi, N. Sahin, M. Sezer. "Bessel polynomial solutions of high-order linear Volterra integro-differential equations". *Computers & Mathematics with Applications*, 62, 1940–1956, 2011.

[8] Falade K.I, "Numerical Solution of Higher Order Singular Initial Value Problems (SIVP) by Exponentially Fitted Collocation Approximate" *Method American International Journal of Research in Science, Technology, Engineering & Mathematics*, 21(1), 48-55, 2017.

[9] Olumuyiwa A. Agbolade and Timothy A. Anake "Solutions of First-Order Volterra Type Linear Integrodifferential Equations by Collocation Method" *Hindawi Journal of Applied Mathematics*, Article ID 1510267, page 3, 2017.

[10] S. Alao, F.S. Akinboro, F.O. Akinpelu, R.A. Oderinu Numerical "Solution of Integro-Differential Equation Using Adomian Decomposition and Variational Iteration Methods." IOSR *Journal of Mathematics (IOSR),* 10(4),20, 2014.

[11] Jalil Rashidinia and Ali Tahmasebi "Approximate solution of linear integro-differential equations by using modified Taylor expansion method" *World Journal of Modelling and Simulation*, 9(4), 300, 2013.
.
.

INTERNATIONAL
ENGINEERING,
SCIENCE AND
EDUCATION
GROUP

INESEG

THE EFFECTS OF PRETREATMENT FACTORS ON SEED GERMINATION AND SEEDLING GROWTH OF ANISE (*PIMPINELLA ANISUM L.)*

Mohamad Hesam Shahrajabian[1,2,3]*, Mehdi Khoshkharam[3], Wenli Sun[1,2], Qi Cheng[1,2]
ORCID:0000-0002-8638-1312   ORCID:0000-0002-9301-801X   ORCID:0000-0002-1705-2996   ORCID:0000-0003-1269-6386

[1]Biotechnology Research Institute, Chinese Academy of Agricultural Sciences, Beijing 100081, China
[2]Nitrogen Fixation Laboratory, Qi Institute, Building C4, No.555 Chuangye, Jiaxing 314000,
Zhejiang, China
[3]Department of Agronomy and Plant Breeding, Faculty of Agriculture, Islamic Azad University,
Isfahan (Khorasgan) Branch, Isfahan, Iran
*Corresponding author:hesamshahrajabian@gmail.com

Abstract:*Seed dormancy is one of the major problems in agricultural studies, especially for medicinal plants. Anise (Pimpinella anisum L.)is an important economic medicinal plant with dormant seeds and distributed only in its natural habitats. An experiment was conducted as a Factorial layout within a completely randomized design with four replications to evaluate the effects of some pretreatment factors on primary growth and germination characteristics of anise.Pre-chilling treatments were 0, 15, 30 and 45 days treatments and hormone treatments were GA₃ (Gibberellic Acid), BA (benzyladenine), kinetin (Kinetinnetin), GA₃+BA, GA₃+kinetin BA+kinetin, GA₃+BA+kinetin, KNO₃, H₂SO₄ and distilled water as a control treatment.Prechilling treatment effects on coleoptile and radicle length, seedling length, germination percentage, mean time for germination, germination rate and seed vigor index showed significant differences (p<0.01) among them. Similarly,different hormone treatments also had significantly different influence on coleoptile and radicle length, seedling length, germination percentage, mean time germination, germination rate and seed vigor index. The highest germination percentage and germination rate was related to the usage of BA+ kinetin. The highest values for radicle length and uniformity of seed germination were achieved in BA and kinetin, respectively. Moreover, application of GA₃+BA+kinetin had given the highest seed vigor index. It seems that application of exogenous GA₃+KİNETİN and BA+kinetin concentration, which is provided mostly by chilling treatment, is the most effective factor for breaking the seed dormancy. On the basis of the results, usage of 45 days moist prechilling accompanied with application of GA₃+kinetin and BA+kinetin in Esfahan cultivar was appropriate.*

Keywords: *Seed dormancy, Seed germination, Seedling growth, Anise*

1.Introduction

Anise (*Pimpinella anisum L.*) is a flowering plant in the family Apiaceae native to the eastern Mediterranean region, west and Southwest Asia [1-2-3]. Anise is also famous in traditional Chinese medicine (TCM), Ayurveda and Unani medicine. Anise has been used for different purposes in the traditional medicine system of Iran [4]. Seed priming treatments have been employed to accelerate germination, seedling growth and yield in most seeds under normal and stress conditions [5-6-7-8-9-10-11]. Seed germination can be controlled by many factors like natural germination and growth inhibitors [12-13-14-15]. These are the derivatives of gibberellic acid (GA_3), abscisic acid (ABA), cinnamic acid, kinetinnetin (KİNETİN), bonzyladenin (BA), coumarin, jasmonic and etc. The variation in seed dormancy and seedling emergence are controlled by environmental conditions. The origin of research into Gibberellins can be traced to Japanese plant pathologists who were investigating the causes of the bakane (foolish seedling) disease that seriously lowered to the yield of rice crop in Japan, Taiwan, and some other Asian countries [16]. Gibberellic acid is a plant growth hormone that has an important role in seed germination [16]. It has been reported that the stimulating effects of GA_3 on seed germination are not similar in all crop species [17]. GA_3 has been also reported to promote growth in cotton, rice and in some halophytes under saline conditions [18-19]. Tsygankova et al. [20] confirmed specific auxin-like, cytokinetinnin-like and minor gibberellins-like effect of synthetic heterocyclic compounds on cell division, cell proliferation, cell elongation and cell differentiation that are the basic processes of plant growth and development. Gibberellins is known to eliminate the chilling requirements of peach and apple seed and increased their germination [21]. Primed with gibberelin improve quality of seeds and germination [22]. Liopa-Tsakalidi et al. [23] also suggest that germination and seedling growth of 11 species responded differently to different levels of GA_3. Fernandez et al. [24] revealed that cold stratification has a direct influence on the production of gibberellins (Gas) in seeds of *Arabidopsis thaliana*. Exogenously applied GA overcomes seed dormancy in several species [25]. Hormone priming increased antioxidant enzyme activity and decrease the amount of reactive oxygen space.Sharifi and Pouresmael [26] concluded that only cold treatments such as gibberellic acid, cytokinetinnin, potassium nitrate, washing and light treatments are not useful. It has been reported that GA is effective in breaking seed dormancy in snowberry [27]. Nkomo and Kambizi [28] noted that prechilling followed by exposure to a temperature higher than 30ºC encourages the germination of *C. Olitorious* seeds. Rouhi et al. [29] concluded that applying 500 ppm concentration of GA_3 and KNO_3 resulted in higher germination in waterlily dormant seeds. Plant hormones are used in breaking seed dormancy [30]. Cytokinins and auxin are the most common plant growth regulators used in in vitro culture of plant tissues [31-32]. Cytokinins constitute a major class of plant growth regulator that is involved in a wide range of physiological processes [33]. Cytokinins have a stimulatory or an inhibitory role in different development processes, such as control of apical dominance in the shoot, root growth and branching, leaf senescence, and chloroplast development [34]. In spite of the fact that Anise is an important and expensive medicinal and spice plant, not enough information is available on the effects of moist pre-chilling and application of hormones on different cultivars of it. So, the aim of this study is to survey the certain effects of different treatments to stimulate seed germination and seedling growth of Anise.

2.Materials and methods

The study evaluates the influence of some pretreatments on growth and germination characteristics of anise (*Pimpinella anisum L.*), an experiment was conducted as Factorial layout within completely randomized design with four replications at Research laboratory of Mojgan Agricultural Company, Mahmood Abad, Isfahan, Iran. Pre-chilling treatments were 0, 15, 30 and 45 days treatments and hormone treatments were GA_3 (Gibberellic Acid), BA (benzyladenine), kinetin, GA_3+BA, GA_3+ kinetin, BA+ kinetin, GA_3+BA+ kinetin, KNO_3, H_2SO_4 and distilled water as a control treatment. First, seeds were surface sterilized in 1.5% (w/v) sodium hypochlorite solution for 15 minutes and then rinsed three times with sterile distilled water. For each treatment, 4 Petri dishes were used and 30 seeds were put into each of them, then, each Petri dish was covered with 10 mm of each specific treatment. In the first trial, seeds were chilled for 15, 30 and 45 days, and after that, seeds were soaked and treated with 10 hormone treatments. In the second experiment, the seeds were treated without pre-chilling treatments. In the thirds experiment, seeds treatments were done with polyethylene glycol. Equation number one and number two were used to calculate germination percentage and germination rate, respectively.

Germination percentage= (Number of germinated seed /total number of seed) $\times$ 100   (1)

1) $GR = \Sigma \dfrac{N}{\Sigma(n \times g)}$ (2)

Where N is the number of germinated seed on growth day and g is the number of germination seeds Analysis of variance (ANOVA) was used to determine the significant differences. Uniformity of seed germination and mean time for seed germination (MTG) was evaluated by equation number 3 and 4. Seed vigor index was calculated by equation number 5.

Uniformity of seed germination= $\dfrac{1}{\dfrac{\sum (D - \overline{D})^2 \times N}{\sum N}}$ (3)

$MTG = \dfrac{\Sigma(nd)}{\Sigma n}$ (4)

n: The number of germinated seed in the specific day.
d: The number of days from the beginning of germination.
$\sum$n: The total number of germinated seed.

Seed vigor index: Germination percentage $\times$ mean of seedling length (mm)(both coleoptile and radicle) / 100   (5)

The means were separated by Duncan's Multiple Range Test   ($p<0.05$). All statistical analysis was performed with the SAS computer statistical software.

3.Results and discussion

Prechilling had a significant impact on coleoptile length, radicle length, seedling length, germination percentage, mean time for germination, germination rate and seed vigor index was evaluated. The highest coleoptile length was related to 45 days chilling (2.45 mm) which had significant differences with other treatments. Although, the higher value of radical length was obtained for 45 days (0.8485 mm) chilling, its difference with 30 days chilling was not significant. The minimum coleoptiles (0.7536 mm) and radical length (0.6819 mm) was related to control treatment. The higher values of seedling length (2.98 mm), and germination percentage (70.02%) was obtained for 45 days of chilling followed by chilling for 30 days, 15 days and 0 days (control treatment). There were significant differences in seedling length and germination percentage between 45 days of chilling and other treatments. Control treatment had obtained the highest mean time for germination (11.18) which had significant differences with 30 days and 45 days pre-chilling, although, its difference with control treatment was not significant. The maximum value for uniformity of germination rate (5.87%), and seed vigor index (2.244) was achieved in 45 days pre-chilling which had significant differences with other treatments. Both the germination rate and seed vigor index was increased significantly from control treatment to 45 days pre-chilling. The maximum and the minimum uniformity of seed germination was related to control treatment (0.2165), and 15 days pre-chilling (0.1075), which had no significant differences with each other (Table 1). Gupta et al. [30] reported that prechilling treatment also improved seed germination in Isabgol.

The highest coleoptiles length (1.663 mm), and seedling length (2.574 mm) was related to the application of GA_3+ kinetin and the minimum one was observed in KNO_3. Patel and Mankad [16] concluded that low concentrations of GA_3 influence all developmental and physiological processes in plants. The maximum and the minimum radical length was related to the application of BA (1.7232 mm), and KNO_3 (0.5286 mm), respectively, which had significant differences with each other. Benzyladenine (BA) at a high concentration was also shown to be effective in shoot regeneration in *P. vulgaris* [35]. Application of BA + kinetin had obtained the highest value for germination percentage (66.33%) and germination rate (4.126%), which had significant differences with other treatments. Sawan et al. [36] demonstrated that kinetinnetin application improved seed viability and seedling vigor as shown by lengths of the hypocotyls, radical and the entire seedling, as well as seedling fresh weight. Gibberellic acid is also known to play an essential role in seed germination, stem elongation and flower development [37]. The maximum and the minimum mean time for germination was achieved in usage of BA + kinetin (66.33), and KNO_3 (25.45), respectively. Narra et al. [38] also found that the seedling under the GA_3 influence showed enhanced germination, seedling elongation and dry weight accumulation on *Trachyspermum ammi*. Although the higher value for uniformity of seed germination was related to kinetin (0.1523), followed by other treatments, there were no significant differences between treatments. application of ga$_3$+ba+ kinetin had obtained the highest seed vigor index (1.545), and the minimum one was related to the application of distilled water (0.4076) (Table 1). The efficacy of BA in inducing multiple shoots was also demonstrated in chickpea [39], mungbean [40] and pigeonpea [41]. Gupta et al. [30] concluded that GA has shown promising effect in breaking seed dormancy with accelerated seed germination (speed of germination, vigor index) and seedling growth (seedling dry weight).

Table 1. Mean comparison for coleoptile length (mm), radicle length (mm), seedling length (mm), germination percentage (%), meantime for germination, germination rate (%), uniformity of seed germination and seed vigor index.

Treatment	Coleoptile length	Radicle length	Seedling length	Germination percentage	Meantime for germination	Germination rate	Uniformity of seed germination	seed vigor index
Prechilling (day)								
0	0.7536d	0.6819bc	1.463c	14.22d	11.18a	0.3626d	0.2165a	0.3287d
15	1.000c	0.5625c	1.554c	35.28c	11.00a	1.489c	0.1075a	0.6328c
30	1.340b	0.7635ab	2.133b	53.74b	7.81b	3.356b	0.1336a	1.239b
45	2.145a	0.8485a	2.986a	70.02a	5.52c	5.87a	0.1352a	2.244a
Hormone								
GA₃	1.352bc	0.8112abc	2.185b	37.91d	10.44a	2.533d	0.1471b	1.056ab
BA	1.428abc	1.7232bcd	2.143bc	61.22b	9.862a	3.837b	0.1066b	1.365ab
KİNETİN	1.536ab	0.8687ab	2.385ab	47.33c	9.575a	3.199b	0.1523b	1.351ab
GA₃+BA	1.345bc	0.6835cd	2.036bc	52.26b	10.61a	3.007bc	0.1474b	1.263bc
GA₃+KİNETİN	1.663a	0.9123a	2.574a	40.23cd	10.66a	2.673cd	0.1132b	1.484ab
BA+KİNETİN	1.425abc	0.7348be	2.176bc	66.33a	9.74a	4.126a	0.1035b	1.464ab
GA₃+BA+KİNETİN	1.563abc	0.8140abc	2.356ab	54.00b	10.28a	3.179b	0.1202b	1.545a
KNO₃	0.7537d	0.5286e	1.343d	25.45e	6.40b	1.855e	0.1148b	0.4661de
H₂SO₄	1.256c	0.5573de	1.915c	25.69e	6.26b	1.632e	0.1242b	0.6842d
Distilled water	0.8223d	0.5647de	1.465d	25.68e	5.48b	1.987e	0.1247b	0.4076e

Common letters within each column do not differ significantly.
GA₃= Gibberellic Acid
KİNETİN= Kinetinnetin
BA= Benzyladenine

4. Conclusion

Seed germination is a complex physiological process that responds to environmental signals such as light, water, and other factors. Also, Seed germination is very important to know the germination pattern of a plant, especially the medicinal plants. Prechilling treatment effects on coleoptile and radicle length, seedling length, germination percentage, mean time for germination, germination rate and seed vigor index were significant. Different hormone treatments had a significant influence on coleoptile and radicle length, seedling length, germination percentage, mean time germination, germination rate, and seed vigor index. Prechilling treatment for 45 days had obtained the highest coleoptile and radicle length, seedling length, germination percentage, germination rate, and seed vigor index. While control treatment had obtained the maximum mean time for germination and uniformity of seed germination. Application of GA₃+kinetin had obtained the highest coleoptile length, seedling length, and mean time for germination. The highest germination percentage and germination rate was related to the usage of BA+kinetin. The higher values for radicle length and uniformity of seed germination were achieved in the application of BA and kinetin, respectively. Moreover, application of GA₃+BA+kinetin had resulted in the highest seed vigor index. All in all, in conclusion, it was shown that GA₃, kinetin, and BA had greatly enhanced the germination parameters in terms of germination percentage, seedling elongation and other characteristics.

References

[1] Kadan, S., Rayan, M., Rayan, A., ''Anticancer activity of Anise (*Pimpinella anisum L.*) seed extract'',*The Open Nutraceuticals Journal*, 6, 1-5, 2013.

[2]   Saxena, S.N., Verma, M., Kakani, R.K., Rathore, S.S., Saxena, R., Sharma, L.K., ''Analysis of medicinally important compounds and antioxidant properties of Anise (*Pimpinella anisum*) seed extract and shoot callus'', *International J. Seed Spices*, 4(1), 55-62, 2014.

[3] Ibrahim Doaʾan Anwar., ''Medicinal benefits of Anise seeds (*Pimpinella Anisum*) and *Thymus Vulgaris* in a sample of healthy volunteers''. *Int. J. Res. Ayurveda Pharm.*, 8(3), 91-95, 2017.

[4] Shojaii, A., Abdollahi Fard, M., ''Review of pharmacological properties and chemical constituents of *Pimpinella anisum''*. *ISRN Pharmaceutics*. Article ID 510795, 8 pages, 2012.

[5] Ashraf, M., Foolad, M.R., ''Pre-sowing seed treatments shotgun approach to improve germination, plant growth and crop yield under saline and non-saline conditions'', *Advances in Agronomy*., 88, 223-271, 2005.

[6] Shahrajabian, M.H., Soleymani, A., Naranjani, L., ''Grain yield and forage characteristics of forage sorghum under different plant densities and nitrogen levels in second cropping after barley in Isfahan, Iran'',*Research on Crops.*, 12(1), 68-78, 2011.

[7] Shahrajabian, M.H., Xue, X., Soleymani, A., Ogbaji, P.O., Hu, Y., "Evaluation of physiological indices of winter wheat under different irrigation treatments using weighing lysimeter",*International Journal of Farming and Allied Sciences,* 2(24), 1192-1197, 2013.

[8] Shahrajabian, M.H., Wenli, S., Qi, C., ''The power of natural Chinese medicine, ginger root in an organic life", *Middle-East Journal of Scientific Research*., 27(1), 64-71, 2019.

[9]   Mahdavi, B., "Effects of priming treatments on germination and seedling growth of Anise (*Pimpinella anisum L.*)", *Agriculture Science Development*., 5(3), 28-32, 2016.

[10] Soleymani, A., Khoshkharam, M., Shahrajabian, M.H., "Germination rate and initial growth of silage corn grown under various fertility systems",*Research on Crops*., 13(3), 1035-1038, 2012.

[11]   Soleymani, A., Shahrajabian, M.H., Khoshkharam, M., "The impact of barley residue management and tillage on forage maize", *Romanian Agricultural Research*., 33, 161-167, 2016.

[12] Bhardwaj, A.K., Kapoor, S., Naryal, A., Bhardwaj, P., Warghat, A.R., Kumar, B., Chaurasia, O.P., "Effect of various dormancy breaking treatments on seed germination, seedling growth and seed vigour of medicinal plants", *Tropical Plant Research*., 3(3), 508-516, 2016.

[13] Shahrajabian, M.H., Soleymani, A., Khoshkharam, M., "Influence of green manuring from different cover crops and farm yard manures on quantitative and qualitative characteristics of forage corn in low input farming", *Research on Crop Ecophysiology*, 12(2), 62-68, 2017.

[14] Shahrajabian, M.H., Wenli, S., Qi, C., "A review of Goji berry (*Lycium barbarum*) in traditional Chinese medicine as a promising organic superfood and superfruit in the modern industry", *Academia Journal of Medicinal Plants*, 6(12), 437-445, 2018.

[15] Soleymani, A., Shahrajabian, M.H., "Changes in germination and seedling growth of different cultivars of cumin to drought stress", Cercetari *Agronomice in Moldova*, 1(173), 91-100, 2018.

[16] Patel, R.G., Mankad, A.U., "Effect of gibberellins on seed germination of *Tithonia rotundifolia* Blake", *International Journal of InnovativeResearch in Science, Engineering and Technology,* 3(3), 10680- 10684, 2014.

[17] Bell, D.T., Rokich, D.P., Mcchesney, C.J., Plummer, J.A., "Effects of temperature, light and gibberellic acid on the germination of seeds of 43 species native to Western Australia", *J. Vegetat. Sci.*, 6, 797-806, 1995.

[18] Zhao, K.F., Li, M.L., Liu, J.Y., 1986. "Reduction by GA_3 of NaCl-induced inhibition of growth and development in Suaeda ussuriensis", *Austr. J. Plant Physiol*., 13, 547-551, 1986.

91

[19] Lin, C.C., Kao, C.H., "NaCl stress in rice seedlings, starch mobilization and the influence of gibberellic acid on seedling growth", *Bot. Bull. Acad. Sin*., 36, 169-173, 1995.

[20] Tsygankova, V., Andrusevich, Y., Shtompel, O., Myroljubov, O., Hurenko, A., Solomyanny, R., Mrug, G., Frasinyuk, M., Shablyn, O., Brovarets, V., "Study of Auxin, cytokinetin and gibberellins-like activity of heterocyclic compounds derivatives of pyrimidine, pyridine, pyrazole and isoflavones", *European Journal of Biotechnology and Bioscience*, 4(12), 29-44, 2016.

[21] El-Barghathi, M.F., El-Bakkosh, A., "Effect of some mechanical and chemical pre-treatments on seed germination and seedling growth of *Quercus coccifera* (Kemes Oaks)", Jerash Private University, 2005.

[22] Shekari, F., Abbasi, A., Mustafavi, S.H., "Effect of gibberellic acid, salicylic acid and paclobutrazol on oxidative stress in wheat seed under accelerated ageing", *Crop Research*. (1, 2 & 3), 25-32, 2015.

[23] Liopa-Tsakalidi, A., Zakynthinos, G., Varzakas, T., Xynias, I.N., "Effect of NaCl and GA_3 on seed germination and seedling growth of eleven medicinal and aromatic crops", *Journal of Medicinal Plants Research*, 5(17), 4065-4073, 2011.

[24] Fernandez, H., Perez, C., Revilla, M.A., Perez-Gar-cia, F., "The level of GA_3 and GA_{20} may be associated with dormancy release in *Onopordum nervosum* seeds", *Plant Growth Regulation*. 38(2), 141-143, 2002.

[25] Hassan, M.A., Fardous, Z., "Seed germination, pollination and phenology of*Gloriosa superb L.* (Liliaceae)", *Bangladesh Journal of Plant Taxonomy*, 10(1), 95-97, 2003.

[26] Sharifi, M., Pouresmael, M., "Breaking seed dormancy in *Bunium persicum* by stratification and chemical substances", *Asian J. Plant Sci*., 5(4), 695-699, 2006.

[27] Rosner, L.S., Harrington, J.T., Dreesen, D.R., Murray, I., "Effect of gibberellic acid and standard seed treatments on mountain snowberry germination", *Native Plants Journal*, 3(2), 155-162, 2002.

[28] Nkomo, M., Kambizi, L., "Germination studies on*Corchorus olitorius L.* (Tiliaceae) (Jew,s Mallow); a wild leafy vegetable for possible domestication in the Eastern Cape, South Africa", *Aspects of Applied Biology,* 96, 55-59, 2010.

[29] Rouhi, H.R., Tavakkol Afshari, R., Shakarami, K., "Seed treatments to overcome dormancy of waterlily tulip (*Tulipa kaufmanniana Regel*.)", *Australian Journal of Crop Science,* 4(9), 718-721, 2010.

[30] Gupta, A., Parihar, S.S., Choudhary, V.K., Naseem, M., Maiti, R.K., "Germination, dormancy and its removal in Isabgol (*Plantago ovata Forsk*)", *Int. J. Agric. Environ & Biotech*., 1(3), 117-124, 2008.

[31] Eudes, F., Acharya, S., Laroche, A., Selinger, L.B., Cheng, K.J., "Novel method to induce direct somatic embryogenesis, secondary embryogenesis and regeneration of fertile green cereal plants", *Plant Cell, Tissue and Organ Culture*, 73, 147-157, 2003.

[32] Abu-Romman, S.M., Al-Hadid, K.A., Arabiyyat, A.R., "Kinetin is the most effective cytokinin on shoot multiplication from cucumber", *Journal of Agricultural Sciences,* 7(10), 159-165, 2015.

[33] Davies, P.J., ''Plant hormones: Their nature, occurrence and function. In P. J. Davies (Ed.), Plant Hormones: Physiology, Biochemistry and Molecular Biology (pp. 1-12)", Kluwer Academic Publishers, Dordrecht. 1995. http://dx.doi.org/10.1007/978-94-011-0473-9_1

[34] Mok, M.C., "Cytokinins and plant development- An overview. In D. W. S. Mok & M. C. Mok (Eds.), Cytokinnis-Chemistry, Activity, and Function (Chapter 12, pp. 155-166)", Boca Raton: CRC Press. 1994.

[35] Malik, K.A., Saxena, P.K., "Thidiazuron induces high-frequency shoot regeneration in intact seedlings of pea (*Pisum sativum*), chickpea (*Cicer arientinum*) and lentil (*Lens culinaris*)", *Aust J Plant Physiol.*, 19, 731-740, 1992.

[36] Sawan, Z.M., Mohamed, A.A., Sakr, R.A., Tarrad, A.M., "Effect of kinetin concentration and methods of application on seed germination, yield components, yield and fiber properties of the Egyptian cotton (*Gossypium barbadense*)", *Environmental and Experimental Botany,* 44, 59-68, 2000.

[37] Sharma, R.K., Sharma, S., Sharma, S.S., "Seed germination of some medicinal plants of Lahaul and Spiti cold desert (Himachal Pradesh): implications for conservation and cultivation", *Current Science*. 90(8), 1113-1118, 2006.

[38] Narra, H., Mamidala, P., Mehta, P.M., "Gibberellic acid and cycloheximide influenced the growth and biochemical constituents of a medicinally important plant- *trachyspermum ammi* (*I.*) *Sprague*",*Current Trends in Biotechnology and Pharmacy*, 4(1), 596-603., 2010.

[39] Polisetty, R., Paul, V., Deveshwar, J.J., Khetarpal, S., Suresh, K., Chandra, R., "Multiple shoot induction by benzyladenine and complete plant regeneration from seed explants of chickpea (*Cicer arietinum L.*)", *Plant Cell Reports*, 16, 565-571, 1997.

[40] Gulati, A., Jaiwal, P.K., "Plant regeneration from cotyledonary node explants of mungbean (*Vigna radiate L. Wilczek*)",*Plant Cell Rep.*, 13, 523-527, 1994.

[41] Prakash, N.S., Pental, D., Sarin, N.B., "Regeneration of pigeonpea (*Cajanus cajan*) from cotyledonary node via multiple shoot formation", *Plant Cell Rep*. 13, 623-627, 1994.

THE RADIOTHERAPY MIGHT BE A VACCINE FOR IMMUNE RESPONSE

Cengiz Kurtman[1], Iryna Sokur[2], Mahmut Kemal Ozbilgin[3]

[1]MD, Prof.Dr, Ankara University Medical Faculty Department of Radiation Oncology, Ankara, Turkey, ORCID: 0000-0001-9865-2370

[2]MD, Chief Doctor of Kherson Regional Oncological Center, Kherson, Ukraine,

ORCID: 0000-0003-0889-0143

[3]MD, Prof.Dr, Celal Bayar University Medical Faculty Department of Histology and Embryology, Manisa-Turkey, ORCID: 0000-0001-6627-5443

Corresponding author; kurtman@medicine.ankara.edu.tr

Abstract: *Radiotherapy (RT) is one of the most important treatment options of cancer and also may activate the immune response. Because of this, we must discuss the question of "is the radiotherapy vaccine". If RT increases the immune response we must learn some more about the RT effects on the cells, cell surface antigene, immune checkpoints and their inhibition (ICI; CTLA4, PD1, PDL1 inhibition). It will be discussed the role of the radiotherapy and biologic effects of the radiotherapy to activate the immune response, radiotherapy dose, radiotherapy timing and the side effects of immune checkpoints inhibitors. Hypofractionated stereotactic body radiotherapy is widely used in clinical practice to achieve immune response, but with high conformal hypofractionated stereotactic radiotherapy the microenvironment around the cancer tissue such as fibroblast may survive and then may help cancer stem cells progression, and this is a very important subject should be taken into consideration in order to be better understood in future studies.*

1.Introduction

In the multimodally approach we are fighting against cancer with Radiotherapy (RT), Chemotherapy (CT), Surgery (S) and Immunotherapy (IT). There is new information about to use IT and RT. In this paper will be discussed the role of radiotherapy for immune response.

The immune system inhibits cancer cell growth and spread. As seen on Figure 1, also over the basal membrane in the stage 0 (in-situ) epithelial cancer, the Langerhans Cell (L) acts as Antigen Presenting Cells (APC) for an immune response [1].

Figure 1. The Langerhans Cell (L) over the basal membrane in the epithelial tissue.

In tumor microenvironment there are many cells; such as normal epithelial cells, mesenchymal cells, endothelial cells, macrophage (M), tumor-associated macrophage (TAM), fibroblast (F), cancer-associated fibroblast (CAF), dentritic cell (DC), antigen presenting cell (APC), T-B lymphocytes, cancer cells and many dead cells of cancer cells and normal cells. There are many dead tissues and necrotic secretions in the carcinoma microenvironment. These increase with treatments and may protects cancer. Inflammatory response increases pressure and may protect cancer. M2, TAM, CAF, peristicle, collagen tissue may protect cancer. (Figure 2).

Figure 2. Cancer microenvironment has many living and dead cells (Tc: T cytotoxic, T: T lymphocyte, DC: Dentritic Cell, F: Fibroblast, CAF: Cancer-Associated Fibroblast, M: Macrophage, TAM: Tumor-Associated Macrophage, C ł: Dead Cells)

During RT planning usually, we include in the treatment volume primary gross tumor volume + clinical target volume + lymph nodes (Figure 3) [2]. But if we want a good immune response we need cancer antigens and lymphatics. Because of this, we must discuss to save regional lymphatics and to give RT before surgery.
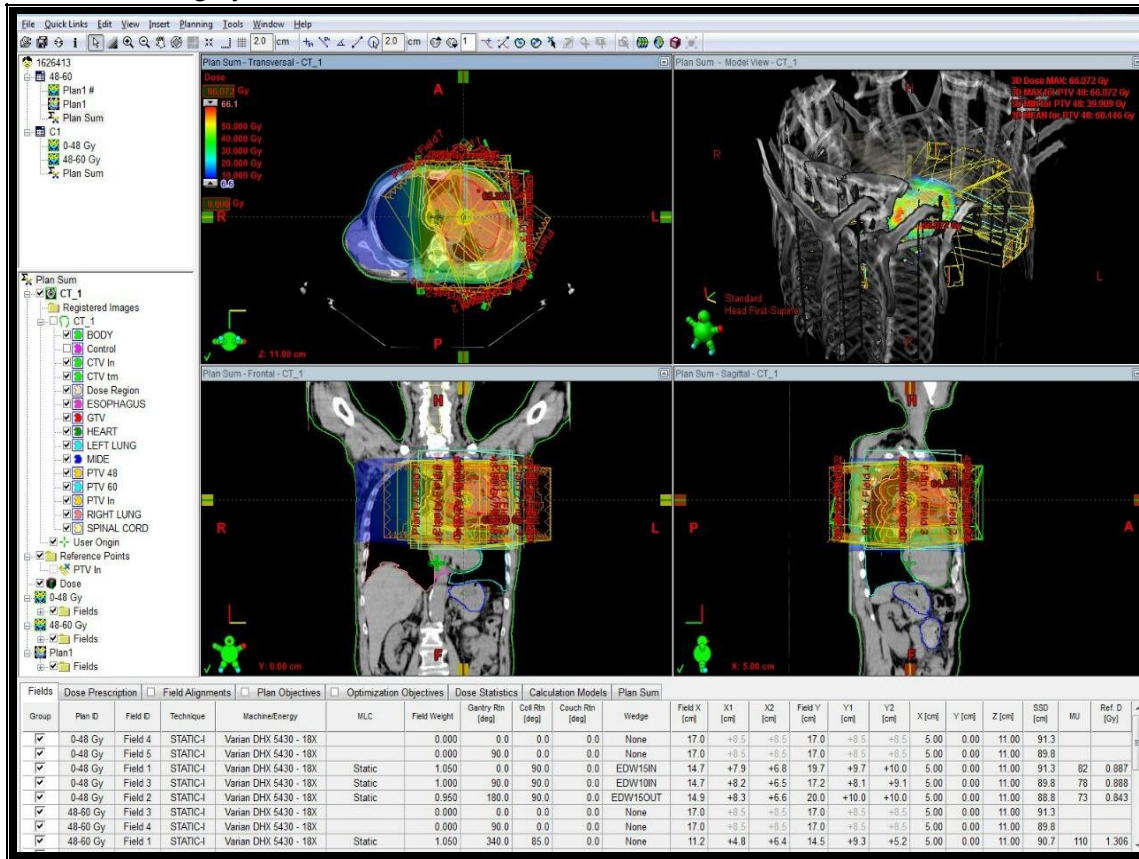
Figure 3. Radiotherapy treatment fields and isodoses on the left lung cancer case.

In the past and in classic radiation biology had 4R [3]; Repair, Redistribution, Reoxygenation (but RT may cause hypoxia, this may bad news and needs Anti VGF), Repopulation (This may bad news because RT may stimulate cancer growth) and 5R; Radioresistant/Radiosensitive tissue or cancer. Now we have 6R; IMMUN REJECTION, this may be good news? Because Radiotherapy activates immune response (Figure 4). Also, we have the 7R; Remodelling means cancer lives in a microenvironment and crosstalk with cancer and microenvironment such as CAF, etc [4, 5].
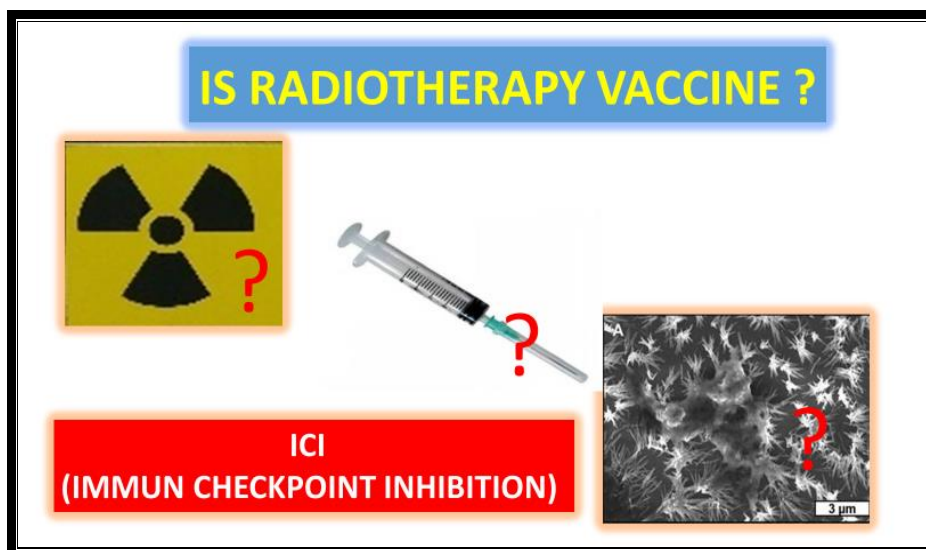
Figure 4. Is the radiotherapy vaccine [1, 6]?

In oncology practice, there are some vaccines, such as; Oncolytic virus, BCG [7]. Also; Sipuleucel-T is a DC-based vaccine containing GM-CSF. White cells (DS, Mo-Ma, B cell) are taken from the patient's with apheresis and transferred to the fabrication, where meeting with recombinant antigen-Sipuleucel-T / Provenge, Dendritic cells mature with GM-CSF and the T cell is matured and activated, then is given back from the vein the patient. This is active cell immunotherapy in castration-resistant prostate cancer, and

Cimavax-EGF (CUBA): If meningitis bacteria inoculated to patient body, produces antibodies against EGF. The EGF amount is reduced [8, 9]. Cancer can not progress and can not metastasis. Another non-vaccine treatment also against the EGF receptor as TKI. Including to above;

Is the radiotherapy vaccine? If RT increases the immune response we must learn some more about immune checkpoint inhibition (ICI; CTLA4, PD1, PDL1 inhibition) [10].

There are some molecules called Major Histocompatibility Antigene (MHC) or Human leukocyte Antigene (HLA) for immune activation after RT; MHC 1 (HLA- A, B, C) cell surface molecules is to deliver intracytoplasmic antigens such of viruses and tumor antigens presented to CD8 + cytotoxic T cells by the cell. MHC 2 (HLA-DP, DR, DQ) are the cell surface molecules, which has been taken by bacterial endocytosis to presented to CD4 + helper T (Figure 5-6) [11].
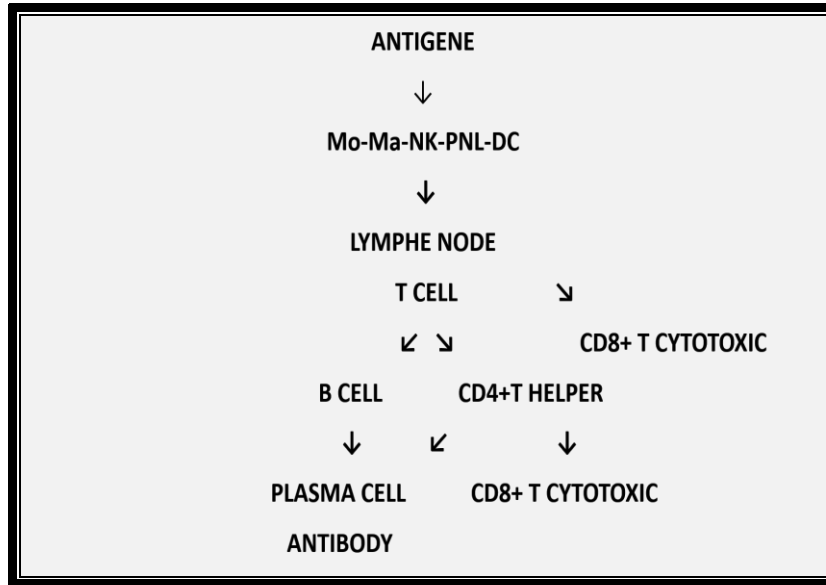
Figure 5. Immun activation after RT
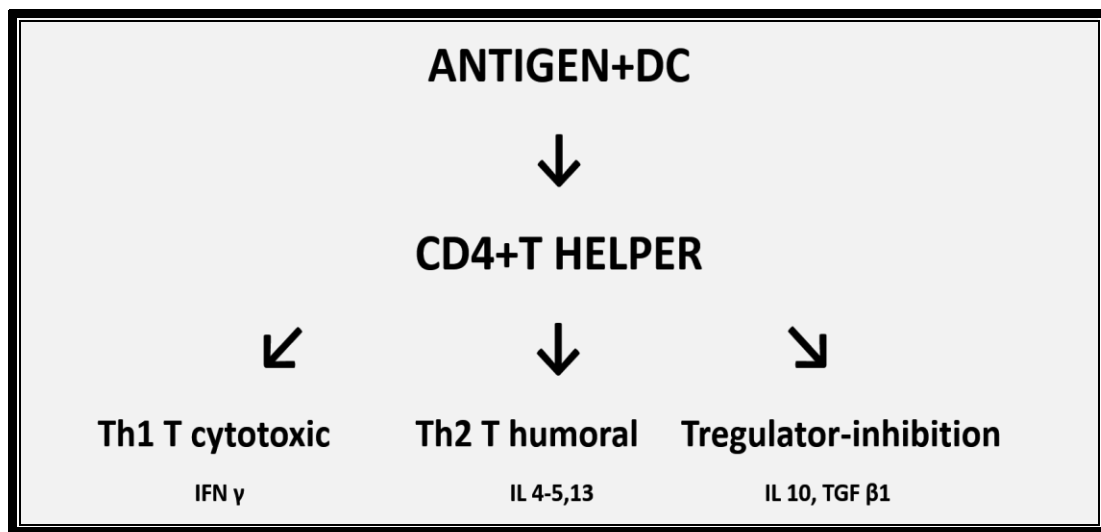
Figure 6. CD4 + T helper

Th1 cells provide the cellular immunity of the person with interferon gamma (IFN-γ), interleukin-2 (IL-2) and tumor necrosis factor-alpha (TNF-alpha). IL-2 specifically proliferates cytotoxic T-cells and activates IL-2 NK-cells. Also, the TNF-alpha stimulates T-cells and NK-cells to attack the tumor. INF-γ helps HLA-expression and enhances antigen presentation to effector T-cells [10-12]. Th2-cells secrete more IL-4, IL-5 and IL-10 than Th1-cells and Th2-cells support the immune response with antibody production. IL-4 stimulates B-cells through IgE. IL-10 contributes to the formation of B-cells, monocytes, and granulocytes [10-12].

2. Radiotherapy response

When we give RT to cancer microenvironment we may see many reactions [13-18];

1. Tumor antigens (MHC1/2) excrete to the extracellular matrix. Macrophages and dendritic cells (Dentritic-Cell DC) take them, go to the lymph glands, and these antigens present to the effector T cells and activate T cytotoxic cells (Tc) (CD8 + T lymphocytes).

2. DNA binding protein HMGB1 (High Mobility protein Group Box 1) Increases with radiation. The HMGB1 protein release to extracellular space. HMGB1 is TLR4-associated dendritic cell activator.

3. ATP (Adenosine triphosphate) appears after RT damage, activate the immune response.

4. When DNA is damaged, ATM (Anti telengectase mutated protein) comes out.

5. NKG2D (Natural Killer group 2D) ligands are increased. NK and active CD8 + T cells attack these ligands on cancer. Also the activated Tc attacks to metaplasia and metastasis.

6. From the endoplasmic reticulum, Calreticulin appears on the tumor surface. Calreticulin pre-apoptotic is released and it is the message to "eat me" in cell translocation.

7. Uric acid and Nitric oxide increases are released into the tumor space and cancer is eliminated by macrophages

8. HSP (heat shock protein) increases. They stimulate the Dentritic Cell (DC). DC stimulates CD8 + Tc.

9. Ceramide is present in the vascular endothelial membrane and also in all membranes. Ceramide is a member of the sphingolipid family, leads to   apoptosis. It also helps in immunotherapy (IT) by providing Dentritic Cell maturation with MHC1 increase.

10. ICAM1 (CD54): Intra Cellular Adhesion Molecule/Inter-Cellular Adhesion Molecule. After RT lymhatic endotelial cell adhesion increased to keep the immune cells for immune response

11. Fas (CD95): First Apoptosis Signal (Apo1 or tumor necrosis factor receptor superfamily member 6) binds to the protein-ligand (FasL), resulting in apoptosis signaling from the nucleus leading to cancer cell death.

12. The formation of ROS (reactive oxygen substrate) also kills cancer.

13. Radiation kills cancer directly but also activate immune responses through the Stimulator of Interferon Genes (STING)-mediated DNA-sensing pathway.

14. After RT, IFN gamma released against cancer to increases immune cell migration to the tumor site, has antiproliferative and antiangiogenic effects, the cytotoxic effect on cancer. IFN causes apoptosis in cancer. Also, IFN gamma / IL-12 are secreted by tumor-infiltrating monocytes/macrophages/ DCs and these activate the Natural Killer (NK) cells and this help to open holes in the cell with perforin granule enzyme and por forming the cytolytic protein. Por caspase or Fas-L caspase stimulus kill cancer.

3. Abscopal effect

(Ab: remote, away from. Scopes: target, purpose, aim, scope); Divided into two; The near abscopal effect (bystander effect, audience effect) and the remote abscopal effect [19-21].
The abscopal effect cannot be obtained in non-T cells rats. After RT, close and distant cancer cells may shrink and disappear. Because the antigens released by RT-receiving cells are taken up by Macrophages and DCs, and in the lymph node these antigens recognized by the effector T-cell and the activated immune system kills close and distant cancer cells. CD8 + Tc and Type1 Interferon increase. As seen in

Figure 7, the left lower metastatic lesion has disappeared after RT to only the left hiler primary and mediastinal lymph nodes because of the abscopal effect of RT [22].
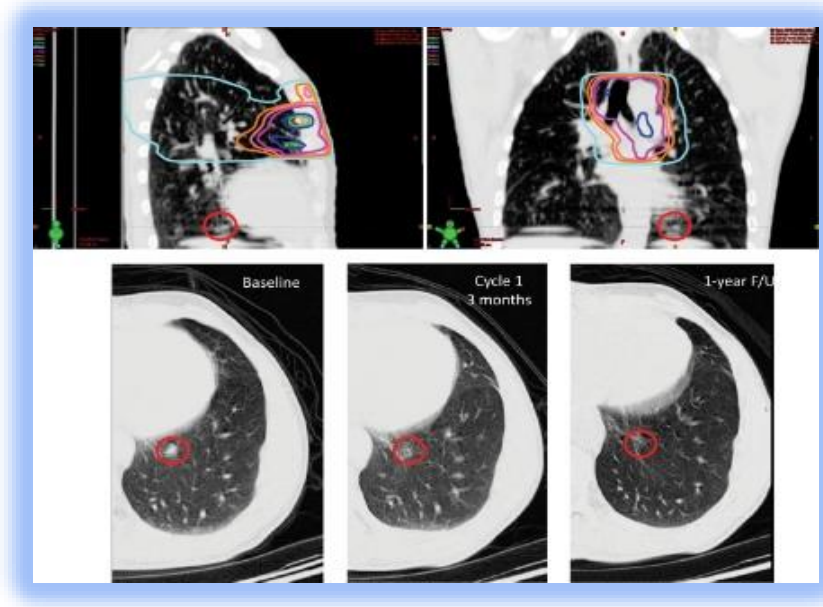
Figure 7. Abscopal effect [22]

BUT, if proliferating cancers and metastases mutate, it may be a new antigenic construct and we can not see the abscopal effect. Cancer cells are heterogeneous and each cancer cell has similar and dissimilar antigens. For this reason, the immune response may not be against every cell. Also, it is very important that a normal person has immune checkpoints (ICP) to protect its self from over immune attack to from autoimmune diseases. If ICP works in cancer patients our immune system can not attack to kill the cancer cells. Because of these, we must discuss how the ICP works and we need ICP inhibition to fight against cancer (Figure 8).
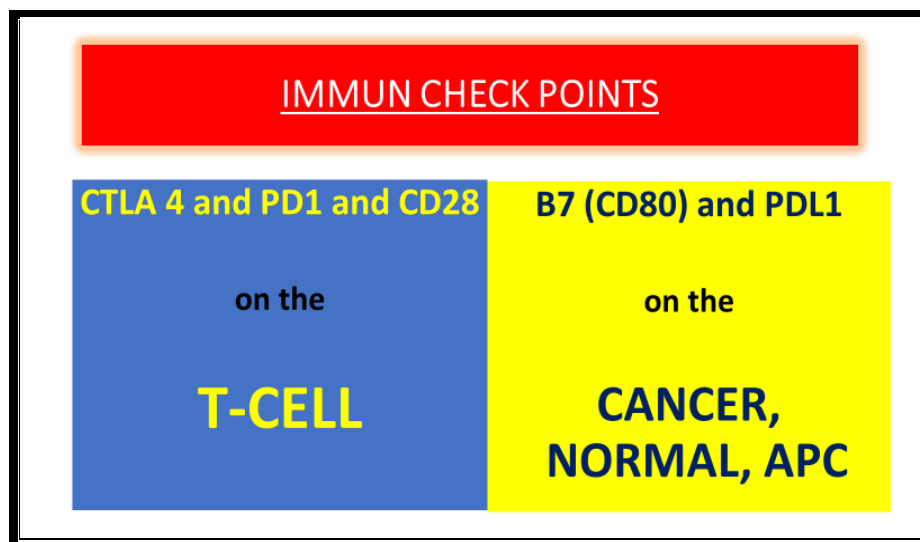
Figure 8. Immun Check Points (ICP)

There are natural immunocompromised checkpoints against autoimmunization (CTLA4, PD1, PDL1) and block the immune response, otherwise, the body will accept its normal cells as foreign. CTLA4 (Cytotoxic T Lymphocyt Associated antigen 4) immunity checkpoint prevents self-attack in normal human and normal tissues, protects us and prevents autoimmune disease. CTLA4 is on T lymphocyte, and if B7 (B; Bursa of Fabricius was used to identify unknown B cell antigens and ligands in studies previously performed with monoclonal antibodies. Now, this terminology is also used in APC and DC. B7 peripheral membrane protein; T cell surface costimulatory molecule) are on the normal and APC or cancer cells. If CTLA4 and B7 binds; T lymphocyte cannot attacks.

The MHC antigen stimulates APC and DC receptors, also at the same time directly stimulates on T cell receptors. CD28 (Cluster of Differentiation 28) in the T cell communicates with B7 in APC provides immune activation. When this activation reaches a certain level, CTLA4 which is on the active T cell binds to the B7 ligands on DS or APC in order to avoid the autoimmune attack and immuno-suppression. If anti-CTLA4 is given, B7 continuously stimulates the T cell and increases the immune response.

B7 and CTLA4 receptor interaction between the tumor cell and APC then inactivates T cell. If Anti CTLA4 is given, T cell becomes active. Anti CTLA4 T blocks CTLA4 on the cell. The APC stimulus continues at T and T attacks cancer. If anti-CTLA4 (Ipilimumab) is given, B7 cannot bind to CTLA4 in dendritic cells or in APC, and the attack continues (Figure 9). Also, APC (antigen presenting cell) stimulation continues on T-lymphocytes, the attack is exacerbated, but it is also necessary to pay careful attention to the attacking of normal tissues which cause hazards and side effects.
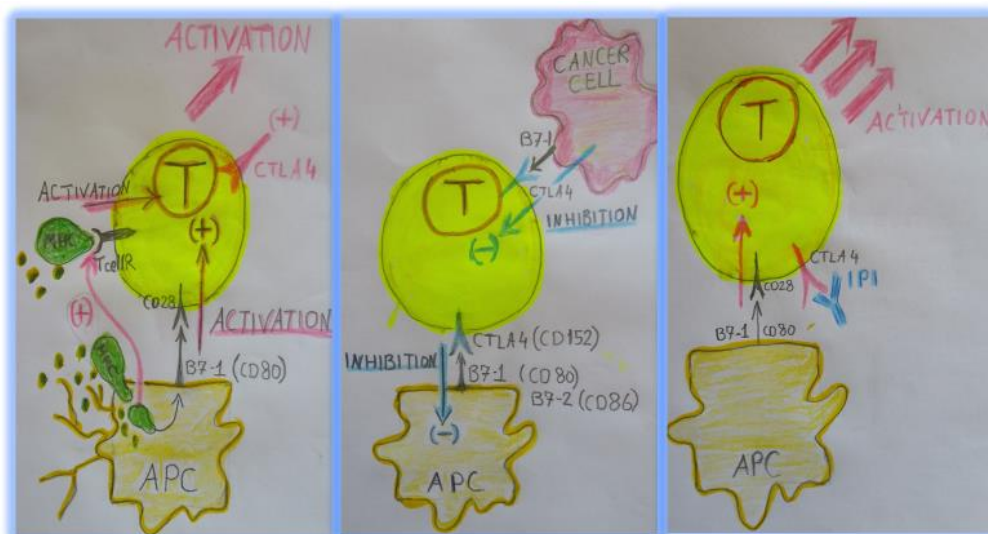
Figure 9. Activation and inhibition with B7, CD28 and CTLA4 interactions

The PD1 is on T CELL and PDL1 is on NORMAL and APC and cancer cells. When RT is given, PD1 and PDL1 are overexpressed. If a contact on T cell PD1+PDL1 on the tumor cell/normal/APC cell deactivates the immune T cell. ICI antibodies (anti-PD, anti-PDL1) continues to activate the immune response against cancer (Figure 10).

PD1 is present in activated T cells and must bind to PDL1 to suppress T cell immunity. PDL1-2 is present not only in antigen presenting cells but also in cancer cells, and T cell inhibition occurs when the PDL1 ligand of APC or tumor cell meets with PD1. Therefore, if anti PDL1 is given, PDL1 and PD1

will not meet, APC will not be suppressed, and it will continuously stimulate APC and the killer cell will attack cancer in the active state. Cancer can not prevent T cell attacks.
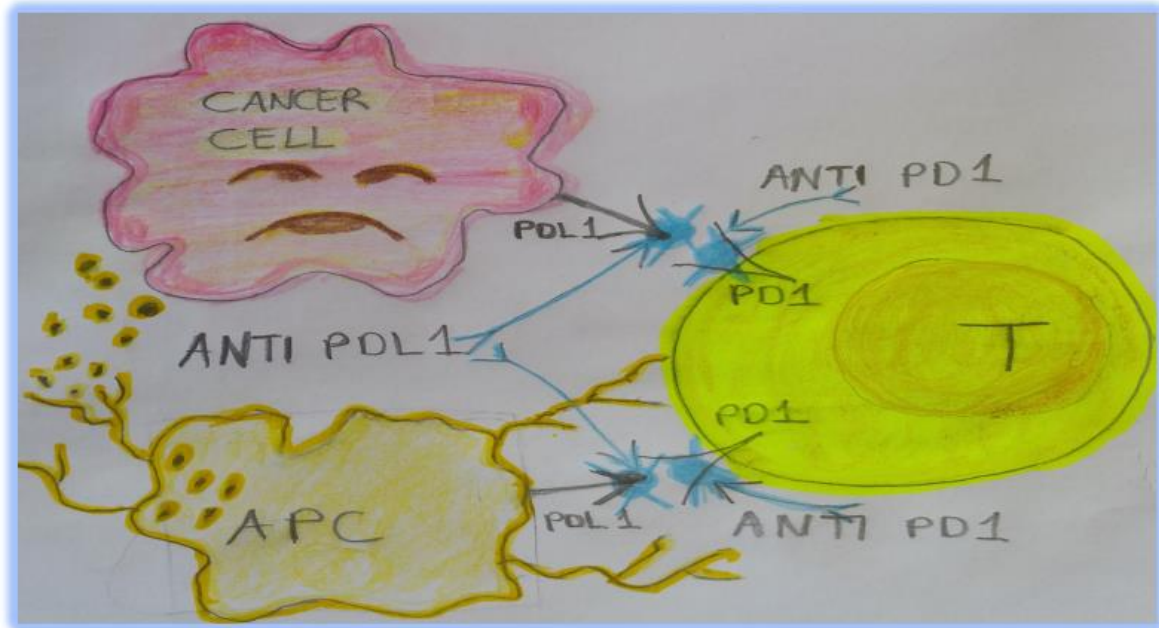
Figure 10. PD1/PDL1 interactions and anti PD1/anti PDL1

Anti PDL1 closes the PDL in cancer and in APC. The PD1 in cancer and in the APC cannot contact with PDL and the T attack continues. if we give an ICI, auto-immunity is exacerbated and side effect increases. If B7 is blocked, the CD28 stimulus is turned off and immune stimulation is reduced [23, 24].

4. Side effects of ICI+RT [25, 26]:

The most common autoimmune side effect is on the skin, like vitiligo, but G3-4 is less. In addition, gastroenteritis, nausea, vomiting, reduced appetite, fatigue can be seen. Also, colitis, pneumonia, hepatitis, nephritis may occur. Attacks on the endocrine system can lead to hypothyroidism, thyroiditis, hypophysitis, colitis, pneumonia, these are threating the life.

CTLA4 is the first and early control point and early side effects can be expected (dermatitis, vitiligo, gastroenteritis, hepatitis, endocrinopathy, thyroid dysfunction). PD1 / PDL1 is the second control point and late side effects can be expected. (Lung pneumonia in the late period).

5. RT Dose and timing [10-14, 27]:

Low-dose RT is insufficient to activate the immune system. Very high doses completely eliminate the anti-tumor effect of the immunizing system. In addition, excessive antigen presentation may also exert a stifling effect on the immune response. Because of this, the dose must be stimulating cytotoxic cells while decreasing T regulatory cells.

Low doses below 2Gy can not kill cells. It is more likely to induce macrophage stimulation, where the macrophages (M2/ TAM) provide anti-inflammatory effects and thus impair the immune response. At doses above 2 Gy, cancer cell surface antigens (MHC1, ICAM, Fas) are exaggerated from the cell.

In X-Ray RT, the input and output doses act on normal tissues and also suppress the immunological response at the around and within cancer. Proton is better in this respect [28].

The hypofractionated RT with stereotactic body RT (SBRT) with 1x20Gy, 3x8Gy, 5x6Gy is recommended (3 or 5 fractions are preferred to 1 fraction. The best is 3x8Gy) such as 3x8Gy or 5x6Gy + anti-CTLA4 (3 mg/kg every 1-3 weeks for 4 doses) instead of a single dose of 1x20Gy or 1x15Gy, 5x3Gy, 3x5Gy, 2x7.5Gy (The best is 2x7.5Gy).

If ICI is given too long before RT, the RT given later will destroy existing cytotoxic T lymphocytes and the response will diminish. If immunotherapy is given just prior to RT, there is an immunologically prepared environment and RT effect is increased. If RT is given first, the cells that are found to recognize and to kill the tumor cells die and the immune response can only be achieved by introducing immunogenic cells from the outside. The best is given; just before RT, or during RT, or immediately after RT. But, in the near future, we must discuss for the use of SBRT because the microenvironment is very important and with hypofractionated stereotactic radiotherapy, the microenvironment around the cancer tissue such as fibroblast may survive and then may help cancer stem cells progression [4, 5].

6. Conclusion

It is clear that the RT activates the immune response [6, 29-33]. It is popular to use hypofractionated SBRT, but we have risk because of the protected fibroblasts around the irradiated volume may survive and then help cancer stem cell progression [4, 5, 31]. After RT there are many changes in the cancer cell or around the tumor microenvironment and these activate the immune response. But the cells have some immune checkpoints to protect autoimmune disease after a certain level of immune activation. If we use the ICI with RT we may see the better immune response but we may pay attention to the side effects of these applications. Hypofractionated stereotactic body radiotherapy is widely used in clinical practice to achieve an immune response, but in the microenvironment around the cancer tissue such as fibroblast may survive and may help cancer stem cells survive and progression, and this is very important subject should be taken into consideration in order to be better understood in future studies.

References

[1] Jaitley S, Saraswathi TR, "Pathophysiology of Langerhans cells", *J Oral Maxillofac Pathol.*, 16 (2), 239–44, 2012.

[2] Purdy JA, "Current ICRU definitions of volumes: limitations and future directions", *Semin Radiat Oncol.*, 14, 27-40, 2004.

[3] Pajonk F, Vlashi E, WH, "Radiation Resistance of Cancer Stem Cells", *The 4 R's of Radiobiology Revisited Stem Cells,* 28: 639-48, 2010.

[4] Ishii G, "Crosstalk Between Cancer-Associated Fibroblasts and Cancer Cells in the Tumor Microenvironment After Radiotherapy", *EBioMedicine*., 17, 7–8, 2017.

[5] Arnold KM, Flynn NJ , Raben A, et al, "The Impact of Radiation on the Tumor Microenvironment: Effect of Dose and Fractionation Schedules", *Cancer Growth and Metastasis*., 11, 1-17, 2018.

[6] Kurtman C, Sokur I, Zaplatina S, et al, "Radiotherapy and Immun Response. Is the Radiotherapy Vaccine? Good News?" *Accepted for publication in Celal Bayar University-Health Sciences Institute Journal*., 6 (2), 2019.

[7] Redelman-Sidi G, Glickman MS, Bochner BH, "The mechanism of action of BCG therapy for bladder cancer - a current perspective", *Nature Reviews Urology*., 11, 153-62, 2014.

[8] Rodríguez PC, Rodríguez G, González G, Lage A, "Clinical development and perspectives of CIMAvax EGF, Cuban vaccine for non-small-cell lung cancer therapy", *MEDICC Rev*., 12, 17-23, 2010.

[9] Saavedra D, Crombet T, "CIMAvax-EGF: A New Therapeutic Vaccine for Advanced Non-Small Cell Lung Cancer Patients", *Front Immunol*., 8, 1-7, 2017.

[10]. Hwang WL, Pike LRG, Royce TJ, Mahal BA, Loeffler JS, "Safety of combining radiotherapy with immune-checkpoint inhibition", *Nat Rev Clin Oncol*., 15, 477-94, 2018.

[11] Esposito A, Criscitiello C, Curigliano G, "Immune checkpoint inhibitors with radiotherapy and locoregional treatment: synergism and potential clinical implications", *Curr Opin Oncol*., 27, 445-51, 2015.

[12] Manda K, Glasow A, Paape D, Hildebrandt G, "Effects of ionizing radiation on the immune system with special emphasis on the interaction of dendritic and T cells", *Front Oncol*., 2, 1-9, 2012.

[13] Demaria S, Golden EB, Formenti SC, "Role of Local Radiation Therapy in Cancer Immunotherapy", *JAMA Oncol*., 1, 1325-32, 2015.

[14] Demaria S, Coleman CN, Formenti SC, "Radiotherapy: Changing the Game in Immunotherapy", *Trends Cancer*., 2, 286-94, 2016.

[15] Shi X, Shiao SL, "The role of macrophage phenotype in regulating the response to radiation therapy", *Transl Res*., 191, 64-80, 2018.

[16] Hanahan D, Weinberg RA, "Hallmarks of cancer: the next generation", *Cell*., 144, 646-74, 2011.

[17] Gameiro SR, Jammeh ML, Wattenberg MM, Tsang KY, Ferrone S, Hodge JW, "Radiation-induced immunogenic modulation of tumor enhances antigen processing and calreticulin exposure, resulting in enhanced T-cell killing", *Oncotarget*., 5, 403-16, 2014.

[18] Kaur P, Asea A, "Radiation-induced effects and the immune system in cancer", *Front Oncol*., 2, 1-10, 2012.

[19] Hu ZI, McArthur HL, Ho AY, "The Abscopal Effect of Radiation Therapy: What Is It and How Can We Use It in Breast Cancer?" *Curr Breast Cancer Rep*., 9, 45-51, 2017.

[20] Jatoi I, Benson JR, Kunkler I, "Hypothesis: can the abscopal effect explain the impact of adjuvant radiotherapy on breast cancer mortality?" *NPJ Breast Cancer*., 4, 1-8, 2018.

[21] Zhang X, Niedermann G, "Abscopal Effects With Hypofractionated Schedules Extending Into the Effector Phase of the Tumor-Specific T-Cell Response" *IJ Rad Oncol Biol Phys*., 101, 63-73, 2018.

[22] Formenti SC, Demaria S, "Combining Radiotherapy and Cancer Immunotherapy: A Paradigm Shift", *J Natl Cancer Inst*., 105, 256-65, 2013.

[23] Garon EB, Rizvi NA, Hui R, et al, for the KEYNOTE-001 Investigators, "Pembrolizumab for the Treatment of Non–Small-Cell Lung Cancer", *N Engl J Med*., 372, 2018-28, 2015.

[24] Antonia SJ, Villegas A, Daniel D, et al, for the PACIFIC Investigators, "Durvalumab after Chemoradiotherapy in Stage III Non-Small-Cell Lung Cancer" *N Engl J Med*., 377, 1919-29, 2017.

[25] Winer A, Bodor JN, Borghaei H, "Identifying and managing the adverse effects of immune checkpoint blockade", *J Thorac Dis*., 10 (Suppl 3), 480-9, 2018.

[26] Kähler KC, Hassel JC, Heinzerling L, et al, for the "Cutaneous Side Effects" Committee of the Work Group Dermatological Oncology (ADO), "Management of side effects of immune checkpoint blockade by anti-CTLA-4 and anti-PD-1 antibodies in metastatic melanoma", *J Dtsch Dermatol Ges*., 14, 662-81, 2016.

[27] Wang Y, Deng W,   Li N, et al, "Combining Immunotherapy and Radiotherapy for Cancer Treatment: Current Challenges and Future Directions", *Front Pharmacol*., 9, 1-11, 2018.

[28] Ebner DK, Tinganelli W, Helm A, et al, "The Immunoregulatory Potential of Particle Radiation in Cancer Therapy", *Front Immunol*., 8, 1-8, 2017.

[29] Rogers SJ, Puric E , Eberle B, et al, "Radiotherapy for Melanoma: More than DNA Damage", *Dermatol Res Pract.,* 3, 1-9, 2019.

[30] Shevtsov M, Sato H, Multhoff G, Shibata A, "Novel Approaches to Improve the Efficacy of Immuno-Radiotherapy", *Front Oncol.,* 9, 1-16, 2019.

[31] Ozpiskin OM, Zhang L, Li JJ, "Immune targets in the tumor microenvironment treated by radiotherapy", *Theranostics*., 30, 1215-31, 2019.

[32] Turgeon GA, Weickhardt A, Azad AA, et al, "Radiotherapy and immunotherapy: a synergistic effect in cancer care", *Med J Aust*., 210, 47-53, 2019.

[33] Thangamathesvaran L, Shah R, Verma R, Mahmoud O, "Immune checkpoint inhibitors and radiotherapy-concept and review of current", *Ann Transl Med*., 6, 1-10, 2018.